SYNTHESIS, CHARACTERIZATION AND TOXICITY OF NANOPARTICLES FOR REAL WORLD APPLICATIONS

A Dissertation

by

AISHWARYA SOORESH

Submitted to the Office of Graduate and Professional Studies of
Texas A&M University
in partial fulfillment of the requirements for the degree of

DOCTOR OF PHILOSOPHY

Chair of Committee,	Kenith E. Meissner
Co-Chair of Committee,	Christie M. Sayes
Committee Members,	Michelle Pine
	Michael J. McShane
Head of Department,	Ibrahim Karaman

May 2014

Major Subject: Materials Science and Engineering

ABSTRACT

Nanotechnology involves the synthesis and characterization of materials at the atomic, molecular and macromolecular scales, which results in a controlled manipulation of structures and devices that have at least one dimension that is approximately 1-100 nm in length. Objects at this scale, referred to as "nanoparticles" (NPs), exhibit physical properties differing from that of their bulk or micron scale counterparts. Unique properties such as small size, improved solubility, surface tailorability and large surface-to-volume ratio open up many research and application avenues for the materials scientist, the biologist and the engineer. These novel properties enable cross-disciplinary researchers the opportunity to improve existing products and to design and develop new products.

The primary aim of this work was to design studies and formulate methodologies that offer valuable insight into the complexities that are often encountered with understanding environmental/human health impacts of a nanotechnology. This dissertation investigates two scenarios of a nanotechnological application. First, a current nanotechnology-based consumer application was considered. Specifically, the incorporation of titanium dioxide NPs into paints and lacquers was studied. A valuable way to gather information critical to the development of safe nanomaterial-containing consumer products is by employing a product life cycle approach. The primary focus here was to formulate methodologies to produce nano-enabled coatings in-house and assess the impacts/benefits of a nanotechnological application that is currently in the

marketplace using a life cycle approach. Material characterization and toxicological evaluations of NPs in their pristine and end-of-life stages were assessed. Next, a potential nanotechnological application was explored. Specifically, the modification of silver NPs for insect vector control was investigated. The research developed here was the first of its kind in engineering a novel silver NP-pesticide conjugate. The efficacy of the newly developed conjugate and the cellular effects in model cell culture systems were evaluated. The findings of this work will provide a useful initial framework in prioritizing future nanotechnological research needs and have a significant impact on material scientists, toxicologists and engineers alike.

DEDICATION

To my parents

ACKNOWLEDGEMENTS

I would like to thank my advisors, Drs. Christie Sayes, Kenith Meissner and Michelle Pine for their guidance, tireless support and extension of knowledge. They have all been exceptional mentors throughout the course of this research. Their constant encouragement, technical advice, financial and moral support has played a key role in the completion of this study. They are experts in their fields and the multidisciplinary nature of all my research projects has enabled me to learn a lot from each one of them and develop a very diverse skill set. Thanks also to Dr. Michael McShane for serving on my committee. I am very grateful to my entire committee and will forever be indebted to all of them!

My sincere appreciation goes to my friends, colleagues, the department faculty and staff for making my time at Texas A&M University a great experience. I would like to particularly thank my lab mates, Mike Berg, Amelia Romoser and Ahmed Ridha of the Sayes lab; Ravish Majithia and Sarah Ritter of the Meissner lab and Ashvin Nagaraja of the McShane lab for the lively discussions, help, and valuable suggestions during the course of this study. I also want to extend my gratitude to all my collaborators at Texas A&M University and RTI International. A large portion of this work would have not been possible without their contributions. A special shout out to my friends, Amanda Cain, Avinash Rani, Rohit Chintala and Arijit De for their encouragement and moral support.

Finally, thanks to my family for their patience, love and encouragement.

TABLE OF CONTENTS

Page

LIST OF FIGURES

Page

LIST OF TABLES

Page

1. INTRODUCTION

Nanotechnology is defined as the ability to fabricate materials at the atomic, molecular and macromolecular scale, which results in a controlled manipulation of structures and devices that have at least one dimension that is approximately 1-100 nm in length [1]. Objects at this scale, referred to as "nanoparticles" (NPs), exhibit fundamentally new properties and functions differing from that of their bulk or micron scale counterparts. Unique properties such as small size, improved solubility, surface tailorability and large surface-to-volume ratio have resulted in the creation of one of the most dynamic science and engineering domains. This opens up many research and application avenues for the materials scientist, the biologist and the engineer. Thus, such a rapidly growing field allows cross-disciplinary researchers the opportunity to improve existing products and to design and develop new products.

The rise in popularity of nanoscale science and engineering stems from nanotechnology being an effective route to alter and enhance properties. Consequently, NPs have been incorporated into hundreds of different types of products and offer great promise in providing new technological breakthroughs. For example, titanium dioxide NPs are produced in high tonnage volumes for use in paints and coatings (as a UV absorber to help prevent UV degradation), cosmetics (in sunscreens to prevent UV damage to skin), and packaging applications [2-4]. Silver NPs have been cited as the most commonly used nano-object in a wide range of consumer products. An increasing number of nano-silver containing products are available, including cosmetics and

personal care products, food and health-food, antimicrobial paints and coatings, hygienic surfaces and packaging materials, and medical applications [5-7]. Zinc oxide NPs find wide applications in cosmetics and personal care products, but other applications such as antimicrobial packaging have also emerged recently [8]. To list the entire spectrum of all the currently used NPs for consumer and industrial applications would require hundreds of entries. The Project on Emerging Nanotechnologies (PEN) is the first publicly available on-line inventory of nanotechnology-based consumer products [9]. When the PEN inventory was first released in March 2006, it listed 212 products, and three years later, the list skyrocketed to 1015 products– an increase of almost 400%, indicating how rapidly this field is progressing. It is estimated that by 2020 nanotechnologies will impact at least $3 trillion across the global economy, and nanotechnology industries worldwide may require at least 6 million workers to support them [10].

While the remarkable properties of these nano-enabled products have the potential to revolutionize several industries and many aspects of human life, human exposure to NPs is inevitable. Public exposures could be due to intentional administration or inadvertent contact. Questions regarding toxicological and environmental/human impact of nanomaterials and concerns regarding the safety of these materials are subjects of considerable debate.

According to the National Institute of Standards and Technology, NIST, 3 or 4 emerging nanotechnology-based consumer products are entering the market per week, with an estimated $2.6 trillion in NP-containing manufactured goods by 2014 [11]. The incorporation of NPs into products causes increased exposure to the workers producing

the materials, the consumer utilizing the product, and eventually the environment in which the product is disposed. The overall safety of NP-exposures arising from widespread use of nano-enabled products remains relatively unknown. In order to develop a successful risk analysis framework, the research and development centered on nanomaterial production should be balanced with its corresponding toxicological information.

The evaluation of the safety of nanomaterials will likely involve a multi-disciplinary approach with communication among several disciplines such as material science, chemistry, physics and engineering in addition to an emerging field known as "nanotoxicology", i.e., studying the toxicological potential of nanomaterials. The potential adverse effects of NPs on biological systems are a major concern. Some studies suggest that NPs can affect biological behavior at both the cellular and sub-cellular levels by systemically being distributed in tissues or organs [12]. There is also some evidence that some NPs may readily travel within the human body and penetrate cell membranes triggering a variety of damaging responses such as the generation of reactive oxygen species or inflammation [12, 13]. Therefore, there is an overwhelming need to evaluate the toxicity of NPs in the cellular environment.

In vitro NP toxicity evaluations could provide some answers critical to evaluating the safety of a nano-enabled product or the bare NP itself. In comparison to *in vivo* or animal testing, *in vitro* cellular models are easy to control, less expensive, more reproducible and more importantly ethically accepted as a testing method. *In vitro* techniques are rapid, cost effective and reduce the use of live animal models in research.

Cell lines selected for *in vitro* assays are intended to represent a response likely to be observed *in vivo*. Controlled conditions facilitate the study of a specific biological pathway or a particular toxicological endpoint. Hence, the choice of cell lines, endpoints, incubation times and realistic dosing concentrations are pivotal experimental design considerations, to name a few. Additionally, appropriate controls need to be included in the study before drawing conclusions [13]. Toxicological evaluations are therefore necessary and an integral component in prioritizing the safety of current and newly developed nano-enabled products. This screening methodology can be used to rank potential toxicities of a host of nanomaterials.

The following section expands on the NPs of interest in this work.

1.1. NP of interest

1.1.1. Titanium dioxide NPs

Titanium dioxide (TiO_2) NPs are manufactured worldwide for use in a range of applications, and hence listed in the top five NPs used in consumer products [14]. It is well documented that the physical and chemical properties of nanosized matter differ substantially from the properties of the same material in its bulk form, because a smaller size ensures a larger portion of atoms on the particle surface [13, 15, 16]. For example, particles on the nanometer size scale can increase resistance to ultraviolet damage, prevent wear and fouling, and improve the rheology, hardness and strength of construction materials [17]. These particles have been shown to replace toxic organic biocides and can be used for air purification, thermal insulation and self cleaning [17].

The paint and lacquer industry, in particular, is a high tonnage user of engineered nanomaterials. Vast amounts of particulates, pigments, binders and fillers are used in paints and lacquers. TiO_2 NPs have traditionally been incorporated into these paint and lacquer formulations as a whitening agent because of its brightness and very high refractive index and to impart special properties such as improved durability, water repellence and scratch resistance [18]. The global use of TiO_2 for paint and surface applications alone exceeds 2.5 million tons annually [19, 20].

The incorporation of NPs into paint and lacquer formulations is a consumer application already in the marketplace. As a result, human exposure to these engineered NPs is inevitable. The route and extent of exposure is heavily dependent on the application of the nano-enabled product in a real world scenario [21]. While several studies have investigated the physiochemical characteristics and material toxicity of pristine TiO_2 NPs [22], little is known about the effects of TiO_2 NPs incorporated into complex matrices such as paint and lacquer formulations. More importantly, changes in physiochemical characteristics and material toxicity during product end-of-life scenarios, i.e. potential release of NPs from the matrices, are unknown and need research emphasis. The development of engineered nanomaterials can develop dynamically only if the safety of humans and the environment is known or, at a minimum, the risk can be assessed [23, 24]. In other words, the identification and characterization of engineered NPs in complex matrices is a prerequisite in order to fill in data gaps in safety assessments. Thus, one valuable way to gather information critical to the development of safe nanomaterials is using a product life cycle approach [25-28].

A product life cycle approach integrates product development with manufacturing, consumer and occupational exposure, enabling an opportunity to elucidate the human and environmental impacts of a technology. Exposure scenarios of bare as well as commercial NPs throughout their life cycle must be considered. This approach provides an opportunity to elucidate the human and environmental safety of a technology by assessing toxicological impact throughout the product life cycle.

1.1.2. Silver NPs

Silver NPs (AgNPs) have been gaining increasing attention over the past few years because of their unique electronic and optical properties; hence, they find wide applications in various fields such as environmental, biomedicine, catalysis, optics and electronics. Several methods are employed in the production of AgNPs, but the biggest challenge of synthesizing uniform and stable AgNPs with a controllable size remains. It is crucial to control the size and shape of AgNPs as the optical properties are dictated by these parameters [29].

Generally speaking, the synthesis of AgNPs can be categorized as a top-down or a bottom-up approach [30]. In the top-down approach, specialized methods such as milling, grinding, etching and pyrolysis are employed to mechanically reduce the silver in its bulk form into the nano-scale regime. Examples of the top-down approach to synthesize AgNPs include gamma radiation, laser ablation, photochemical reduction, electrochemical reduction, and sputtering [31-35]. The top-down approach is often employed for large scale production of NPs, however, the main disadvantage of this approach is the limited control on AgNP formation which results in imperfections in the

crystals. Furthermore, this synthesis scheme is time consuming and often yields a broad distribution of NP sizes, which impacts the applicability of the newly generated NPs for any real world application [36, 37] . The bottom-up strategy, on the other hand, often employs wet chemical methods such as organic synthesis, self assembly approach or colloidal aggregation to generate AgNPs [37].

The simplest and the most commonly used bottom-up technique to synthesize metal NPs in the bulk phase is the chemical reduction of metal salts [38]. Synthesis involves the use of a soluble metal salt, a reducing agent, and sometimes a capping or stabilizing agent to prevent aggregation [30]. Careful selection of reducing agents and colloidal stabilizers allows for successful synthesis of NPs. Commonly used stabilizing agents include polymers and surfactants [39]. Although this preparation is simple, great care must be taken to make sure that the NPs produced are stable. Controlling the size and shape of NPs is a challenge. Factors such as solution concentrations, reaction temperature, reaction time, and reducing agent greatly influence the particle size [34]. Other factors such as rate of mixing, purity of water/reagents, and cleanliness of glassware are also known to play an important role during the synthesis scheme.

One of the most attractive properties of AgNPs is their high surface-to-volume ratio which results in high surface reactivity [40-44]. Indeed, if the surface of the NP is not protected with a capping or stabilizing agent, interactions between particles occur thereby reducing the high surface energy and resulting in aggregation [29, 45-48]. For this purpose, polymers, surfactants and inorganic capping materials are often introduced during the NP synthesis schemes [49]. The mode of action in preventing aggregation is

by electrostatic repulsion, steric hindrance or both [37]. In addition to stabilization, these capping agents can also be carriers of specific functionalities for novel applications [37, 50]. Thus, the ultimate goal of nanosilver synthesis for real world applications is to achieve NPs with the following characteristics: (1) narrow size distribution, (2) well defined shape, (3) known chemical composition with no impurities, and (4) no aggregation or agglomeration [29]. By utilizing a capping agent that acts as a colloidal stabilizer and enhances water suspendability, these highly desirable characteristics can be achieved for AgNPs [51, 52].

The high surface-to-volume ratio of AgNPs also results in improved antimicrobial properties and hence AgNPs have been widely used for the production of nano-enabled packaging [53]. AgNPs have also been postulated as ideal candidates for antimicrobial surface coatings, antimicrobial paints and even food and drink additives. The proposed mechanism of action of Ag is thought to arise from leaked Ag ions which causes damages on bacterial cell walls upon binding with cellular proteins or DNA, and thereby inactivating the enzyme phosphomannose isomerase [6, 7, 54].

The use of these NP-enabled products in their intended (and potentially unintended) manner would result in either individual colloids or NPs incorporated into larger composites entering into the human body [55, 56]. Furthermore, the physical and chemical properties and observed antimicrobial effects of AgNPs can also influence their reaction with commensal microbial populations within the gastrointestinal tract. Some of these responses could be detrimental to surrounding tissues by causing inflammation and alterations in the immune response depending on the physicochemical nature of the NP,

the target microbial populations and the physiological conditions existing within specific locations of the gastrointestinal tract [57]. The microbial populations within the gastrointestinal tract have coevolved with us and it directly influences gastrointestinal tract form, function, and stability. The microbial consortia within the intestines are vital to many aspects of normal host physiology, immune development, and in controlling infections. When NP-containing food products are ingested, these particles are exposed to the spectrum of pH levels that exist from the stomach to the large intestines. These conditions could facilitate the release of NPs from the food matrix and/or metal ions from the particle core. Food-incorporated, aggregated, or free particles could get disseminated within the gastrointestinal tract. Changes in the pH of the surrounding environment will modify the particles' size, increase the amount of leached metal ions, and influence the production of reactive oxygen species (ROS) from the surface of the colloid [6, 58-61]. Perturbations in the microbial communities could be expected when there are changes associated with the NP surface or, as has previously been reported, when a digestion procedure is incorporated into the experimental design [62-65].

1.2. Overview of the dissertation

The primary aim of this dissertation was to design studies and formulate methodologies that offer valuable insight into the complexities that are often encountered with understanding environmental/human health impacts of a nanotechnology. A current and novel nano-technological application was studied in this work.

Section 2 employs a life cycle assessment for a current nanotechnology-based consumer application, specifically the incorporation of TiO_2 NPs in paints and lacquers. Methodologies were formulated to produce the nano-enabled products in-house. Simulated wear-and-tear scenarios were performed on the nano-enabled products to mimic real world end-of-life scenarios. The pristine NPs and the worn-and-torn powders were analyzed via material characterization techniques and toxicity evaluations. A product life cycle approach such as this provides a rich framework for assessing the benefits and risks of nanotechnologies and possibly aid in identification of the risk triggers.

Section 3 of the dissertation utilizes cutting-edge nanoscience methodologies to effectively address the shortcomings of current pesticides by engineering a novel pesticide encapsulated NP. First, chemical reduction methods to produce monodisperse AgNPs were investigated. The lab-synthesized AgNPs was then surface modified with deltamethrin, a nonionic surfactant as the capping agent. The resultant aqueous suspension termed as a pesticide encapsulated nanosilver particle was thoroughly characterized. Furthermore, the effects of the newly developed NP-pesticide conjugate in killing mosquitoes were compared to its active ingredient deltamethin in a time-course and dose-dependent manner.

Section 4 investigates *in vitro* effects of the pesticide encapsulated NP. Even though cellular effects of the individual components i.e., deltamethrin and AgNPs are well-characterized, any modifications of those effects due to the conjugation process have not been previously studied. Therefore, the effects of the newly created AgNP-

pesticide conjugate on basic cellular responses were assessed utilizing an *in vitro* cellular model. The long-term goal of this interdisciplinary research was to develop efficacious pesticides with minimal toxicity in mammals. A paradigm-shifting technology such as this offers new possibilities for vector and pathogen control. This example of a potential NP-based technology will have a significant impact on basic understanding of synthesis, characterization, and toxicology, as well as in the application of such technologies towards vector control.

Section 5 explores the physicochemical changes and possible perturbations to microbial communities within the gastrointestinal tract upon AgNP exposure. A simulated digestion protocol was designed to evaluate the effect of colloidal silver particles when exposed to planktonic bacterial cultures and biofilms. The model system included four precursor steps in which the silver was exposed to varying pH conditions and incubation times. Such an *in vitro* digestion model will aid to a more accurate hazard assessment strategy of ingested NPs.

Conclusions and future research directions are presented in Section 6.

2. A LIFE CYCLE APPROACH FOR TWO PROTOTYPICAL HOME-USE CONSUMER PRODUCTS CONTAINING ENGINEERED NANOMATERIALS

2.1. Introduction

Engineered nanomaterials offer great advantages to the building industry with regard to sustainable development. It is well documented that the physical and chemical properties of nanometer sized matter offer specific benefits over the same material in bulk form [13, 15]. For example, in the building industry, NPs can increase resistance to ultraviolet damage, prevent wear and fouling, and improve the rheology, hardness, and strength of construction materials [17]. In many cases, individual engineered NPs are incorporated into larger composite products which provide the benefits of nanotechnology but with a generally regarded decreased risk of direct particle exposure [66, 67]. To date, a total of 250 products produced by over 100 companies incorporate nanocomposites into building or renovation plans with estimated revenues surpassing $1 billion [68]. Although nanocomposites have been hypothesized to substantially decrease the potential for direct exposure to NPs [66, 67], the potential for human and environmental risk throughout the product life cycle is uncertain. Only a few laboratory studies have been designed and performed to test this concept, though in many cases, a decrease in exposure through the inhalation route has been concluded [69].

The paint and lacquer industry, in particular, uses many tons of TiO_2 NPs as a whitening agent and to provide properties such as improved durability, water repellence, and scratch resistance [18]. The global use of TiO_2 for paint and surface applications

alone exceeds 2.5 million tons annually with the specific use of nanoscale TiO_2 is conservatively estimated around 30,000 tons [19, 20, 70]. As a result, human exposure to these engineered NPs is inevitable. The route and extent of particle exposure, however, is dependent upon the application and use of the nano-enabled product in real world scenarios [21].

The identification and characterization of engineered NPs in complex matrices is a prerequisite to fill data gaps in assessments of human and environmental safety as nano-enabled products are developed. Little is known about the effects of TiO_2 NPs incorporated into complex matrices such as paint and lacquer formulations. More importantly, changes in physiochemical characteristics and material toxicity during product end of life scenarios, i.e. potential release of NPs from the matrices, are unknown and need research emphasis. One way to gather information critical to the development of safe nanomaterials is employing a product life cycle approach [25-28] which integrates product development with manufacturing and consumer/occupational exposure. This approach provides an opportunity to elucidate the human and environmental safety of a technology by assessing toxicological impact throughout the product life cycle.

The product life cycle should include an evaluation of not only the production, distribution, formulation, and use of nano-enabled goods, but also an account of potential exposures to humans and the environment. Exposures in the form of precipitated particles from water waste or airborne particles from aerosolization

processes are examples of by-products from nano-enabled goods that could cause potential adverse health effects.

This section characterizes pristine bulk material and degraded NP-enabled products and investigates the toxicological response of human pulmonary cells to these materials. Three commercially available TiO_2 NPs were incorporated into paint and lacquer formulations and simulated wear-and-tear scenarios were performed on the nano-enabled products. Pristine and worn-and-town powders were then exposed to immortalized human lung epithelial cells (A549) to investigate the effect on cellular viability and ROS generation. This product life cycle approach provides a rich framework for assessing the benefits and risks of emerging nanotechnologies. The impact of this research will help enable sustainable opportunities of nanotechnology in the built environment.

2.2. Methods

2.2.1. NPs used in the study

Three commercially available TiO_2 NPs currently used for applications in industrial coatings were used in this study. These pristine NPs differed in surface treatment and were designated as TiO_2-1, a silica/alumina-treated rutile pigment, TiO_2-2, a zirconia/alumina-treated rutile pigment, and TiO_2-3, an aluminum hydroxide/silica-treated rutile pigment. Materials TiO_2-1 and TiO_2-2 were obtained from Tronox Limited with trade names CR-826 and CR-828, respectively. The third material, TiO_2-3, was acquired from Cristal Global with trade name Tiona 596. All TiO_2 NPs were multipurpose grade rutile pigments having excellent optical properties and high

durability. The properties of the three focal TiO_2 NPs used in this study are listed in Table 2.1.

Table 2.1. Material properties of the three pristine TiO_2 NPs used in the study.

Property	TiO_2-1	TiO_2-2	TiO_2-3
Applications	• Interior and exterior industrial coatings • Interior and exterior architectural coatings • Marine finishes coatings • Water and solvent-based industrial coatings • Powder coatings • General industrial coatings		
Surface treatment (as specified by supplier)	Dense silica/alumina-treated rutile pigment	Zirconia/alumina-treated rutile pigment	Aluminum hydroxide/silica treated rutile pigment
TiO_2 content (as specified by supplier)	93%	95%	94%
Durability (as specified by supplier)	Very high	High	-
Average particle size (as specified by supplier)	200 nm	190 nm	-
pH	8.0	8.0	8.0
Zeta potential (mV) (measured in-house)	21.2 ± 0.20	31.1 ± 0.72	19.2 ± 0.62

2.2.2. Nano-enabled products

To mimic real word applications, the three TiO_2 NPs were incorporated into paint and wood coatings. The laboratory-formulated paint and wood coatings were prepared as described below.

Paint on drywall. The paint formulation used included base paint (with and without TiO_2) mixed via commercial specifications[11]. EcoVAE Interior Quality Flat formulation was used as a reference for base paint without TiO_2 (Celanese Corp., Irving, TX). Per the specifications, water, latex, and thickener were mixed using an air mixer and Cowles blade for 30 minutes. While mixing, other additives i.e. defoamer, dispersant, surfactant, fillers, and pigment extenders (except TiO_2) were added to the mixture and well blended. Finally, 16 wt% pristine TiO_2 NPs were added to the base paint formulation. Base paint without TiO_2 served as a control.

In an effort to validate this laboratory-formulated paint, a commercial water-based interior flat paint sample was included in this study (Olympic, PPG Industries, Pittsburgh, PA). This commercial paint sample was mixed using the air mixer and Cowles blade described above to ensure a well-blended material with no settling.

As a final step, paint formulations were poured into cast as a 25 mil (mil is an industry specific term where 1 mil is equivalent to 0.0254 mm) wet film using a Gardco 8-path slot coater to achieve uniform paint thickness on the dry walls. This coated surface was then air-dried at room temperature for 2 days. An average paint thickness of 0.20 mm, equivalent to ~8 mils was observed.

Wood coatings. Wood coatings were prepared by the addition of 1 wt% of DPT (diphenyl (2,4,6-trimethylbenzoyl)phoshpine oxide) to a polyester based resin (polyester tetraacrylate, also known as acrylic ester). To this resin, 2 wt% TiO_2 was incorporated. Resin without TiO_2 served as a control. A clean dry wood surface was coated with polyester resin and laminated to a polyethylene terephthalate (PET) film. The wood

surface was then cured for 180 seconds at λ=365 nm. Once cured, the PET film could be easily stripped off leaving the final product coated and completely dry. A second coat was applied to ensure adequate coating thickness. The 16 wt% TiO_2 addition in paints and the 2 wt% TiO_2 addition in wood coatings were based on industrial specifications [71-73].

2.2.3. Wear-and-tear process

The nano-enabled paint on drywall and wood coatings were subjected to wear-and-tear scenarios to mimic real world end-of-life stages. The Taber test is one of the most commonly employed techniques for simulating the abrasive damage to surfaces[74, 75]. The surfaces of formulated TiO_2-enabled paint on drywall and TiO_2 in wood coatings were abraded by attaching a jumbo collet to a Taber Abraser 5900 Reciprocating machine (Testing Machines Inc., New Castle, Delaware). Ten abrasive cycles with a rotation speed of 60 cycles per minute and a normal force of 10 N were employed for each sample. Abrasion was caused by friction at the contact line between the sample surface and the jumbo collet. Powders from each sample, representative of an end-of-life scenario, were collected in vials.

The steps involved in the paint formulation and subsequent wear-and-tear process on the drywalls are depicted in Figure 2.1. The worn-and-torn paint powders were designated as base paint (i.e., no TiO_2), base paint plus TiO_2-1, base paint plus TiO_2-2, and base paint plus TiO_2-3.

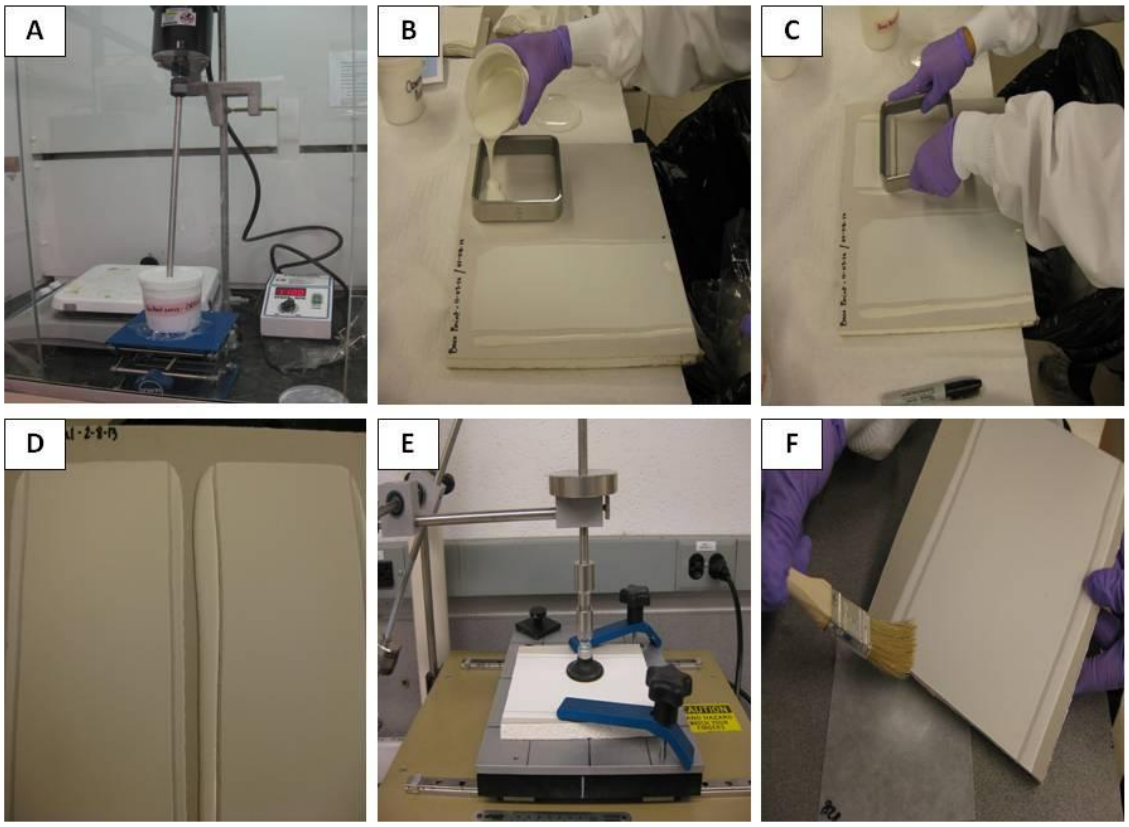

Figure 2.1. Paint formulation on dry wall. Steps involved in the paint formulations on the dry wall are depicted: (A) Prepare and mix base paint, (B) pour formulated paint into slot coater, (C) draw down the paint, (D) allow paint to dry, (E) simulate wear-and-tear scenario using taber abrasion apparatus and (F) collect powders for further analyses.

The steps involved in the wood coating and subsequent wear-and-tear processes are depicted in Figure 2.2. The worn-and-torn wood powders were designated as uncoated wood (i.e., no TiO_2), wood plus TiO_2-1, wood plus TiO_2-2 and wood plus TiO_2-3.

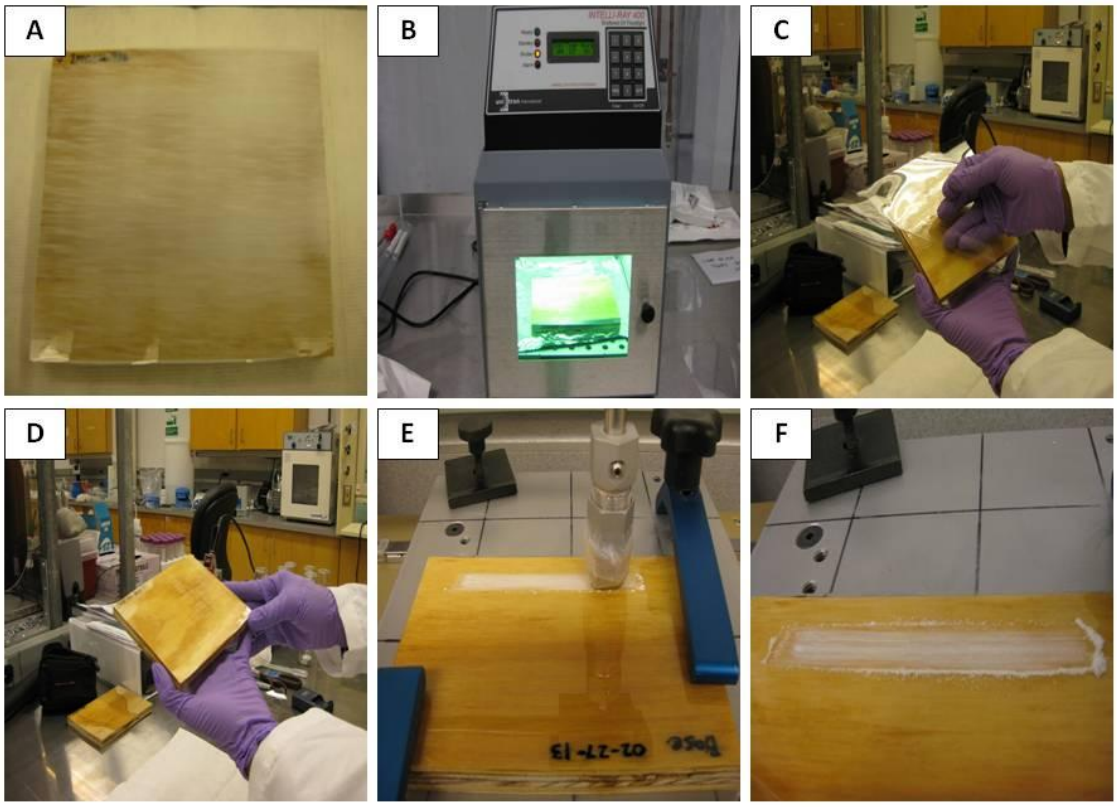

Figure 2.2. Wood coating process. Steps involved in the wood coating process are depicted: (A) Coat clean wood surface with polyester and cover with PET film, (B) UV-curation for 180 sec, (C) peel off the PET film, (D) final coated wood product, (E) simulate wear-and-tear scenario using taber abrasion apparatus and (F) collect powders for further analyses.

2.2.4. Material characterization

The following material characterization techniques were employed to analyze the pristine TiO_2 NPs (as described in Section 2.2.1) as well as the worn-and-torn nano-embedded paint and wood powders (as described in Section 2.2.3).

Transmission electron microscopy (TEM). Samples were suspended in ultra-pure water in preparation of TEM analysis. Grids were prepared by dropping 3 μL of each suspended sample on to a 200 mesh copper grid (Ted Pella, Inc., Redding, CA) and dried overnight. Transmission electron micrographs were imaged using Hitachi H-7000 electron microscope operated at an accelerating voltage of 100 kV. Images were recorded using Gatan CCD camera and 4pi Revolution® software.

Scanning electron microscopy (SEM). Samples for SEM analysis were deposited onto a carbon adhesive surface affixed to SEM stubs and coated with gold/palladium for 2 minutes using a Hummer® sputtering system (Anatech, Ltd., Battle Creek, MI). Scanning electron micrographs were obtained using a FEI Quanta 200 environmental scanning electron microscope. Images were recorded using high vacuum mode, typically 15kV, spot size 2.5, and a working distance of 10 mm. Elemental analysis was performed for each sample using the attached x-ray detector and Inca® x-sight software (Oxford Instruments X-ray Technology) was used to process the energy dispersive X-ray spectroscopy (EDX) spectra.

Fourier transform infrared spectroscopy (FTIR). Chemical compositions of samples were probed using a Thermo-Fischer Smart Orbit-Single Bounce ATR (Thermo Scientific, Madison, WI) using a Nicolet 6700 FTIR in the 400–4000 cm^{-1} range. Spectra

were recorded in transmission mode with a resolution of 4 cm^{-1}. Thirty-two scans were collected and averaged for each spectrum.

2.2.5. Toxicological responses

Cell cultures. Initial cytotoxicity was probed using immortalized human lung epithelial (A549) cells (ATCC, Manassas, VA). Cells were maintained in F-12K medium supplemented with 10% fetal bovine serum and 1% penicillin and streptomycin. Cells were cultured at 37 °C in a humidified atmosphere with 5% CO_2 and passaged every 3 days. Passage numbers 2–10 were used in the experiments.

Cell viability. Exposure to toxic agents can compromise cell membranes, thereby allowing cellular contents to leak out [12]. Cell viability was assessed using trypan blue, a diazo dye, which is only permeable to cells with compromised membranes. Thus, dead cells are stained blue while live cells are colorless. Percentage viability was measured via the Countess® Automated Cell Counter.

A549 cells were seeded with 1 x 10^4 cells/cm^2 in 24 well plates in complete growth medium and allowed to proliferate for 48 hours until 80% confluent. Cells were gently washed with phosphate buffered saline (HyClone, Logan, UT), followed by exposure to increasing concentrations (0, 0.1, 1, 10, 100, and 1000 ppm) of the three pristine TiO_2 NPs in complete medium and incubated for 24 hours. Cell viability was assessed using trypan blue exclusion assay via the Countess® Automated Cell Counter (Invitrogen) as per the manufacturer's instructions. The purpose of performing a dose-response cytotoxicity study using the pristine TiO_2 samples was to determine a relevant concentration to subsequently perform reactive oxygen species measurements.

Intracellular ROS measurement. The DCFH-DA (2′,7′-dichlorofluorescein diacetate) assay was used to measure the levels of intracellular ROS. This is a cell-based assay for measuring hydroxyl, peroxyl, or other ROS activity within a cell. DCFH-DA is cell-permeable fluorogenic probe which is diffused into cells and deacetylated by cellular esterases to non-fluorescent 2', 7'-dichlorodihydrofluorescin (DCFH). In the presence of ROS, DCFH is rapidly oxidized to highly fluorescent 2', 7'-dichlorodihydrofluorescein (DCF). Consequently, the fluorescence intensity is directly proportional to the ROS levels within the cell cytosol and can be measured using a fluorescence plate reader.

DCFH-DA (Cell Biolabs, Inc.) was used to measure the levels of ROS after exposure to TiO_2 in pristine and incorporated form. A549 cells were seeded with 1 x 10^4 cell/cm^2 in a 96 well plate in complete growth medium. Upon reaching 80% confluency, cells were gently washed with PBS followed by treatment with 100 μM DCFH-DA and incubated at 37°C for 30 min. Cells were then exposed to pristine TiO_2 NPs, worn-and-torn paint samples, or worn-and-torn wood samples and incubated for 24 hours. Hydrogen peroxide (1000 μM) was used as the positive control. Unexposed cells in complete medium served as a negative control. After the 24 hour incubation, fluorescence was measured at 480 and 530 nm (excitation and emission, respectively) using a fluorescence plate reader (Synergy Mx Multi-Mode Microplate Reader, BioTek Instruments, Inc., Winooski, VT). The study was designed for an n=8 replicates per treatment and each experiment were performed twice.

2.2.6. Statistical analysis

Each value represents the mean of at least three separate analyses plus or minus the standard error of the mean (SEM). Multiple comparisons were performed using analysis of variance (ANOVA) followed by post-hoc testing if $p<0.05$. Differences between treatment groups were analyzed via the Turkey-Kramer Multiple Comparisons test or the Kruskal Wallis test comparing all pairs of columns to untreated cells. Probability values of $p < 0.05$ were considered to be statistically significant. Statistical analyses were performed using INSTAT software v 3.0 (GraphPad, Inc., San Diego, CA).

2.3. Results, discussion and data interpretation

2.3.1. Life cycle approach to TiO_2-embedded products

TiO_2 pigments exists in two morphological crystalline forms, rutile and anatase, with each phase possessing a unique crystal structure [2, 76]. The structures can be described in terms of (TiO_2^{6-}) octahedron: octahedrons connected by their vertices form anatase while octahedrons connected at their edges gives rise to rutile. These differences in crystal structures cause differences in the mass densities and electronic band structure, and consequently affect their photoactivity [2]. In general, rutile is claimed to be less photoactive than anatase due to surface defects and thus commonly used as a white pigment in the coating industry [76, 77].

To further improve pigment dispersion, the surface of TiO_2 is treated with alumina, silica, zirconia, aluminum phosphates of other metals or often a combination of these [78]. Surface modifications with inorganic hydrates decreases the photoactivity of

titania pigments by increasing electron-hole recombination sites [79]. Hence, the surface treatment techniques dictate the photoactivity of titania pigments and the effectiveness of the coating determines the degree of photoactivity [80]. From a toxicological point of view, surface modifications physically inhibit the diffusion of oxygen and thereby reduce the generation of free radicals. Other advantages of surface treatments include improved wetting ability in different media (water, solvent, and polymer), and improved compatibility with binder and color stability [81].

The unique physiochemical properties associated with individual nanomaterials are expected to result in different human and environmental impacts between various nanomaterials. Additionally, particles from different stages throughout the product-life cycle of the same nanomaterial are expected to have differential risk associations. To investigate the risk of various form factors a product life-cycle approach can be implemented to assess pristine, formulated, and worn-and-torn NPs.

The life cycle approach for engineered nanomaterials incorporated into paints and coatings has four main stages in which exposure may occur. These four main stages are: (1) raw material production, (2) product manufacturing, (3) consumer use scenarios, and (4) product end-of-life disposal. Environmental release or hazards to humans are the two main exposure risks. The release of pristine particles or formulated composites as industrial air emissions, industrial wastewater processes, or trash produced by consumers are major sources of environmental concern. With human exposure, release from worn-and-torn formulated composites, as in the case of weathered products or during "do-it-yourself" home projects, into aerosolized particulate matter in the air or solid

particulates that deposit on surfaces are major sources of concern. Further identification of potential hazards from such sources requires toxicity testing using appropriate model test systems depending on the type of exposure.

The three pristine TiO_2 NPs chosen for this study are currently used in the manufacturing of paint products and were designated TiO_2-1, TiO_2-2, and TiO_2-3. These pristine particles are then incorporated into paint and lacquer formulations, applied to drywall and wood, respectively, and subjected to simulated wear-and-tear scenarios. This wear-and-tear simulation, designed to mimic a consumer sanding a surface, results in powders representing end-of-life-cycle particles (Stage 4), which are analyzed and compared to the pristine particles (Stage 1). Here we compare the physiochemical properties of the pristine and end-of-life cycle properties.

2.3.2. Material characterization

TEM and SEM reveal critical information about the particle size, shape, aggregation states and morphology. EDX confirms the elemental composition of a given sample. Figure 2.3 shows the transmission and scanning electron micrographs of the three pristine TiO_2 samples. These micrographs confirm primary particle size to be 200 nm for all three TiO_2 NP types.

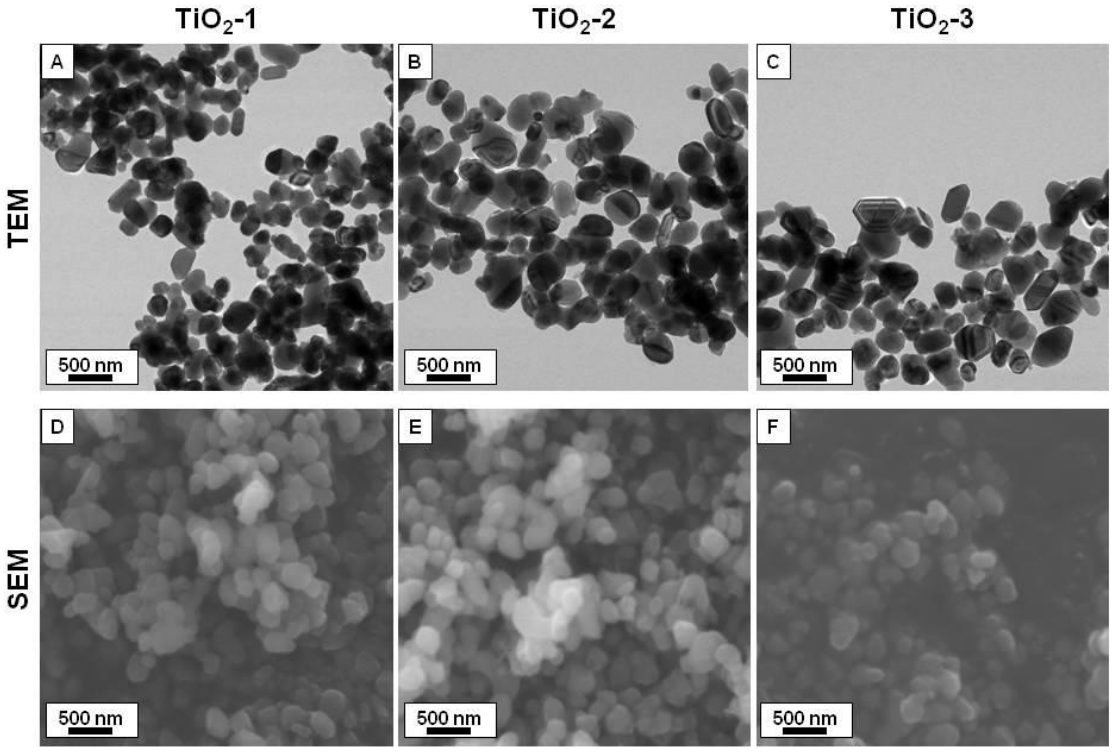

Figure 2.3. Transmission electron micrographs (top) and scanning electron micrographs (bottom) of the pristine TiO_2 NPs. Three different TiO_2 NPs were used in the study, and designated as TiO_2-1, TiO_2-2 and TiO_2-3. (A) TEM of TiO_2-1, (B) TEM of TiO_2-2, (C) TEM of TiO_2-3, (D) SEM of TiO_2-1, (E) SEM of TiO_2-2 and (F) SEM of TiO_2-3.

Figure 2.4 shows the transmission electron micrographs of the worn-and-torn paint powders. Micrographs of the base paint formulations mixed with TiO_2 NPs (i.e., base paint plus TiO_2) clearly indicate TiO_2 NPs embedded in the matrix. The micrographs also show the reference material (i.e., base paint without TiO_2) is devoid of TiO_2 particles. Micrographs suggest aggregate particle size to be approximately 600 nm for all three TiO_2 nano-enabled paint products.

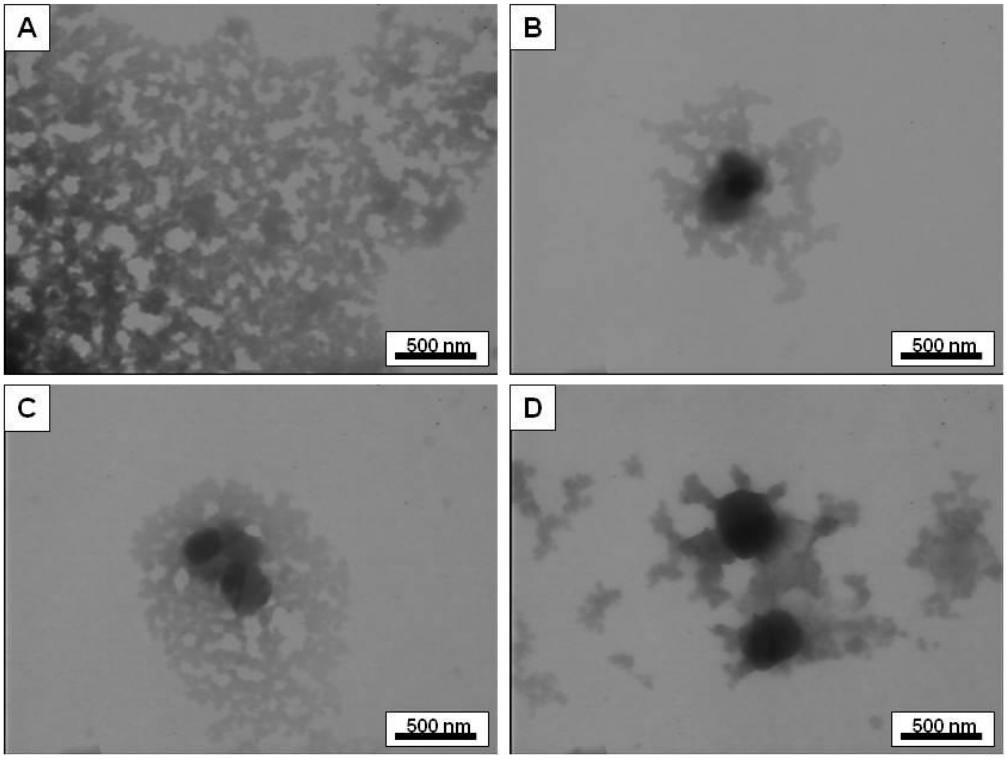

Figure 2.4. TEM of worn-and-torn paint surfaces. Transmission electron micrographs of (A) worn-and-torn reference material, (B) base paint plus TiO_2-1, (C) base paint plus TiO_2-2 and (D) base paint plus TiO_2-3.

Scanning electron micrographs and elemental analysis further confirm the presence of TiO_2 in the worn-and-torn paint surfaces (Figure 2.5). The micrograph of the reference sample does not contain any TiO_2. Additionally in Figure 2.5, the EDX spectra confirm the absence of TiO_2 in the reference material and the presence of TiO_2 in other samples with characteristic peaks of Ti (0.45, 4.5 and 4.9 keV). The background material also shows representative peaks for carbon and oxygen. The strong Si peak in samples can be attributed to the paint ingredient Diafil 525, which contains amorphous Si. The calcium (Ca) peak is present in native drywall in the form of calcium carbonate.

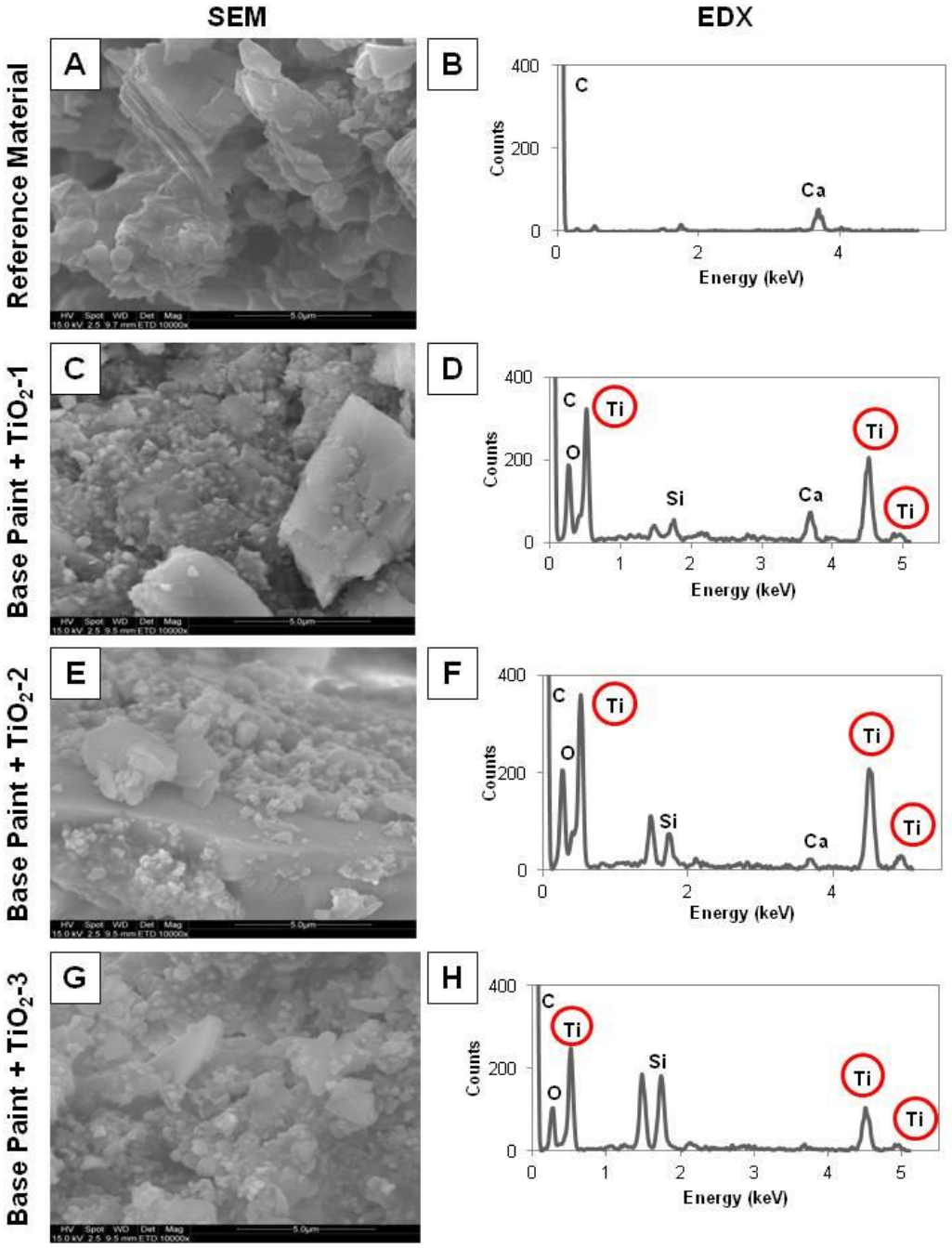

Figure 2.5. SEM and EDX spectra of worn-and-torn paint surfaces. Scanning electron micrographs and corresponding elemental analyses of worn-and-torn paint surfaces. (A) SEM of worn-and-torn reference material, (B) EDX of worn-and-torn reference material, (C) SEM of base paint plus TiO_2-1, (D) EDX of base paint plus TiO_2-1, (E) SEM of base paint plus TiO_2-2, (F) EDX of base paint plus TiO_2-2, (G) SEM of base paint plus TiO_2-3 and (H) EDX of base paint plus TiO_2-3.

Figure 2.6 shows the transmission electron micrographs of the worn-and-torn wood samples. As shown in the micrographs, the reference sample (i.e., uncoated wood) does not have any characteristic TiO_2 particles while all the other samples (wood coating with TiO_2) show TiO_2 NPs embedded in the complex wood matrix. Micrographs suggest that a bimodal particle size population exists in each sample. Aggregate particle sizes are approximately 200 nm and approximately 600 nm for all three TiO_2 nano-enabled wood samples.

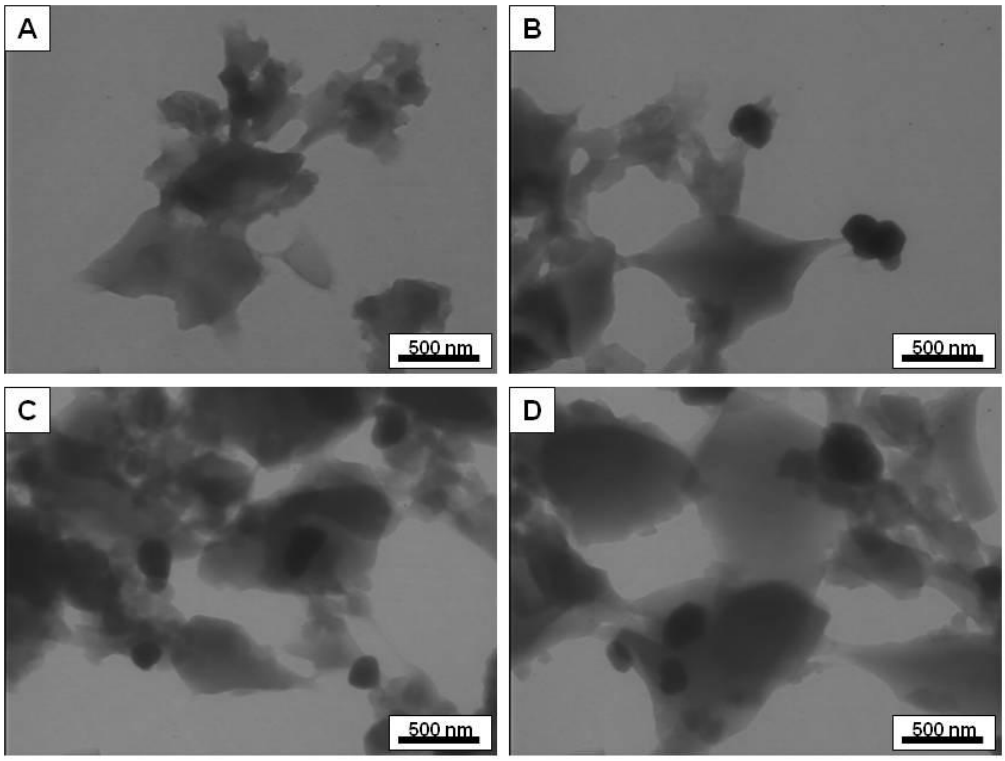

Figure 2.6. TEM of worn-and-torn wood surfaces. Transmission electron micrographs of (A) worn-and-torn reference material, (B) wood plus TiO_2-1, (C) wood plus TiO_2-2 and (D) wood plus TiO_2-3.

Figure 2.7 shows the scanning electron micrographs and elemental analysis of the worn-and-torn wood surfaces. The reference material does not show any characteristic Ti peak in the EDX spectra and no TiO_2 was seen in the micrographs. On the other hand, samples with incorporated NPs clearly indicate the presence of TiO_2 NPs in both the EDX spectra as well as the SEM images. Because only 2 wt% TiO_2 was included in the resin matrix, the EDX peaks are not as strong as the paint samples (16 wt%), but the micrographs confirm the presence of the NPs.

Taken together, these microscopy and elemental analyses techniques confirm the presence of TiO_2 embedded in the complex paint formulations on the drywall and wood coatings after the wear-and-tear process. In both microscopy techniques, the individual primary particles are clearly distinguishable, thus providing motivation to understand the potential impacts of exposure to nano-enabled products. NPs incorporated into composites can be abraded and dislodged from the parent material. These individual NPs, while not identical to the engineered particles added into the product during the enabling phase, are still reactive on their surface and free to react with surrounding matrices independent of the composite.

In addition to electron microscopy, pristine and worn-and-torn samples were also analyzed using FTIR. The fundamental vibrations of TiO_2 appear in the in the low energy region of the infrared spectra. A peak in the 500-520 cm^{-1} range can be attributed to the presence of TiO_2 in samples [82-85]. Additionally, bands in the low energy region between 340 cm^{-1} and 520 cm^{-1} can be assigned to the stretching vibrations of the Ti-O-Ti bonds [82, 86, 87].

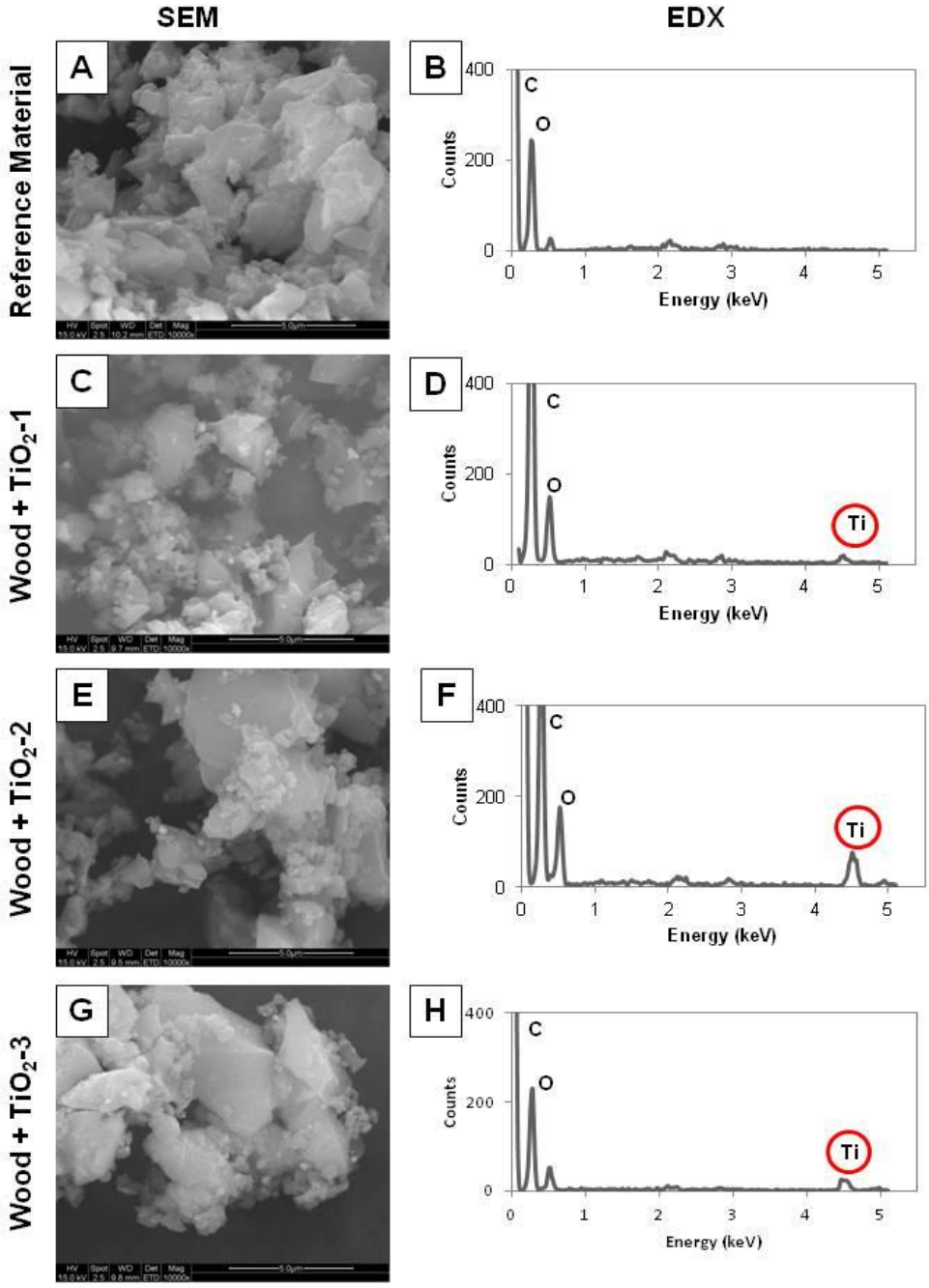

Figure 2.7. SEM and EDX spectra of worn-and-torn wood surfaces. Scanning electron micrographs and corresponding elemental analyses of worn-and-torn wood surfaces. (A) SEM of worn-and-torn reference material, (B) EDX of worn-and-torn reference material, (C) SEM of wood plus TiO_2-1, (D) EDX of wood plus TiO_2-1, (E) SEM of wood plus TiO_2-2, (F) EDX of wood plus TiO_2-2, (G) SEM of wood plus TiO_2-3 and (H) EDX of wood plus TiO_2-3.

Figures 2.8A, 2.8B and 2.8C show the FTIR spectra of the pristine TiO_2 NPs, the worn-and-torn paint samples and the worn-and-torn wood samples, respectively. On analyzing the spectral peak positions, the characteristic structure of TiO_2 in the 340-520 cm^{-1} range is observed in all three pristine TiO_2 samples (Figure 2.8A).

Figure 2.8B shows the FTIR spectra of the worn-and-torn paint samples. The FTIR spectrum of the base paint with no TiO_2 is also shown. As seen from the spectra, the characteristic structure of TiO_2 in the 340-520 cm^{-1} range is present in all three worn-and-torn paint samples but absent in the base paint spectrum. In order to further quantify this TiO_2 peak, the worn-and-torn paint samples were corrected for background using the base paint sample as the reference spectra. Figure 2.9 overlays the FTIR spectra of the three pristine TiO_2 NPs to the corresponding worn-and-torn paint plus TiO_2 samples. The structure at approximately 500 cm^{-1} is clearly visible in all three worn-and-torn paint samples and matches well with the pristine sample spectra. Therefore, in addition to microscopy techniques such as TEM and SEM, and elemental analysis via SEM-EDX, these FTIR spectra further confirm the presence of TiO_2 in the complex worn-and-torn paint matrix. At 16 wt% of TiO_2 included in the paint formulations, FTIR is able to detect the presence of the characteristic TiO_2 peaks in all the worn-and-torn paint samples.

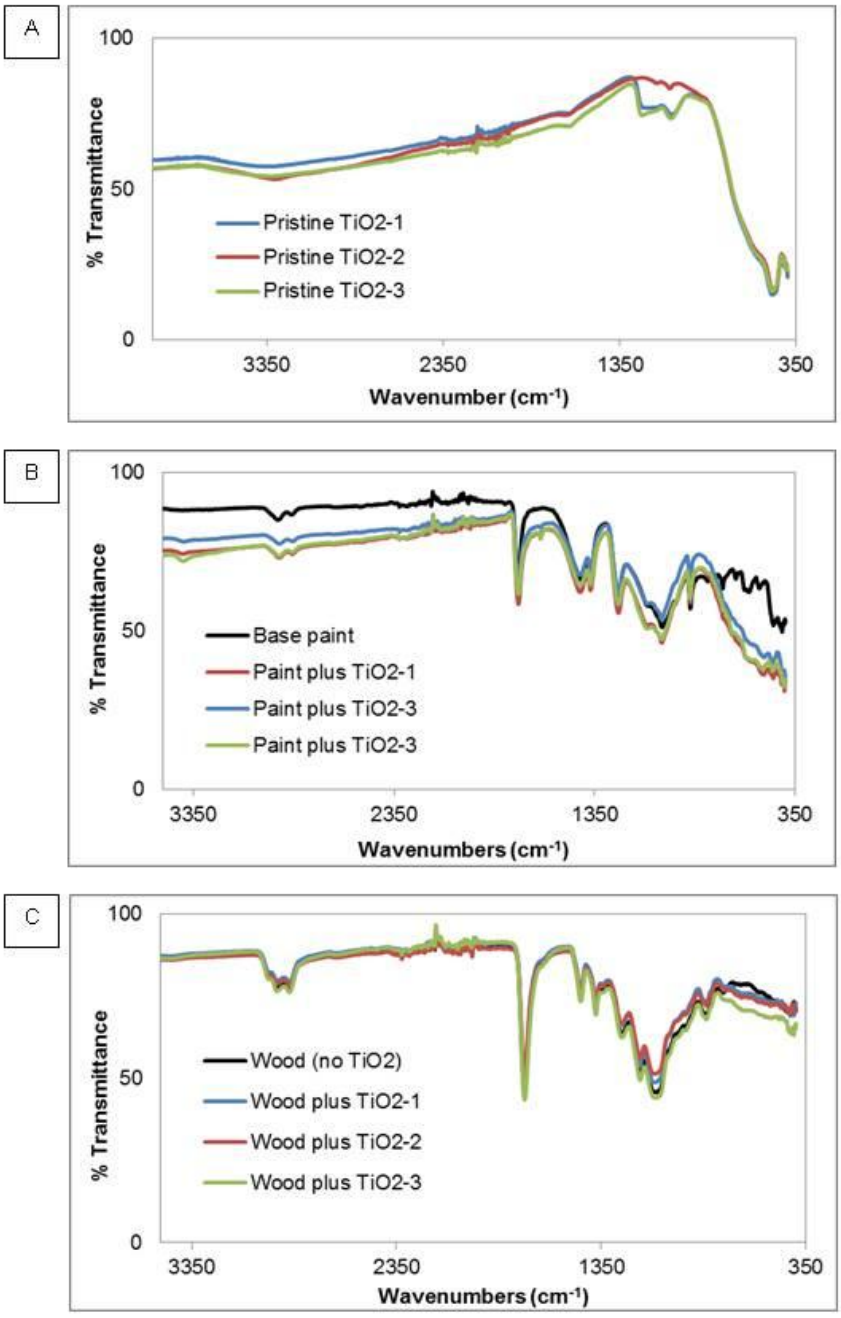

Figure 2.8. FTIR spectra. (A) Pristine TiO_2, (B) worn-and-torn paint surfaces and (C) worn-and-torn wood surfaces.

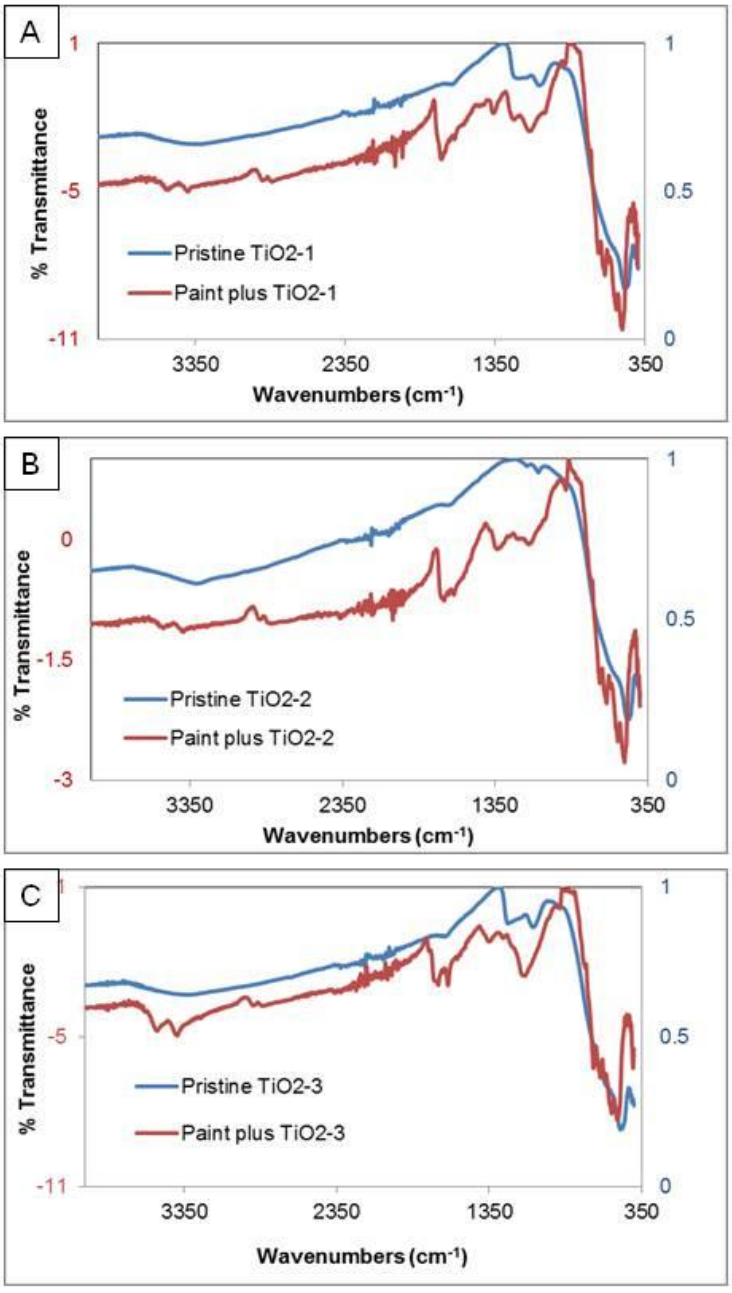

Figure 2.9. FTIR spectra comparing pristine TiO_2 to worn-and-torn paint surfaces. The blue spectra represent the pristine sample while the red spectra represent the worn-and-torn paint samples. The worn-and-torn paint samples were corrected for background using the paint without TiO_2 sample as the reference spectra. (A) Pristine TiO_2-1 and paint plus TiO_2-1, (B) pristine TiO_2-2 and paint plus TiO_2-2 and (C) pristine TiO_2-3 and paint plus TiO_2-3.

Figure 2.8C shows the FTIR spectra of the worn-and-torn wood samples. The FTIR spectrum of the wood with no TiO_2 is also shown. From these spectra it is evident that the characteristic structure of Ti at 520 cm^{-1} is not prominent in all three worn-and-torn wood samples. Similar to the paint samples, the worn-and-torn wood samples were also corrected for background using the wood with no TiO_2 sample as the reference spectra to quantify the presence of TiO_2. Figure 2.10 overlays the FTIR spectra of the three pristine TiO_2 NPs to the corresponding worn-and-torn wood plus TiO_2 samples. After correcting for background, the characteristic peak of Ti at 520 cm^{-1} is still not prominent in any of the worn-and-torn wood samples. Because the samples contain only 2 wt% TiO_2 in the wood resin matrix formulation, the signal appears to be below the detection limit of the FTIR system used in this work. As a result, the signal from the TiO_2 in the worn-and-torn wood matrix is not visible by FTIR but is detectable by other material characterization techniques such as TEM, SEM and SEM-EDX which confirmed the presence of TiO_2 in the complex worn-and-torn wood matrix.

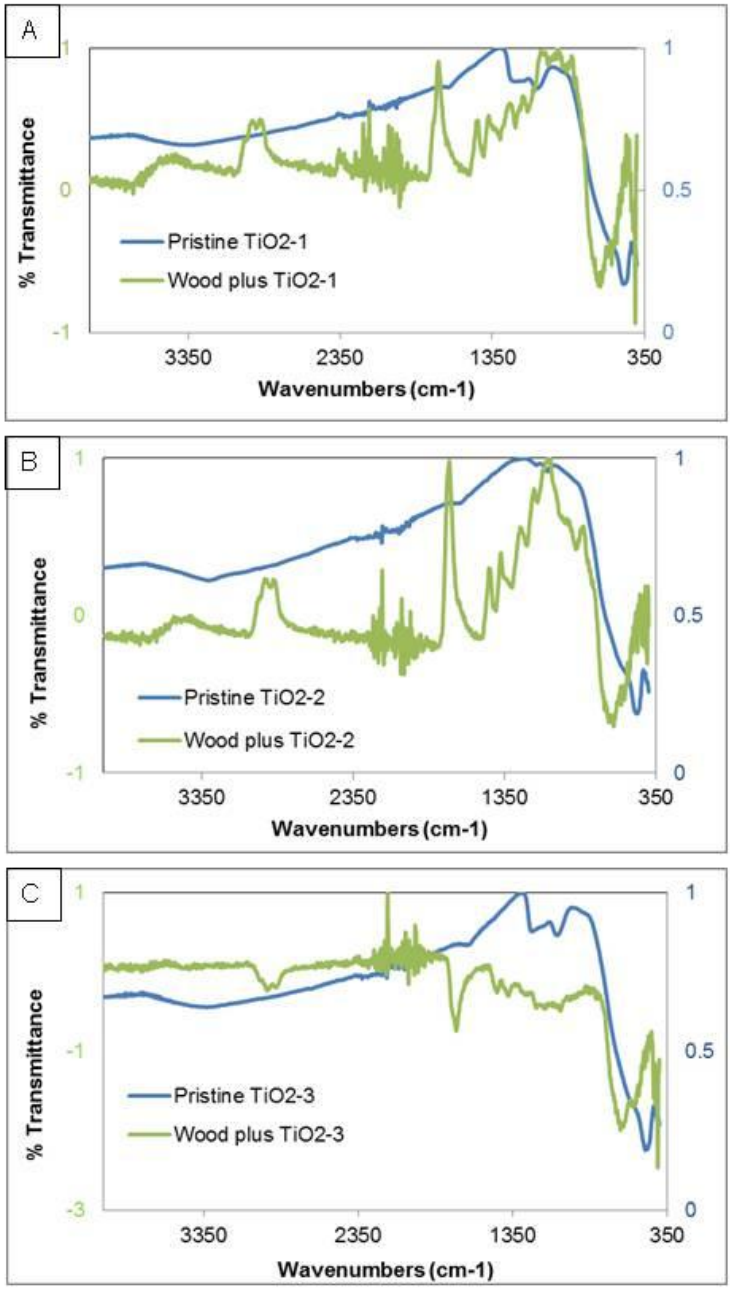

Figure 2.10. FTIR spectra comparing pristine TiO_2 to worn-and-torn wood surfaces. The blue spectra represent the pristine sample while the green spectra represent the worn-and-torn wood samples. The worn-and-torn wood samples were corrected for background using the wood without TiO_2 sample as the reference spectra. (A) Pristine TiO_2-1 and wood plus TiO_2-1, (B) pristine TiO_2-2 and wood plus TiO_2-2 and (C) pristine TiO_2-3 and wood plus TiO_2-3.

2.3.3. Toxicological responses

As with any new technology, the identification of potential health risks is a prerequisite for a proper assessment of the usefulness and safety of the nanomaterials and new products that may be developed. Studies suggest some nanomaterials can affect biological behaviors at the cellular (e.g., viability) and sub cellular (e.g., ROS generation) levels. Human and environmental health risks can only be determined through assessment of the hazards posed and the potential for exposure to the nanomaterials in various life-cycle stages. The most likely route of occupational exposure to nanomaterials used in consumer products is inhalation [11, 88]. Additionally, as the wear-and-tear simulation of this study produced air-borne powders, inhalation is the most likely route of consumer exposure at the end-of-life cycle stage. Therefore, a model lung system consisting of A549 cells was chosen for use in this study.

A549 cells were exposed for 24 hours to increasing concentrations (0, 0.1, 1, 10, 100, and 1000 ppm) of all three pristine TiO_2 NPs. Based on the cellular response to these low, medium, and high ranges of doses, a "medium dose" was chosen as the primary dosing concentration for subsequent toxicological endpoint evaluation. The results of the trypan blue exclusion assay are summarized in Figure 2.11. A549 cells exhibit a fairly monotonic dose-response relationship (i.e., cell viability decreases with increase in dose) upon exposures to all three NP types. Cellular viability is significantly reduced ($p<0.01$) as compared to untreated cells at the highest dose of 1000 ppm for all three TiO_2 NP types. Since cellular viability was unaltered at the lower doses of 0.1, 1

and 10 ppm, and significantly altered at the highest dose of 1000 ppm, the 100 ppm dose was selected as the primary dosing concentration. Thus, for the subsequent toxicity endpoint measurement, the A549 cells were exposed to a dosing concentration of 100 ppm as this dose showed decreased viability without complete cell death.

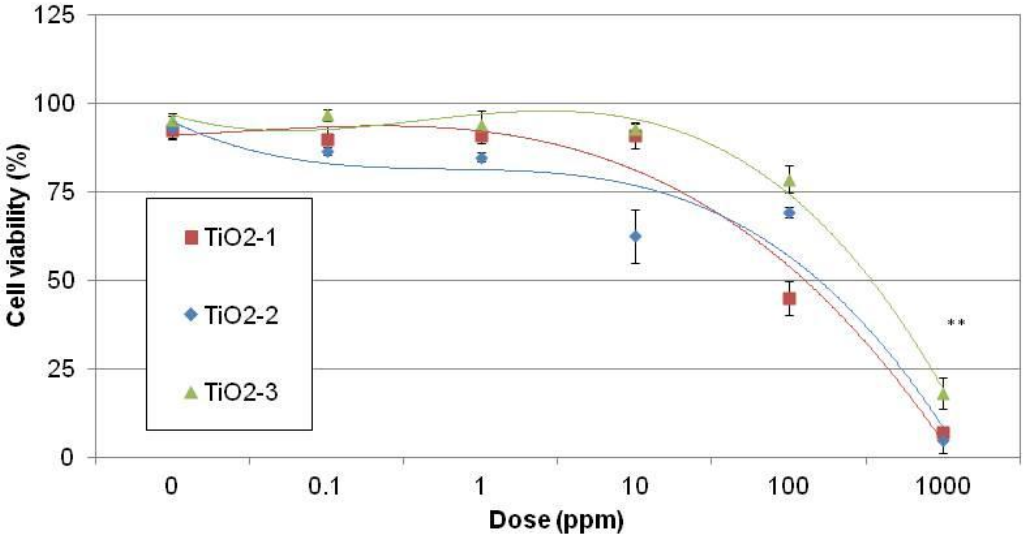

Figure 2.11. Toxicological response. Cell viability as measured using trypan blue exclusion assay. A549 cells were incubated with increasing concentrations of the three pristine TiO_2 NPs for 24 hours. Data were normalized to the control values and are represented as the mean ± SEM (, P<0.01).**

A central hypothesis in the field of nanotoxicology is that NPs are able to induce cellular dysfunction as a result of oxidative stress. The presence of excessive ROS can cause cellular oxidative stress, which in turn leads to DNA damage and lipid degradation. Recent evidence indicates that the possible mechanism of TiO_2 NP-induced toxicity involves DNA damage via oxidative stress [89]. Thus, ROS production of TiO_2 NPs in their pristine and end-of-life stages was tested *in vitro.*

Cellular generation of ROS was measured in A549 cells after a 24 hour exposure to pristine TiO_2, worn-and-torn paint samples and worn-and-torn wood samples. Data were normalized to the appropriate control values and these results are summarized in Figure 2.12. Statistically significant increase in oxidant production as measured via increased DCF fluorescence was observed with all three pristine TiO_2 NPs (Figure 2.12A). The ROS generation in the TiO_2-1, TiO_2-2 and TiO_2-3 samples was 1.72, 1.96 and 1.65 fold greater than the unexposed control, respectively. This differential effect of the three pristine particles supports the idea that surface treatment is an important factor in toxicity of nanomaterials.

The results of the ROS production from the worn-and-torn paint and wood samples are shown in Figures 2.12B and 2.12C, respectively. Only two out of the three worn-and-torn paint samples containing TiO_2 (i.e., base paint plus TiO_2-2 and base paint plus TiO_2-3) exhibited significant increase in intracellular oxidants compared to the control (Figure 2.12B). This may be due to differential adhesion, chemical attraction, or wetting of the paint matrix to the TiO_2 NP surface. The water based paint emulsion wets particles differently based on surface chemistries, thus the different particle types may reside in different phases of the emulsion. When the paint dries, one particle type may be "coated" with organic phases and thus not cause ROS generation while other particles may have simply dried as a mixture and still have active sites. In contrast, the worn-and-torn wood samples containing TiO_2 did not cause any significant ROS generation in comparison to the control; however there was a significant difference among the three NP types (Figure 2.12C).

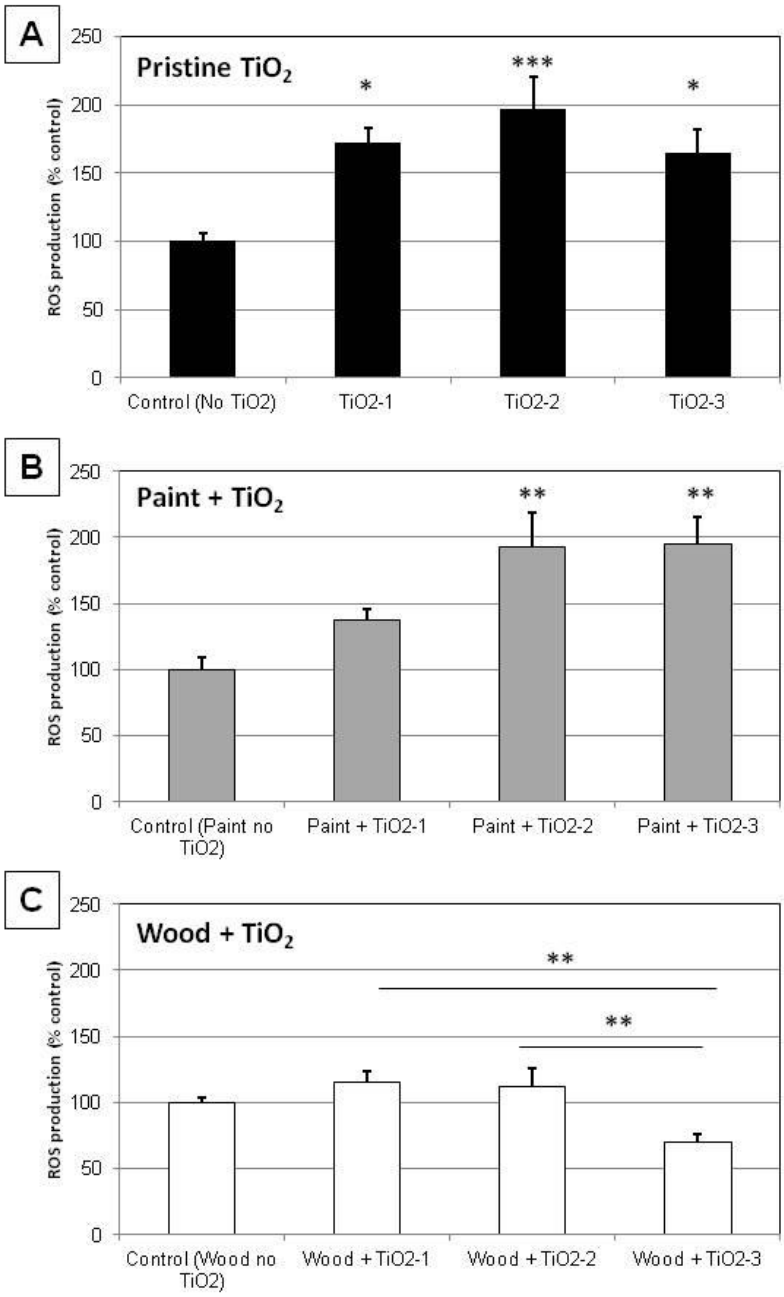

Figure 2.12. Intracellular ROS generation as measured using DCFH-DA. Cells were exposed to 100ppm of (A) pristine TiO_2, (B) worn-and-torn paint samples and (C) worn-and-torn wood samples, and incubated for 24 hours. Data were normalized to the control values and are represented as the mean ± SEM (*, P<0.05; **, P<0.01; ***, P<0.001).

2.3.4. Commercial paint

An off-the-shelf commercial paint was purchased and used in this study. This product was a water-based interior flat paint and served as a comparison to our formulated nano-enabled paints. Paint-on-drywall samples were made, allowed to cure, and underwent the wear-and-tear simulation in the same fashion as the laboratory-formulated versions. The transmission electron micrograph, scanning electron micrograph and elemental analysis confirm the presence of TiO_2 in the worn-and-torn commercial paint particles (Figure 2.13).

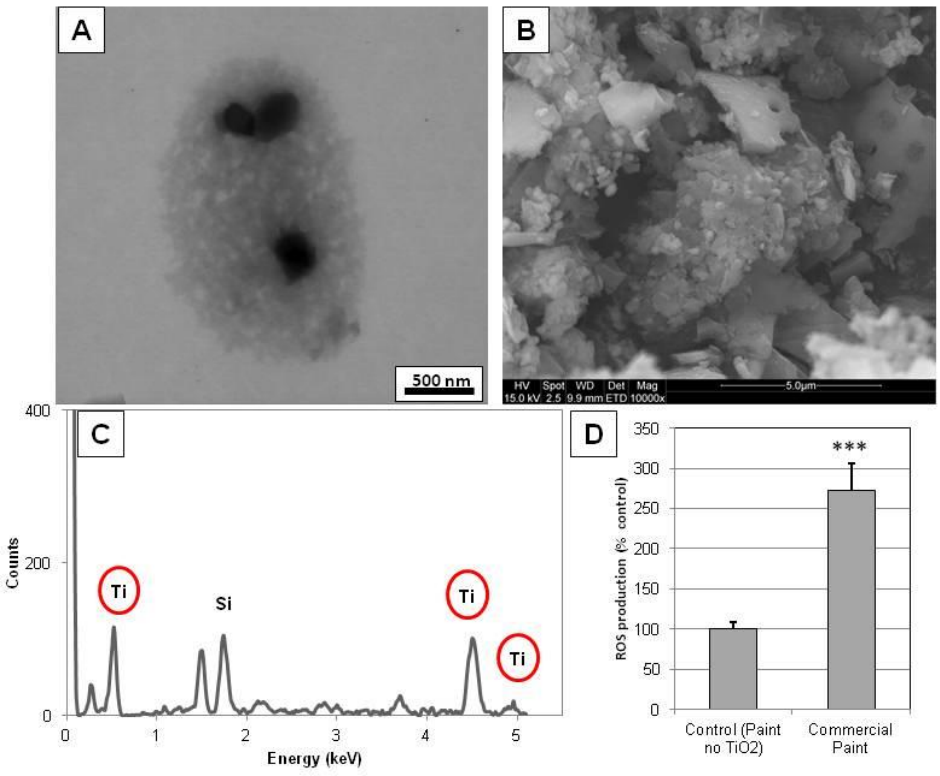

Figure 2.13. Worn-and-torn commercial paint. Material characterization and ROS production of worn-and-torn commercial paint sample. (A) TEM, (B) SEM, (C) SEM-EDX spectra and (D) ROS generation.

The TiO_2 NPs were also of a similar particle size as compared to the nano-enabled paint formulated products in Figure 2.4 and Figure 2.5. Furthermore, the ROS generation in A549 cells upon exposure to this commercial paint sample exhibited a statistically significant intracellular oxidant increase as compared to the control cells. These results indicate that our formulated paint products are representative of typical consumer products.

2.4. Summary

In summary, electron microscopy and elemental analysis as material characterization tools were able to detect the NPs in the worn-and-torn matrices. FTIR, on the other hand, proved to be a useful tool for the nano-enabled paint samples, but the nano-enabled wood samples warrant further investigation. These results validate the usefulness of TEM, SEM and EDX as a predictive tool for analyzing worn-and-torn nano-enabled products. FTIR as a material characterization technique, however, is only valid when relatively high concentrations of the NPs are incorporated into the products. Furthermore, *in vitro* toxicological assessments of both of pristine and worn-and-torn powders provide a more realistic platform for data interpretation and the identification of risk triggers. Thus, the application of a life cycle approach will help provide critical information to evaluate potential health and environmental risks and benefits of a nano-scale technology.

3. SYNTHESIS AND CHARACTERIZATION OF A NOVEL AGNP-PESTICIDE CONJUGATE*

3.1. Introduction

Every day, people and animals contract debilitating and life threatening diseases due to bites from infected flies, ticks, and mosquitoes. Not only do diseases such as malaria, West Nile virus, and Dengue Fever cause physical suffering but they also result in severe economic losses. Additionally, animals become reservoirs for arthropod borne diseases which increase the livestock morbidity and mortality and decreases reproductive capacity. This leads to a perpetual cycle of infectivity and loss.

When it comes to arthropod vector control, a conceptual paradigm shift is urgently needed. Strategies are being developed which aim to control vector populations by killing the larval stages. Biopesticides such as the Cry and Cyt toxins produced by the bacterium Bacillus thuringiensis (Bt) and insect growth regulators (IGRs) such as methoprene and novaluron are effective larvacides. Bt toxins have been incorporated into transgenic crops to combat agricultural insect pests. However, both Bt toxins and IGRs currently have limited use as sprays since they do not kill the adult stage and widespread coverage of breeding areas in remote locations is logistically challenging [90, 91]. Current chemical vector control strategies are limited to the same four classes of synthetic insecticides (organochlorine, organophosphate, pyrethroid, and carbamate)

---

* Reprinted with permission from Sooresh, A., et al., *Surface Functionalization of Silver Nanoparticles: Novel Applications for Insect Vector Control.* ACS Applied Materials and Interfaces, 2011. **3**(10): p. 3779-3787. Copyright 2011 American Chemical Society.

that have been used for over 30 years [92]. In this period, no new chemicals or classes of insecticides have been successfully incorporated into vector control programs against adult mosquitoes. One major problem with using traditional insecticides for vector control is that, over time, the insects develop resistance. Because insecticides either inhibit acetylcholinesterase (organophosphates and carbamates) or modulate the voltage gated sodium channels (pyrethroids and DDT), the development of resistance to one molecular target means many insecticides are rendered ineffective.

The research presented here is a first of its kind testing the efficacy of a novel nanoconjugate in a miniature biological model system. This biological model is the mosquito, an insect with an open circulatory system and a hydrophobic, porous external surface. This waxy cuticular surface has orifices ranging 0.5 to 2 μm, much larger than the nanometer size scale. The model nanoconjugate, termed pesticide encapsulated nanosilver (PENS), is 20 nm in diameter. It is made of deltamethrin molecules tethered to the surface of nanosilver particles and designed to be a new tool to fight disease carrying insect vectors.

For many different NP-types their high surface area to volume ratio results in high surface reactivity [40-44]. AgNPs offer the possibility of altering their surfaces in order to introduce specific functionalities for environmental applications [29, 45-47]. In addition, because silver is an electron dense metal, the PENS nanoconjugate can be traced in vectors, in the environment, and in animals. Lastly, by employing a metal NP as the core of the conjugate, the risk of inactivating the primary function of the pesticide (e.g. deltamethrin) by forming covalent bonds is eliminated.

In this section, a novel synthetic scheme to produce a NP-pesticide core-shell nanoconjugate to be used as an active agent against insect vectors, such as mosquitoes is presented. Lab synthesized 15 nm stable AgNPs were surface functionalized with deltamethrin as the capping agent resulting in a stable colloidal suspension. The physiochemical properties of both the pristine nanosilver particles and the PENS conjugate were characterized. These properties include size, size distribution, chemical composition, agglomeration states and stability of particles. Two mosquito bioassays were also conducted to quantify the uptake of PENS via silver metal detection and to assess the mortality of mosquitoes. The act of tethering a synthetic organic molecule such as deltamethrin to a nanosilver core allows for effective tracking of organics in complex biological matrices such as mosquitoes. This is a paradigm-shifting technology and offers new possibilities for vector and pathogen control.

3.2. Materials and methods

3.2.1. Synthesis of AgNPs and PENS

AgNPs were synthesized by reducing silver nitrate salt solution ($AgNO_3$, 1×10^{-3} M) with 1% (w/w) sodium citrate ($Na_3C_6H_5O_7$). In a typical experiment, the $AgNO_3$ solution was heated to boiling with vigorous stirring; $Na_3C_6H_5O_7$ was mixed with a 30 μM tannic acid solution and heated separately [38]. The citrate-tannic acid solution was added drop-wise to the silver salt solution. The color of the mixture slowly turned from colorless to yellow indicating the reduction of Ag^+ ions [34]. The solutions were removed from the heating mantle and allowed to cool.

Conjugation of the nanosilver core particle with deltamethrin. Deltamethrin ((S)a-cyano3-phenoxybenzyl-(1R)-cis-3-(2,2-dibromovinyl)-2,2-dimethylcyclopropane carboxylate), 90 ppm (180 μM)) was then tethered to the surface of the resultant nanosilver particle suspension via a heating gradient and vigorous stirring. The color of the mixture slowly turned from yellow to orange, indicative of the surface functionalization. The suspension was monitored at 420 nm using Ultraviolet Visible spectroscopy for absorbance peaks. The resultant aqueous suspension is the pesticide encapsulated nanosilver particle, termed PENS. Deltamethrin is a synthetic pyrethroid pesticide and a nonionic surfactant that serves as a colloidal stabilizer during synthesis.

3.2.2. Characterization of AgNPs and PENS

The size, morphology, crystallinity, absorbance, and zeta potential of the pristine nanosilver particles and the pesticide encapsulated nanosilver particles were measured.

Transmission electron microscopy and energy dispersive X-ray spectroscopy. Electron microscopy grids were glow-discharged using PELCO easiGlow (Ted Pella, Inc., Redding, CA) to make the grid surface hydrophilic. One micro liter of the nanosilver particle or PENS suspension was deposited onto a 400 mesh carbon grid. Each grid was analyzed on a JEOL 2010 transmission electron microscope at an accelerating voltage of 200 kV. These grid samples were also probed for elemental analyses using energy dispersive X-ray spectroscopy.

UV-visible absorption spectroscopy. UV-Visible absorption spectra were collected over a wavelength range of 200 to 700 nm using a Synergy Mx Multi-Mode Microplate Reader (BioTek Instruments, Inc., Winooski, VT).

Particle charge. Particle charge or zeta potential of the nanosilver particle and PENS suspension were also measured using a Zeta Sizer Nano Series ZEN 3600 Spectrometer (Malvern Instruments Ltd, Malvern, Worcestershire, United Kingdom).

Fourier transform infrared spectroscopy. Solutions of deltamethrin, AgNP and PENS were dried on a polished 25 x 2 mm ZnS disc (ClearTran, Internation Crystal Labs, Garfield, New Jersey) and analyzed using FTIR System 2000 and Spectrum 100 infrared spectrometers (Perkin-Elmer). Spectra were recorded in transmission mode with a resolution of 4 cm^{-1}. Thirty-two scans were collected and averaged for each spectrum.

3.2.3. Mosquito bioassays

Experiments were conducted using adult female mosquitoes of Aedes aegypti (L.). The mosquitoes were fed with 10% glucose in distilled water. Two mosquito bioassays were conducted. First, a mosquito bioassay was conducted to evaluate the uptake of nanosilver particles in the mosquito hemolymph. Second, a mosquito bioassay to compare viability of mosquitoes on exposure to deltamethrin and PENS was carried out. For both the mosquito bioassays, i.e., the hemolymph analysis and the viability tests, clear borosilicate glass vials (maximum capacity of 75 mL) were coated with 15 mLs of solutions (deltamethrin, AgNPs, or PENS) using a Roller Culture Apparatus (Wheaton Industries Inc., Millville, NJ). For the hemolymph analysis, vials were coated with high concentrations of solutions to ensure easy detection of silver uptake. For the viability tests, vials were coated with varying concentrations of deltamethrin and PENS. The roller action ensured uniform coating of suspensions on the walls of the vials. The experimenter was blinded to the treatment groups; and on the day of the experiment, 20

non blood-fed mosquitoes (5 days old) were placed into each of the coated glass vials and observed at specified intervals as described. Additionally, an uncoated vial served as the "negative control".

Mosquito bioassay #1: hemolymph collection and total silver content analysis. Four clear borosilicate glass vials were used in these studies: vial 1 was uncoated, vial 2 was coated with nanosilver, vial 3 was coated with deltamethrin, and vial 4 was coated with PENS. Vials 2 and 4 were each coated with 90 ppm solutions of nanosilver (in water) or PENS (in water). The uncoated vial served as the "negative control" and a 90 ppm deltamethrin coated vial served as the "positive control". The mosquitoes were exposed to each treatment and were observed continuously for the first four hours and the bioassay finalized at 24 hours when survivorship was recorded. The experiment was repeated four times.

Mosquitoes from the bioassay described above were utilized to analyze their silver content in hemolymph. Mosquitoes from the negative control vials, vial 1 (uncoated) and vial 2 (nanosilver), were alive after 24 hours (Figure 3A and C) and their hemolymph was collected at that time. The mosquitoes in the vials 3 (deltamethrin) and 4 (PENS) were observed knocked down 5 min after bioassay initiation, however, they were still moving. At 15 min from bioassay initiation, the mosquitoes were completely immobile and presumed dead. They were continuously observed for the next 4 hours to determine if there was recovery from knock down, but they were scored as dead at 4 hours.

All mosquitoes were then chilled on ice for 15 min after which each was carefully placed on a clean microscope slide under a dissecting microscope. A 10 μL anticoagulant citrate buffered solution (98 mM NaOH, 186 mM NaCl, 1.7 mM EDTA, and 41 mM citric acid, pH 4) was then injected into the thorax using sterile glass needles (Femtotips™; Eppendorf, Hamburg, Germany) connected to a FemtoJet®pump (Eppendorf, Hamburg, Germany) [93]. After 15 min on ice, hemolymph was collected by capillary action using new Femtotips™ through a perforation made between the last two abdominal sclerites of each of the 20 mosquitoes exposed per treatment. Hemolymph was collected by ejecting it from the tips with the aid of the pump and approximately 25 μL of hemolymph was obtained from each group of mosquitoes.

The collected hemolymph was then qualitatively analyzed to measure the total silver content via inductively coupled plasma-mass spectrometry (ICP-MS, Perkin Elmer DRC 2 spectrometer, Waltham, MA). Each sample was diluted by a factor of 100 using a calibration blank solution (5% hydrochloric acid and 1% nitric acid by volume). The resultant solution was heated at 60˚C for 2 hours to dissolve the residual silver particles. The citrate buffer solution was also analyzed to establish background silver concentration levels.

Mosquito bioassay #2: viability tests comparing deltamethrin and PENS. For these studies, mosquitoes were introduced into vials coated with varying concentrations of either deltamethrin or PENS and observed every hour for the first 12 hours. The bioassay was finalized at 24 hours when survivorship was recorded. Both knockdown and death were recorded.

3.2.4. Statistical analysis

Hemolymph values are expressed as the mean plus or minus standard error of the mean (± SEM). Differences between treatment groups were analyzed by a one way analysis of variance (ANOVA) followed by post-hoc testing using the Tukey-Kramer multiple comparison test. Probability values of $p < 0.05$ were considered to be statistically significant. The IBM PC programs INSTAT v3.0 and PRISM v5.0 software (GraphPad, San Diego, CA) were used to calculate and graph results.

3.3. Results

3.3.1. Synthesis and characterization of AgNPs and PENS

A primary goal of nanosilver synthesis for practical applications is to produce monodispersed NPs with a well-defined shape. Therefore, careful selection of the reducing agent and stabilizer are critical steps which can be more easily controlled when the NPs are synthesized "in-house". Hence, we were able to successfully synthesize water soluble, highly monodispersed, and spherical nanosilver particles with a known chemical composition. For these experiments, sodium citrate served the dual role of both a reducing agent and a stabilizer. The well-defined nanosilver core particles were then conjugated with deltamethrin, resulting in PENS, which was also produced in water as opposed to harsh non-polar solvents.

Transmission electron microscopy and energy dispersive X-ray spectroscopy. Figures 3.1 and 3.2 show the transmission electron micrographs and the EDX spectra of the pristine AgNPs and PENS respectively. Electron micrographs of pristine AgNPs show 15 nm monodispersed spherical NPs. Electron micrographs of the PENS clearly

show a nanosilver core encircled by organic molecules. This organic molecule is the deltamethrin that was added during the conjugation reaction. Hence, these transmission electron micrographs confirm conjugation. Furthermore, the EDX of nanosilver shows only silver signature peaks, whereas the EDX of PENS shows the presence of both silver and bromine. These two elements are indicative of silver particles and the deltamethrin ($C_{22}H_{19}Br_2NO_3$). These results further confirm the conjugation.

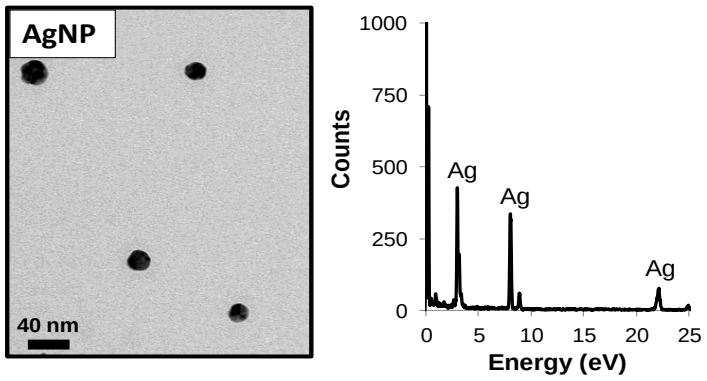

Figure 3.1. TEM and elemental analysis of pristine AgNPs.

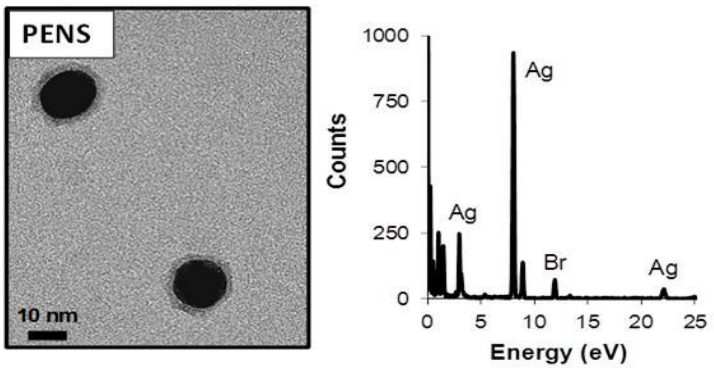

Figure 3.2. TEM and elemental analysis of PENS.

UV-Visible absorption spectroscopy. Figure 3.3 shows the measurements from the UV-Visible absorption spectroscopy. During the synthesis of nanosilver and on conjugating deltamethrin to the nanosilver core, the solution mixture turned from colorless to yellow. This color change is indicative of the reduction of Ag^{+} ions as revealed by the peak at 420 nm [35]. It is important to note that the overall spectral shape of the plasmon absorption remained the same for both pristine nanosilver particles and PENS. The λ_{max} was observed at 400nm for both particles – this is characteristic of 15nm AgNPs.

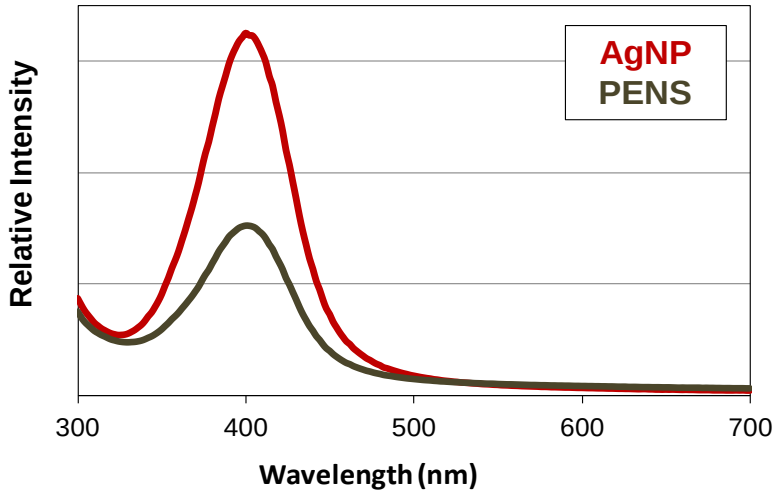

Figure 3.3. UV-Visible spectra of pristine AgNPs and PENS.

Particle Charge. The overall charge that the particle acquires in a particular medium can be determined by measuring the zeta potential of the suspension. The resulting repulsive force can be used to predict the colloidal stability and agglomeration state of NPs. Particles with a large positive or negative zeta potential repel each other

leading to a non-aggregated solution with high stability. Conversely, low zeta potential values result in the tendency of NPs to flocculate, or coagulate loosely thereby causing agglomeration [94]. The zeta potential of pristine AgNP and PENS were found to be around -40 mV verifying that both the nanosilver and PENS particles were charged and stable. A high zeta potential value of -40 mV also suggests that both the nanosilver particles and PENS particles are not likely to aggregate. Since deltamethrin was a nonionic surfactant that serves as a colloidal stabilizer during synthesis, it does not affect the charge of the final AgNP solution.

Fourier transform infrared spectroscopy. The molecule of deltamethrin can be divided into two characteristic parts - Wedge 1 and Wedge 2 as shown in Figure 3.4. Wedge 1 is the proposed "active site" of the molecule that aids in conjugation because it contains ester groups (CO), the cyanide group (CN), active dimethyl groups (CH_3) and electronegative Br atoms [95]. Thus, in the vicinity of interacting atoms such as a nanosilver core, Wedge 1 offers a relatively flexible structure thereby permitting the reactive CO, CN, CH_3 or the Br groups to aid conjugation [96, 97]. Wedge 2, on the other hand, is relatively rigid and provides support for such interaction to occur [96, 97].

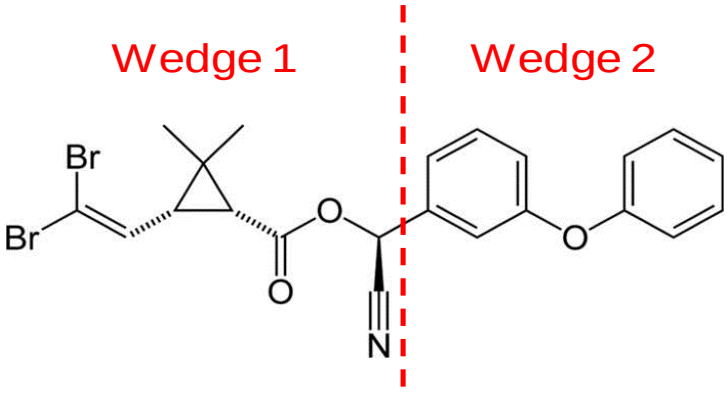

Figure 3.4. Structure of deltamethrin ($C_{22}H_{19}Br_2NO_3$). Wedge 1 is the proposed "active site" of the molecule, while wedge 2 is relatively rigid and provides support for any interaction to occur.

Figure 3.5 shows the FTIR spectrum of deltamethrin, AgNP and PENS deposited as a thin film on the ZnS disc. The FTIR spectrum shown for deltamethrin includes only the fingerprint region between 1800 and 600 cm^{-1}. In this region, the main absorption bands of deltamethrin are assigned to the C=O carbonyl asymmetric stretching (ν = 1734 cm^{-1}), C=C stretching of the aromatic rings (ν = 1488 cm^{-1}), CH_2 deformation in R-CH_2-CN structure (ν = 1459 cm^{-1}) and the deformation vibrations of the cyclopropane rings (ν = 884 cm-^{1}). The band represented at 1122 cm^{-1} can be related to the C-O stretching of the cyanate group (-O-CN) [98-100]. It is interesting to note a clear shift in these bands for the PENS spectra. These shifts in the bands indicate that the reactive groups such as CO, CN and CH_3 of the deltamethrin molecule permit interaction with other molecules in its vicinity. Since the nanoconjugate PENS was created by tethering deltamethrin molecules to a nanosilver core, this shift in the bands for PENS can be attributed to the interaction of the CO, CN and CH_3 groups of the deltamethrin with the nanosilver particle core. Furthermore, the band observed at 1250 cm^{-1} (for both

deltamethrin and PENS) can be assigned to the aryl-O of diphenyl ether which involves aryl-O stretching, out-of-phase C-O-C stretching and ring vibrations. This band corresponds to rigid portion or Wedge 2 of the schematic which does not participate in bonding [96-100]. Additionally, the band at 922 cm^{-1} for deltamethrin was assigned to the asymmetric wagging vibrations of the terminal $(C=C)Br_2$ group [98-100]. Stretching characteristic peaks of carboxlyate C=O were found in 1583 cm^{-1} (asymmetry flex vibration of C=O) and 1393 cm^{-1} in the PENS spectra. These two bands confirm the presence of the nanosilver particles in the PENS sample [101]. Specifically, these carboxylate peaks are indicative of citrate-stabilized nanosilver particles. These results clearly show the interaction of the deltamethrin molecule with the nanosilver particles and further confirm conjugation in PENS. Taken together, these characterization techniques confirm the presence of 15 nm stable nanosilver and the conjugation of deltamethrin to the nanosilver core.

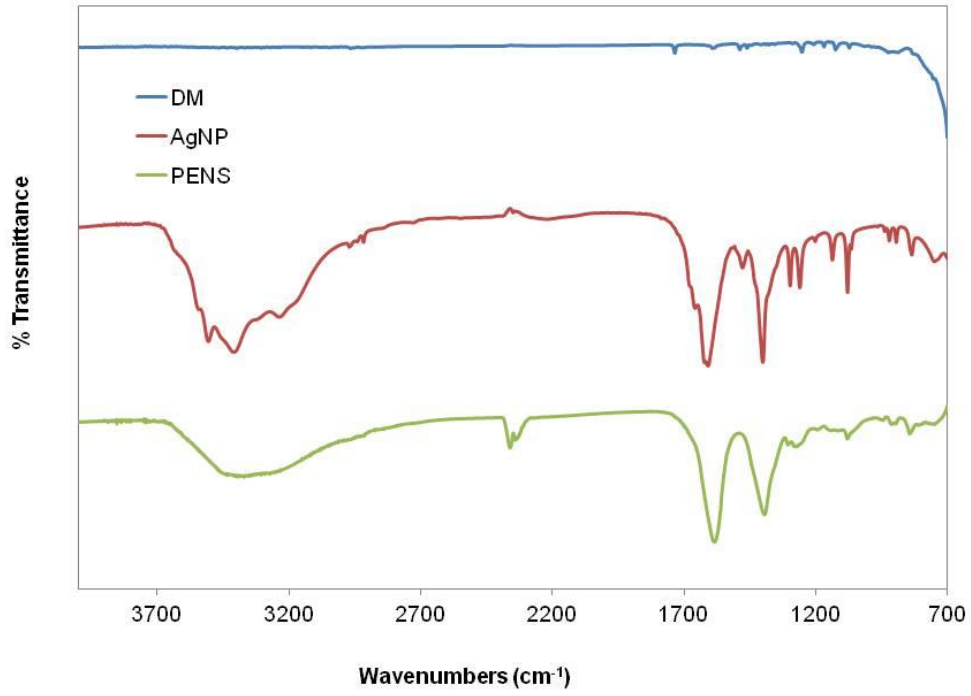

Figure 3.5. FTIR spectra. FTIR spectrum of deltamethrin, AgNP and PENS at the spectral signature region between 1800 and 600 cm^{-1}.

3.3.2. Mosquito bioassays

Mosquito bioassay #1: hemolymph collection and total silver content analysis. Figure 3.6 shows the results from the first mosquito bioassay. i.e., hemolymph collection and evaluation of total silver content. The mosquito bioassay was performed in coated vials: vial 1 was the "negative" control (uncoated); vial 2 was coated with 90 ppm nanosilver particles; vial 3 was the "positive" control (coated with 90 ppm deltamethrin), and vial 4 was coated with PENS (90 ppm deltamethrin and 90 ppm nanosilver particles). All mosquitoes in vials 3 and 4 were completely knocked down within 15 minutes of exposure; the mosquitoes in vial 2 were alive and had a 10% knockdown (i.e.

only 2 out of the 20 exposed mosquitoes were knocked down); and the mosquitoes in vial 1 survived through the 24 hours exposure time period.

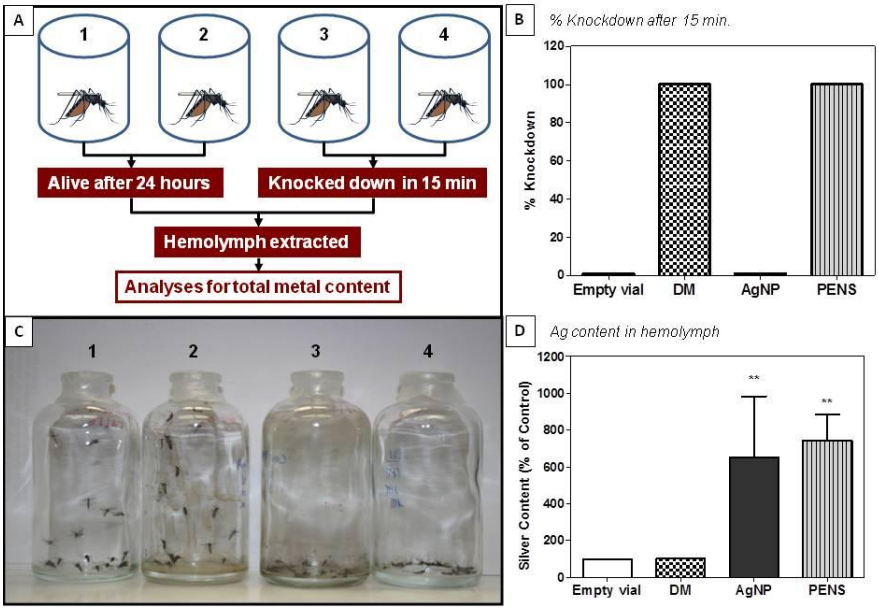

Figure 3.6. The effects on mosquitoes. (A) Schematic diagram of mosquito bioassay, (B) percentage knock down in vials after 15 min, (C) photograph of vials after 15 min of exposure (vial 1 was the "negative" control (uncoated); vial 2 was coated with 90 ppm nanosilver particles; vial 3 was the "positive" control (coated with 90 ppm deltamethrin), and vial 4 was coated with 90 ppm PENS), and (D) ICP-MS analyses of total silver content in mosquito hemolymph.

ICP-MS analysis revealed that the mosquitoes exposed to the uncoated "negative" control vial and the deltamethrin coated vial had virtually undetectable levels of silver (0.04 ng and 0.041 ng of silver, respectively). Therefore, the silver concentration in mosquitoes from the uncoated vials was set at 100% and the levels of Ag from mosquitoes exposed to deltamethrin, nanosilver and PENS were compared to the control. Hemolymph collected from mosquitoes in the nanosilver and PENS coated

vials had silver levels that were higher than those of controls or those in the deltamethrin coated vial by a factor of six and seven, respectively ($p < 0.01$). The citrate buffer solution was also analyzed for total silver content. No significant amount of silver was detected. Thus, these results show that tethering a synthetic organic molecule to a nanosilver particle core enabled the detection of silver metal and facilitated the uptake of the pesticide into the mosquito hemolymph.

In an effort to evaluate the magnitude of exogenous silver potentially introduced via the mosquito hemolymph extraction procedure, we compared the number of AgNPs in the collected hemolymph to the maximum number of silver particles possibly on the surface of the femtotip (i.e. mosquito injection needle) during collection. The following reasoning was used: transmission electron micrographs verified the spherical and monodispersed nature of AgNPs and confirmed the size as 15 nm (Figure 3.1A). On the basis of this size, the total silver content measured from ICP-MS (2.11 ng) and the density of metallic silver (10.5 g/cm^3), the number of nanosilver particles in the collected hemolymph from 20 mosquitoes was calculated as 1.14×10^8 [102]. Therefore, the average number of particles per mosquito was 5.76×10^6.

The ratio of the cross-sectional area of the femtotip to that of nanosilver particles yields the maximum number of particles that are potentially on the tip of the needle as it is injected into the mosquito. This ratio was calculated to be 1.11×10^3. Hence, the amount of nanosilver particles measured from ICP-MS analysis (5.76×10^6) is over three orders of magnitude higher than the amount of silver potentially introduced to hemolymph via needle puncture (1.11×10^3). These two calculations confirm that the

silver content measured via ICP-MS was indeed from the collected hemolymph and not due to exogenous silver introduced during sample collection.

Mosquito bioassay #2: viability tests comparing deltamethrin and PENS. Figure 3.7 and Figure 3.8 show the effects of deltamethrin or PENS on mosquito viability over time and dose, respectively. Mosquitoes that remained alive are represented by the blue bars, mosquitoes that were knocked down are represented by the red bars, and the green bars represent the mosquitoes that were scored as dead. Mosquito viability (i.e., % alive, % knock down and % dead) was recorded every hour for the first 12 hours and again at 24 hours when the bioassay was finalized. The figures show the mosquito viability at the 1st, 2nd, 3rd, 4th, 12th and 24 hour time point (data from 5th through 11th hour not shown). The doses used in the bioassay were: (a) $9x10^{-3}$ ppm, (b) $9x10^{-3}$ ppm, (c) $9x10^{-5}$ ppm, and (d) $9x10^{-6}$ ppm of deltamethrin or PENS.

The results from this mosquito bioassay show that mosquitoes exposed to both deltamethrin and PENS at 9 $x10^{-3}$ ppm resulted in 100% death after 24 hours (Figures 3.7A and 3.8A respectively). Four hours of mosquito exposure to 9 x 10^{-4} ppm deltamethrin resulted in 5% knockdown and 95% death; while 4 hours of mosquito exposure to 9 x 10^{-4} ppm PENS resulted in 15% knockdown and 85% death. At this concentration, 100% mosquito death was observed in deltamethrin vial while 95% death (with 5% knockdown) was observed after PENS exposure at the end of the 24 hour period (Figures 3.7B and 3.8B). These results prove the effectiveness of the nanoconjugate in comparison to deltamethrin over time and dose.

Exposure to 9 x10^{-5} ppm deltamethrin resulted in 90% mosquito death (Figure 3.7C); however, exposure to the PENS had no effect at this concentration (Figure 3.8C). The mosquitoes exposed to 9 x 10^{-6} ppm deltamethrin had a 15% knockdown rate with 85% staying alive (Figure 3.7D), whereas, the mosquitoes exposed to 9 x 10^{-6} ppm PENS had a 100% survival rate through the 24 hours exposure time period (Figure 3.8D). All the mosquitoes survived the entire 24 hour period in the uncoated "negative control" vial (data not shown). Hence, both PENS and deltamethrin were shown to be completely effective after 24 hours of exposure to 9 x 10^{-3} ppm. Additionally, even though exposure to the deltamethrin resulted in 100% mosquito mortality at the 9 x 10^{-4} ppm concentration, the PENS exposure also resulted in 95% mosquito death and the remaining 5% were knocked down proving its effectiveness. These results show that the newly developed nanoconjugate PENS did not inactivate the primary function of the pesticide and was able to kill mosquitoes even at low concentrations.

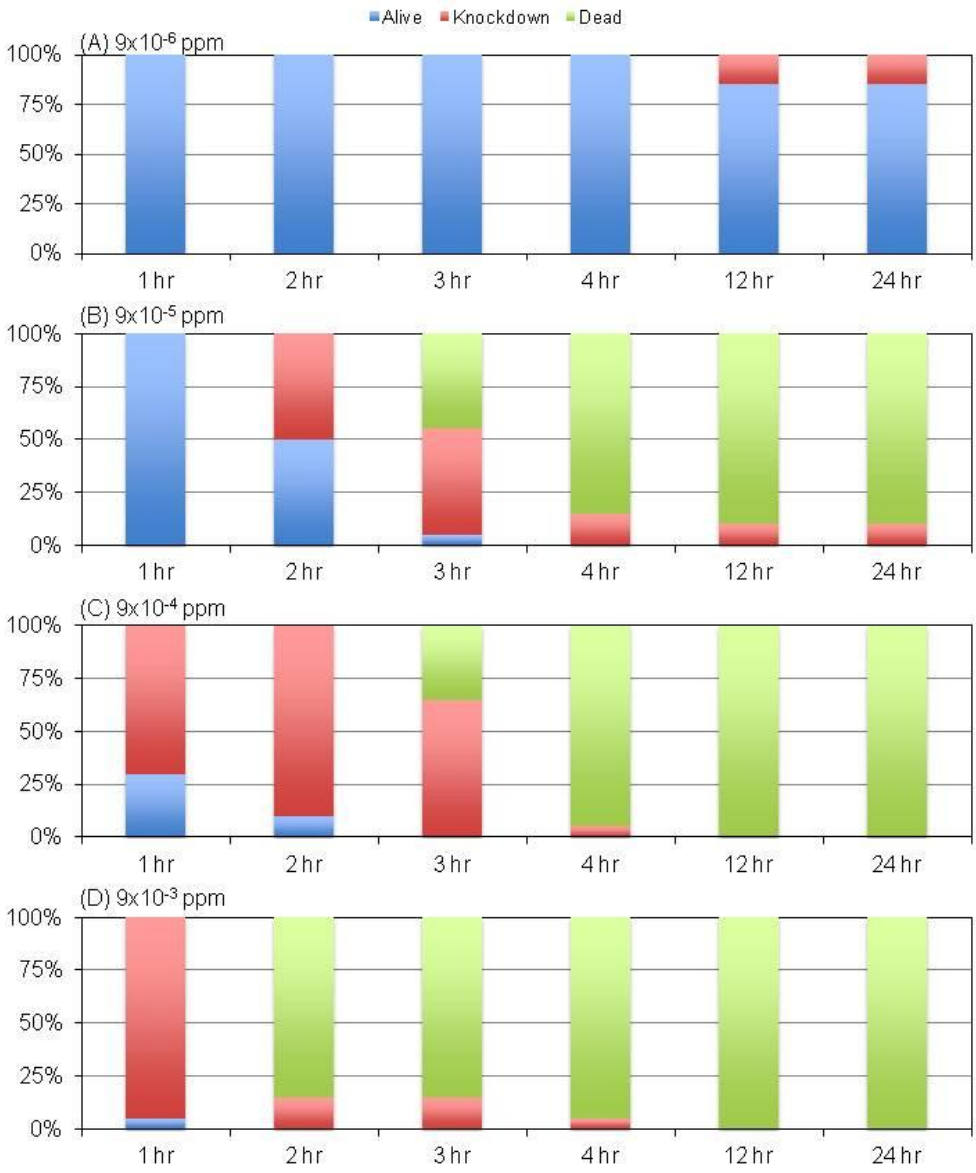

Figure 3.7. The effects of deltamethrin in the mosquito bioassay over time and dose. The blue bars represent mosquitoes that remained alive, the red bars represent the mosquitoes that were knocked down, and the green bars represent the mosquitoes that died. Mosquitoes were counted over the following time points: 1, 2, 3, 4, 12, and 24 hours. The doses used in the bioassay were: (a) $9x10^{-6}$ ppm, (B) $9x10^{-5}$ ppm, (C) $9x10^{-4}$ ppm, and (D) $9x10^{-3}$ ppm of deltamethrin.

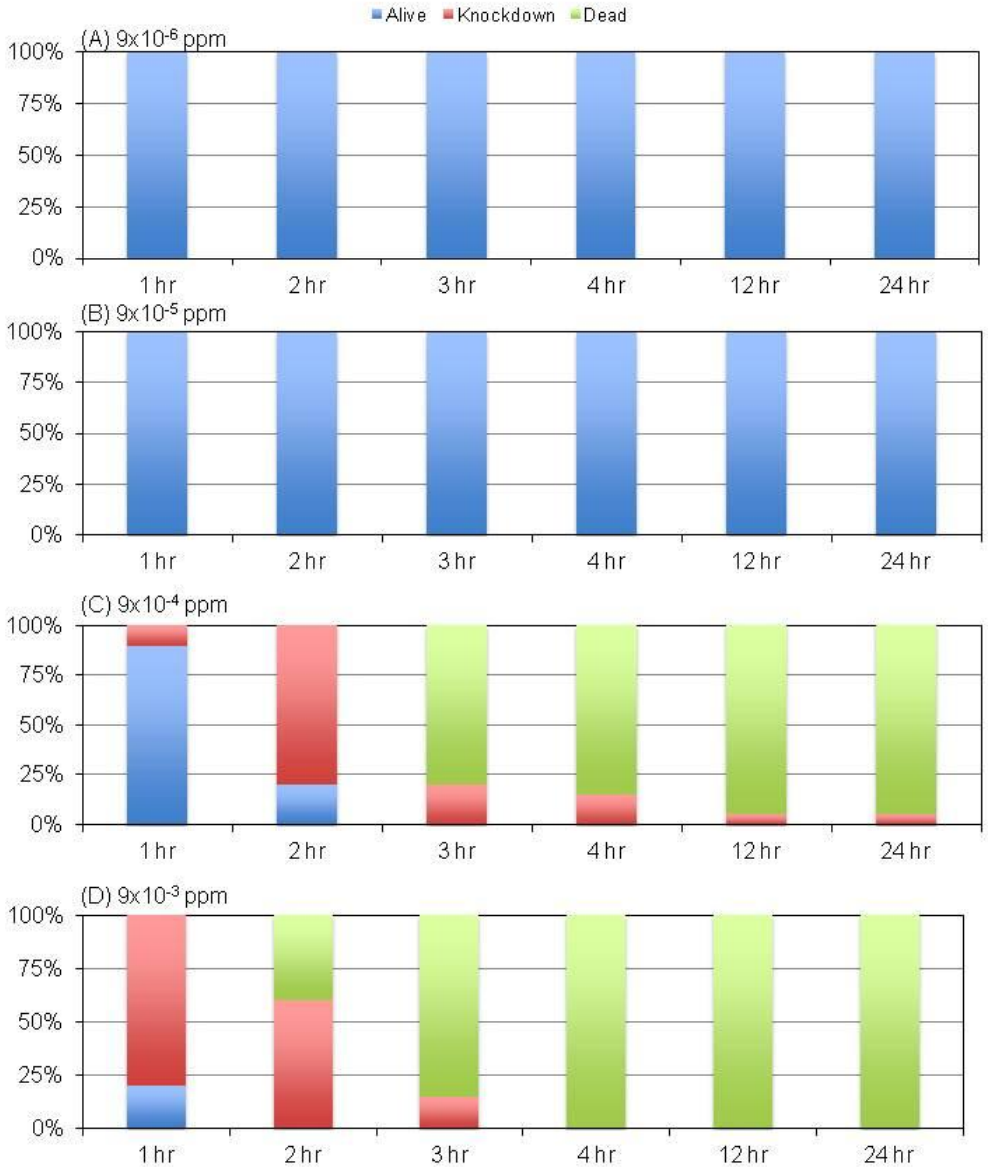

Figure 3.8. The effects of PENS in the mosquito bioassay over time and dose. The blue bars represent mosquitoes that remained alive, the red bars represent the mosquitoes that were knocked down, and the green bars represent the mosquitoes that died. Mosquitoes were counted over the following time points: 1, 2, 3, 4, 12, and 24 hours. The doses used in the bioassay were: (A) $9x10^{-6}$ ppm, (B) $9x10^{-5}$ ppm, (C) $9x10^{-4}$ ppm, and (D) $9x10^{-3}$ ppm of PENS.

3.4. Discussion and data interpretation

The research presented here showcases the conjugation of monodispersed, stable AgNPs to the insecticide deltamethrin. It also explores the possibilities of using the newly created and effective PENS in the fight against disease carrying insects. Effective insect vector control is essential to prevention of vector-borne infectious diseases. Every day flies, ticks, and mosquitoes infect humans and animals around the world with life threatening pathogens causative of diseases for which there are currently no vaccines or effective treatments. Therefore, alternate methods to combat infectious diseases are needed.

Current vector control strategies that target the adult insect or arthropod are limited to the same four classes of synthetic insecticides (organochlorine, organophosphate, pyrethroid, and carbamate) that have been used for over 30 years [103]. Introduction of insect growth regulators (IGRs) such as methoprene and novaluron as well as biopesticides such as the Cry and Cyt toxins produced by the bacterium Bacillus thuringiensis (Bt) have been shown to be effective larvacides. Bt toxins have been incorporated into transgenic crops to combat agricultural insect pests. However, both Bt toxins and IGRs currently have limited use as sprays since they do not kill the adult stage and widespread coverage of breeding areas in remote locations is logistically challenging [90]. Therefore, the development of new and/or improved vector control strategies is paramount in the fight against the irrepressible spread of disease.

Many countries continue to extensively utilize the organochlorine pesticide dichlorodiphenyltrichloroethane, better known as DDT, as well as the pyrethroid

pesticide deltamethrin to control mosquitoes that carry malaria [94]. Even though the pyrethroids are safer than many of the other insecticides, they are neurotoxic to people, and human exposure needs to be effectively and accurately monitored. The structural diversity of the synthetic pyrethroids presents a challenge for the development and analysis of human exposure biomarkers [104].

Another factor complicating biomonitoring of pyrethroids is that many of the metabolites are nonspecific and are derived from the breakdown of multiple pyrethroids. Only cyfluthrin and deltamethrin yield compound specific metabolites [104]. However, several of the common metabolites (specific and nonspecific) also occur naturally in the environment due to microbial transformation and photolysis [105]. Therefore, measurement of urinary metabolites may not accurately depict pyrethroid exposure. The successful conjugation of a pesticide to a NP surface allows for effective tracking of organics in complex biological matrices. The presence of noble metals in biological fluids and other complex matrices allows for ease in detection of organometallic substances, such as PENS describes herein. Analytical methods such as mass spectroscopy, emission spectroscopy, and electron microscopy are all better suited to detect and characterize biological substances that contain elements of high electron density, such as elemental or particulate silver.

Lab synthesized NPs offer several advantages in comparison to purchased NPs. When NPs are prepared from scratch, a well-known chemical composition offers the possibility of altering their surfaces to introduce specific functionalities. While purchased NPs tend to aggregate or agglomerate more easily when suspended in water

affecting the particle size, the primary particle size of homemade NPs can be controlled to a great deal due to the synthesis scheme employed. These pristine (i.e., impurity free) "home-made" NPs have a well-defined size and a uniform shape. Furthermore, since these NPs were created in the lab using chemical reduction methods, laboratory synthesis offers the additional advantage of calculating the resulting concentration of the AgNP and PENS solutions via reaction stoichiometry. Based on the average diameter of AgNP as observed via TEM (i.e., 15 nm), the weight of silver salt used in reaction (i.e., 8.45 mg) and the total reaction volume (i.e., 60 mLs), the concentration of the final solutions (as total atoms/L or number of moles/L) were calculated.

When conjugating an organic molecule to the surface of a NP, an "active site" of the molecule must be identified. In this case, it is deltamethrin is conjugated to the surface of a AgNP. Based on the evidence provided by the FTIR spectroscopy studies, wedge 1 (which contains an ester group, a cyanide group, dimethyl groups, and bromine atoms) is the “active site”. Further evidence is observed in the transmission electron micrographs showing pristine nanosilver particles before conjugation and an organic corona surrounding the nanosilver particles after conjugation with deltamethrin. When considering the effects of the PENS conjugate to mosquitoes, the bioassay resulted in mosquito knockdown and subsequent death. PENS was comparable to deltamethrin in killing mosquitoes at a low concentration ($9x10^{-4}$ ppm). Measurable levels of nanosilver particles were detected in mosquito hemolymph following exposure to either the silver particle or to PENS. Even though deltamethrin resulted in mosquito mortality at $9x10^{-5}$

ppm concentrations while PENS did not, we have clearly demonstrated that the conjugation process does not inactivate the insecticide.

3.5. Summary

In summary, tethering a synthetic organic molecule to an engineered metal-based NP allows for the detection of the metal conjugate in complex matrices, such as mosquito hemolymph. The novel synthetic scheme, material characterization techniques, and *in vivo* mosquito bioassays described here is a refreshing concept for the exploitation of a core-shell nanoconjugate that can be used as an active agent against insect vectors. By simply altering the chemistry of the synthesis scheme, we describe new possibilities of creating several NP-pesticide core-shell conjugate models that can be tested in other biological systems. This example of a NP-based technology will have a significant impact on both basic understanding of synthesis, characterization, and toxicology as well as having an impact in the application of such technologies towards vector control.

4. EFFECTS OF PENS ON VIABILITY AND REACTIVE OXYGEN SPECIES GENERATION IN NEURONAL (PC12) CELLS

4.1. Introduction

Improvement of existing compounds and the development of new methods to eradicate insect vectors that carry infectious diseases is an ongoing process that continues to be of extreme importance to human health. While there are many ways to approach the need for development of effective, safe insect vector control agents, our research team has utilized nanoscience to modify an existing insecticide. We previously described the synthesis and extensive characterization of a novel conjugate comprised of a AgNP core encapsulated by the pyrethroid pesticide, deltamethrin. Size, size distribution, chemical composition, agglomeration states and stability of the conjugate were thoroughly analyzed. Most importantly, exposure to low concentrations of PENS resulted in mosquito knockdown and mortality [106].

The rationalization for utilizing AgNPs to modify a currently utilized insecticide is that these particles have unique antimicrobial and optical properties at the nanometer size scale [107, 108]. This results in specific physicochemical characteristics that may differ from those of conventional particles (i.e. ionic, bulk, particulate, or micronized). For instance, the high surface area to volume ratio in nanomaterials results in high surface reactivity [37, 50, 109-113]. AgNP disinfectant sprays exhibit antiviral properties and also serve as broad-spectrum fungicides [114, 115]. AgNPs can also be deposited on natural and synthetic textiles which can be useful in hospitals to control

infection [116]. Thus, AgNPs are unique in that they offer the possibility of altering their surfaces to introduce specific functionalities for a host of environmental and biomedical applications [37, 113, 117].

Ultimately, insecticides should not only be effective against the targeted pest, but they should also be safe for people to use. Currently, pesticides are not species- specific, and humans can also be poisoned by exposure to these chemicals. The World Health Organization underscores the lack of alternative, cost-effective and safe insecticides and emphasizes the need for new, alternative insecticides [118]. Hence, the development of new methods and compounds to eradicate insect vectors that result in low to little mammalian toxicity are urgently needed. The ultimate long-term goal of this interdisciplinary research was to eventually develop efficacious insecticides with minimal toxicity in mammals.

Even though cellular effects of the individual components of PENS (i.e., AgNPs and deltamethrin) are well-characterized, any modifications of those effects due to the conjugation process have not been previously studied. Therefore, in this section, the primary goal was to assess the effects of our newly created pesticide-particle conjugate on basic cellular responses utilizing an *in vitro* model. The assays chosen to evaluate cellular responses, cellular viability and ROS production, were based on known characteristics of the individual components of PENS.

AgNPs have been shown to induce the generation of ROS [119] followed by both apoptosis and necrotic cell death in several cell lines [119-121]. For this study, pristine AgNPs were synthesized in-house using tannic acid as the capping agent. We

therefore hypothesize that the use of a polyphenolic antioxidant such as tannic acid as the capping agent would actually suppress ROS production instead of increase it.

It is well established that deltamethrin exposure results in increased ROS generation and eventually neuronal cell death via apoptosis in PC12 (neural) cells [122, 123]. Similarly, accumulation of ROS coupled with the induction of oxidative stress in rats has been well documented following pyrethroid insecticide exposure [122, 124-126]. PC12 cells (pheochromocytoma of the rat adrenal medulla), a well-defined neurodevelopment model has served as the standard cell line in studies assessing exposures to neurotoxins [127, 128]. In contrast to primary neuronal cultures, the PC12 cells provide a homogeneous population that continues to divide unless differentiation is triggered by the addition of nerve growth factor. Therefore, the PC12 cell line was chosen as the model culture system for all experiments.

In the previous section, a novel synthesis scheme to produce the pesticide encapsulated nanosilver was described. Material characterization techniques confirmed that the PENS molecule consisted of deltamethrin molecules forming a thin shield-like adsorptive layer around the AgNP core. Furthermore, the efficacy of the conjugate was tested using a dose-dependent and time-course mosquito bioassay. Our results indicated that this newly developed nanoconjugate did not inactivate the primary function of the pesticide and was effective in killing mosquitoes at low concentrations [106]. In this section, the PENS conjugate was tested in neuronal cultured cells to compare the cytotoxic responses to the unconjugated pesticide deltamethrin and pristine AgNPs. The following results describe the *in vitro* effects of exposure to PENS.

4.2. Materials and methods

4.2.1. Dosing solutions and particle characterization

AgNPs were synthesized by reducing silver nitrate salt (99.9999% metal basis, Sigma-Aldrich, St. Louis, MO) using sodium citrate dihydrate and tannic acid solutions (Sigma-Aldrich, St. Louis, MO) as the reducing and capping agents respectively. Deltamethrin was also purchased from Sigma-Aldrich. Conjugation of the AgNP core particles with deltamethrin was carried out as reported previously [106]. The resultant aqueous suspension is referred to as PENS. Thus, the dosing solutions for all experiments included PENS, deltamethrin, and lab-synthesized pristine AgNP.

Molar concentrations of the PENS and AgNPs were calculated based on stoichiometry as previously described [106]. All suspensions were diluted in phenol red-free cell culture media to make up a 90 μM stock solution. Actual dosing concentrations were 5 μM, 10 μM, and 45 μM. The AgNPs and the PENS suspension in cell culture media were characterized via transmission electron microscopy. For TEM analyses, one micro liter of the AgNP or PENS suspension was deposited onto a 400 mesh carbon grid. Each grid was analyzed on a JEOL 2010 transmission electron microscope at an accelerating voltage of 200 kV.

4.2.2. Cell cultures

PC12 cells were maintained in Dulbecco's Modification of Eagles Media (DMEM) F-12 medium (Kaighn’s modification of Ham’s F-12 medium, HyClone, Logan, UT) supplemented with 10% fetal bovine serum (FBS) (Atlanta Biologicals, Norcross, GA) and Normocin Antibiotic Solution (Invivogen, San Diego, CA). Cells

were grown in T75 culture flasks at 37 °C in a humidified atmosphere of 5% CO_2 and 95% O_2 until 80% confluent. Cells were harvested via trypsinization (MP Biomedical, Solon, OH).

4.2.3. Cell viability

Cells were seeded at a concentration of 1 x 10^5 cells per well in 12 well plates in growth medium and allowed to proliferate for 72 hours until they reached 80% confluency. Cells were gently washed with phosphate buffer saline (HyClone, Logan, UT), followed by exposure to PENS, deltamethrin and lab-synthesized AgNPs as outlined in section 4.2.1 in serum free and phenol red free medium and incubated for 24 hours. Cell viability was assessed using trypan blue via the Countess® Automated Cell Counter (Invitrogen) as per the manufacturer's instructions. N=3 wells per treatment and each experiment was performed in triplicate.

4.2.4. Bright field microscopy

Bright field microscopy was employed to assess morphological changes on PC12 cells upon exposure to dosing solutions. Cells were cultured in 6 well plates and exposed for 24 hours to the high dose of 45 μM of PENS, deltamethrin, or lab-synthesized AgNPs. Following exposure, cells were washed with PBS and the medium was changed to phenol red-free DMEM only. Cells were immediately imaged at a total magnification of 20X with an Olympus IX71 inverted fluorescence microscope (Center Valley, PA). Images were processed with Olympus CellSens software.

4.2.5. Intracellular ROS measurement

DCFH-DA (2′,7′-dichlorofluorescein diacetate) was used to measure the levels of intracellular reactive oxygen species (Cell Biolabs, Inc.). The PC12 cells were seeded at a cellular density of 105 cells per well in a 96 well plate in growth medium. Upon reaching 80% confluency, cells were gently washed with PBS followed by treatment with 100 μM DCFH-DA and incubated at 37°C for 30 min. Cells were then exposed to dosing solutions in phenol red free medium with 10% charcoal-stripped FBS and incubated for 24 hours. Hydrogen peroxide (1000 μM) was used as the positive control. Fluorescence was measured at 480 and 530 nm (excitation and emission, respectively) using a fluorescence plate reader (Synergy Mx Multi-Mode Microplate Reader, BioTek Instruments, Inc., Winooski, VT). N= 8 wells per treatment and each experiment was performed in duplicate.

4.2.6. Statistical analysis

Each value is the mean of at least three separate analyses plus or minus the standard error of the mean (SEM). Data were normalized to the control values and are represented as the mean ± SEM. Multiple comparisons were performed using analysis of variance (ANOVA) followed by post-hoc testing if $P<0.05$. For the viability assays as well as reactive oxygen species data, PENS, deltamethrin and AgNP were analyzed via the Kruskal Wallis test followed by a Dunn post-test comparing all pairs of columns. Statistical analyses were performed using INSTAT software v 3.0 (GraphPad, Inc., San Diego, CA).

4.3. Results

4.3.1. PC12 cell viability following exposure to PENS, deltamethrin, or AgNPs

The PC12 cells were exposed for 24 hours to PENS, deltamethrin, or lab-synthesized AgNPs. The primary goal was to study the cellular effects of PENS (via viability and ROS measurements) and compare the effects to the individual components i.e., deltamethrin and AgNPs.

Transmission electron microscopy (TEM) reveals critical information about the particle size, shape, aggregation states and morphology. TEM was previously employed to characterize the pristine AgNPs and the PENS conjugate suspended in water [106]. TEM revealed monodispersed, spherical 15nm particles with no visible aggregation. TEM was once again employed to characterize physicochemical properties of the particles suspended in physiologically relevant media - i.e., cell culture media. Transmission electron micrographs of the lab-synthesized AgNPs and the PENS conjugate in cell culture media are shown in Figures 4.1A and 4.1B, respectively. These micrographs confirm that the particles remained spherical and non-aggregated upon suspension into cell culture media.

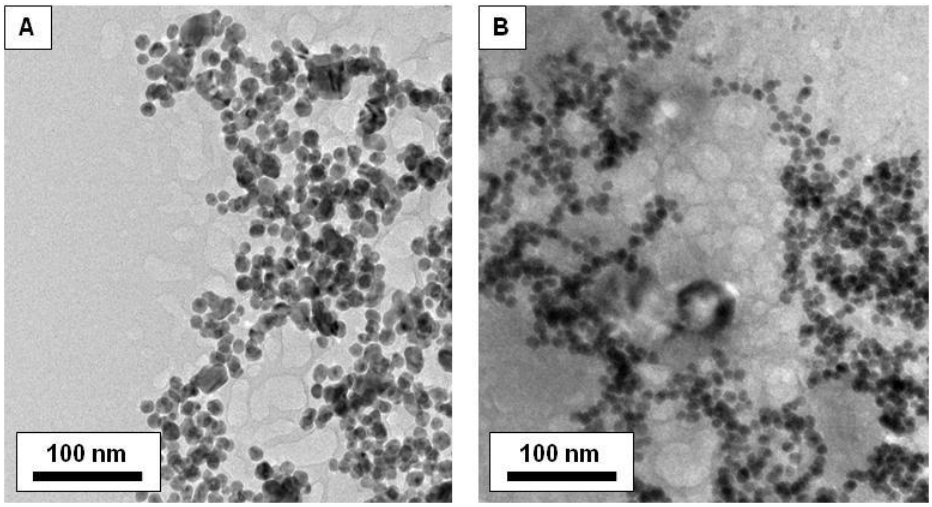

Figure 4.1. Transmission electron micrographs. (A) lab-synthesized AgNPs and (B) PENS suspended in cell culture media.

Figure 4.2 shows the effects on cell viability upon exposure to PENS deltamethrin, or lab-synthesized silver as compared to untreated cells at 5, 10, or 45 μM. PC12 cells exposed to deltamethrin exhibit a fairly monotonic dose-response relationship (i.e., cell viability decreases with increase in dose). Cells exposed to the conjugate PENS follow a similar trend to that of cells exposed to deltamethrin. Cells exposed to silver caused a caused a sharp decline in viability as compared to undosed cells at the 45 μM.

The cell viability remains higher following PENS treatment at the highest concentrations when compared to cells treated with either deltamethrin or AgNPs. Exposure to PENS resulted in a 17% decline in viability at the highest concentration of 45 μM while exposure to deltamethrin caused a 47% decrease and to silver caused 57% decline. Similarly, exposure to 10 μM deltamethrin reduced viability by 14% while viability of PENS treated cells remained unchanged. Thus, viability was significantly

higher in cells exposed to PENS as compared to deltamethrin and AgNP at the 45 µM concentration. These results suggest that cellular viability was less adversely affected by PENS than by the deltamethrin and AgNP at the highest concentration of 45 µM concentration.

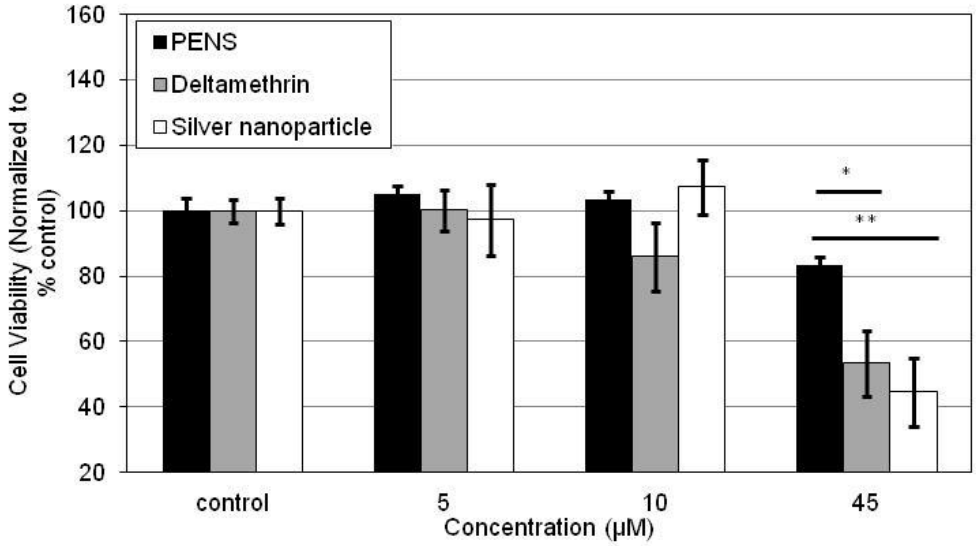

Figure 4.2. Comparison of effects following PENS, deltamethrin, and AgNP exposures on cell viability data at 5, 10 and 45 µM concentrations. Viability was higher in cells exposed to PENS as compared to deltamethrin at the highest concentration of 45 µM. Data were normalized to the control values and are represented as the mean ± SEM (*, P<0.05; **, P<0.01).

4.3.2. Morphological assessment via bright field microscopy

Cell morphological changes were assessed using bright field microscopy following 24 hour exposure to the highest dose (45 µM) of PENS, deltamethrin, or AgNPs as shown in Figure 4.3. While exposure to lab-synthesized AgNPs resulted in cell shrinkage as compared to media alone, cell exposure to deltamethrin resulted in cells

with irregular membrane borders. It is interesting to note that the cells exposed to the PENS conjugate resulted in no obvious morphological changes. This would suggest that the PC12 cells are less adversely affected by the PENS conjugate in comparison to both deltamethrin and AgNPs.

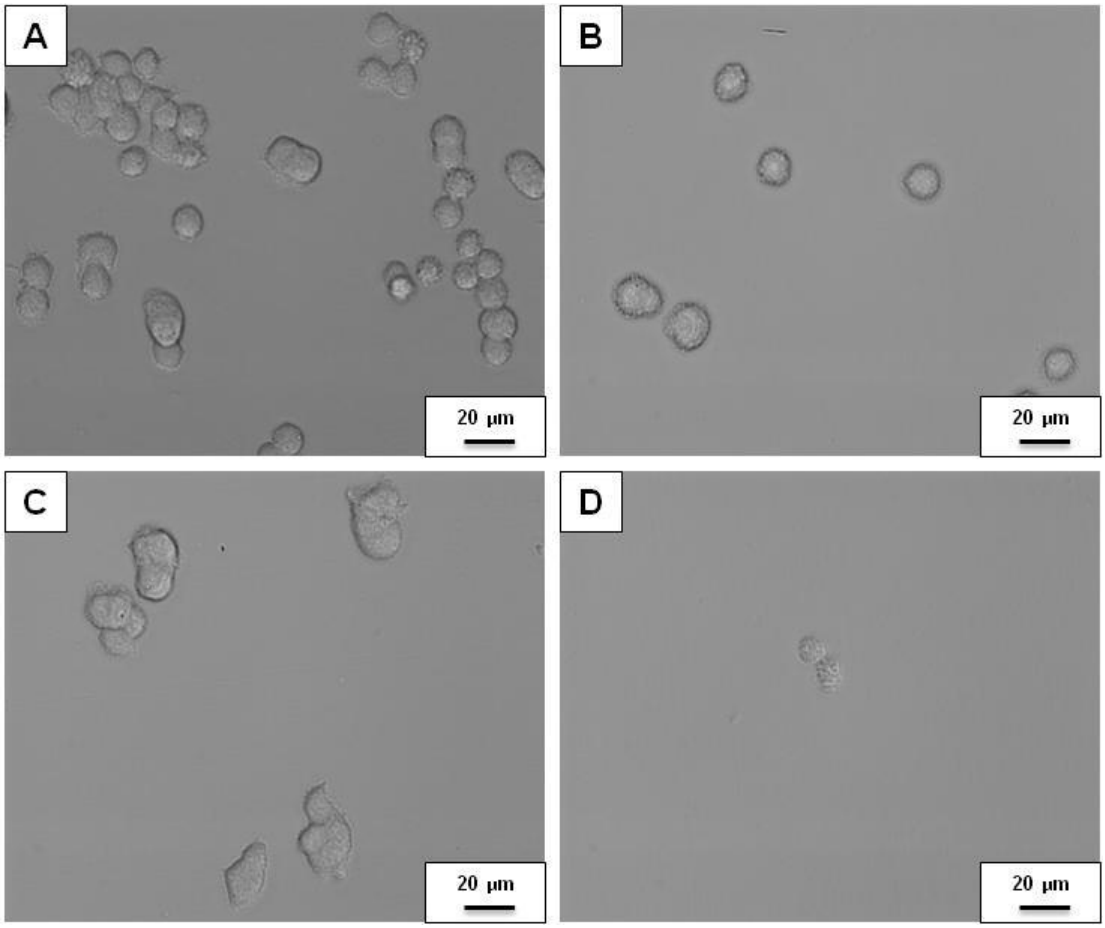

Figure 4.3. Bright field microscopy of PC12 cells. PC12 cells were exposed to the highest dose of 45 µM of PENS, deltamethrin or lab-synthesized AgNPs and incubated for 24 hours to assess morphological changes. The images include: (A) unexposed control cells, (B) cells exposed to PENS, (C) cells exposed to deltamethrin and (D) cells exposed to AgNPs.

4.3.3. Intracellular ROS measurement

Both deltamethrin and silver particles have been shown to increase production of reactive oxygen species *in vitro* [119, 129-133]. Therefore, we wanted to determine if our novel pesticide-particle conjugate, PENS, induced similar effects as deltamethrin or AgNP on cellular production of ROS. Cellular generation of ROS was measured in PC12 cells 24 hours after PENS, deltamethrin, or lab-synthesized AgNP exposures and the results are shown in Figure 4.4.

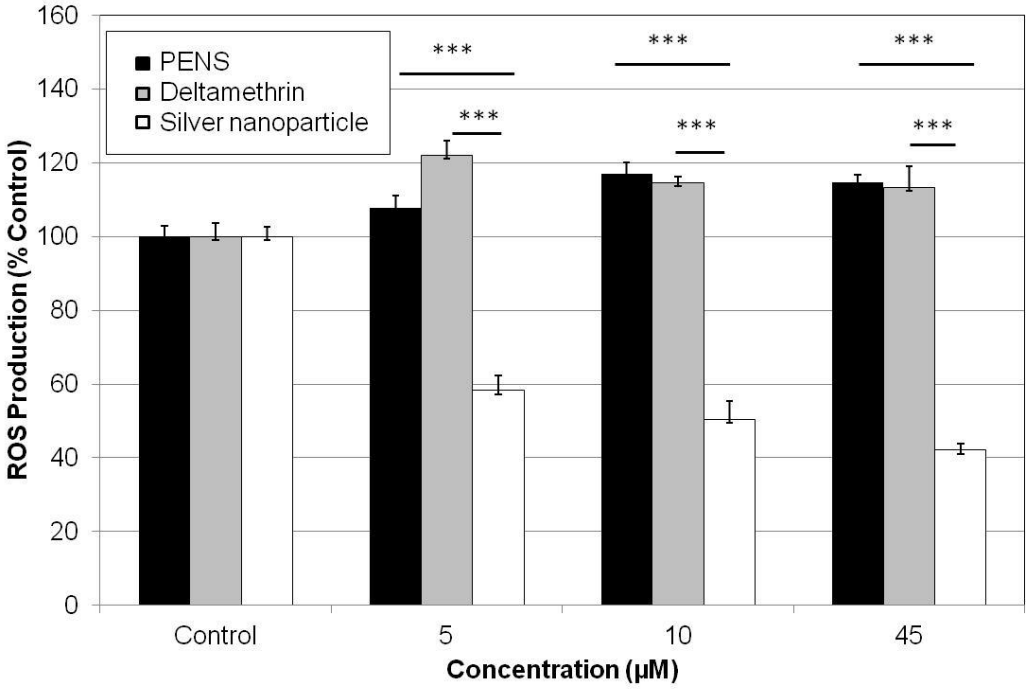

Figure 4.4. ROS production by PC12 cells following 24 hour exposure to PENS, deltamethrin, or AgNPs. Intracellular reactive oxygen species production was measured using DCFH-DA. Cells were exposed to 5, 10 and 45 µM concentrations of PENS, deltamethrin or lab-synthesized AgNPs and incubated for 24 hours. Data were normalized to the control values and are represented as the mean ± SEM (, P<0.01; ***, P<0.001).**

As seen from the figure, PENS and deltamethrin were not statistically significant from each other with regards to the ROS at all exposure concentrations. This suggests that the cells exposed to the PENS conjugate are responding in a manner similar to those exposed to the deltamethrin**.** On the other hand, ROS production upon comparing PENS to lab synthesized AgNPs, and deltamethrin to lab synthesized AgNPs were statistically significant at all concentrations.

4.4. Discussion and data interpretation

Development of new insect vector control agents that are safe, effective, and affordable is a high priority, especially in areas where humans are suffering from diseases spread by infected mosquitoes, ticks, and flies. There is an urgent need to engineer highly specific and targeted products that are safer than conventionally used pesticides. As described in Section 3, the physiochemical properties of PENS were extensively characterized (size, chemical composition, agglomeration state, and particle stability), and most importantly, mosquitoes exposed to PENS were knocked down and killed.

In an attempt to further explore these "next generation pesticides", this section evaluated the safety of the conjugate. The overall aim was to develop a tool in the fight against insect vectors that was effective and at least as safe, if not safer than, currently used insecticides. The *in vitro* effects following exposure to the newly created PENS conjugate on cellular viability and oxidative stress response in the mammalian neuronal cell line-PC12 were assessed. Specifically, we were interested in studying the cellular effects of PENS via cell viability and ROS measurements. The effects due to exposure to

the conjugate were then compared to those induced by the individual components (i.e., deltamethrin and AgNPs).

PC12 cells are a widely used neuronal model system that readily recapitulates key events in neuronal cell development [128]. Deltamethrin is known to increase ROS generation and eventually lead to neuronal cell death via apoptosis in PC12 (neural) cells [122, 123]. Other pyrethroids such as cypermethrin have also been reported to produce oxidative stress *in vitro* [125]. Li et al have also shown that deltamethrin treatment induces oxidative stress in the brain, including increased levels of lipid peroxidation products and decreased activities of enzymes such as superoxide dismutase (SOD) and glutathione reductase [122]. A recent study by the same group provides evidence that deltamethrin exposure promoted free radical formation in rat brain (in vivo) and further validated reactive oxygen species generation in PC12 cells *in vitro* [134]. Furthermore, deltamethrin-treated PC12 cells also induced the expression of the transcription factor NF-E2-related factor 2 (Nrf2) and heme oxygenase-1 (HO-1), a Nrf2-regulted gene [133]. Hence, several studies have reported deltamethrin-mediated oxidative stress in PC12 cells and shown that ROS is one of the mediators of this process [123, 135-137].

Exposure to AgNPs cause both apoptosis and necrotic cell death due to increased cellular ROS levels in several cell lines [119-121]. However, our results show a significant suppression of intracellular ROS in PC12 cells after exposure to known concentrations of our lab-synthesized silver particles. The majority of AgNPs that are reported to cause cell death due to ROS production are heavily coated to improve stability. Specifically, the coatings used for this purpose include: citrate coated AgNPs

[138], PVP coated AgNPs [119], hydrocarbon coated AgNPs [139] or peptide coated AgNPs [140]. In addition to surface coating, AgNP toxicity is also dependent to a great extent upon the NP size [120, 139, 141-143]. In our study, however, stable, spherical, monodispersed AgNPs were synthesized in-house using sodium citrate as the reducing agent and tannic acid, a polyphenol, as the capping agent to achieve particle stability [38, 144, 145]. Moreover, it is well established that polyphenolic compounds exert protective effects against glutamate cytotoxicity [146]. Furthermore, the ability of poylphenols to chelate metal ions is also well documented [147]. Thus our results demonstrate that the use of a polyphenolic antioxidant capping agent such as tannic acid will suppress ROS production in this particular cell line. These findings emphasize the importance NP coating and composition has on cellular viability and ROS production.

Another important point to be noted here is that when the PENS conjugate and the home-made AgNPs were re-suspended in cell culture media, the particles did not aggregate and instead stayed monodispersed, stable and spherical as shown by the transmission electron micrographs (Figure 1). Hence, dosing PC12 cells with the PENS conjugate and lab-synthesized AgNPs suspended in cell culture media is not only physiologically relevant but also a true representation of the biological effects to the newly developed nanoconjugate as well as the pristine AgNPs.

4.5. Summary

In summary, our current study was a first step towards evaluating the safety of our newly developed conjugate, PENS. Assessment of the *in vitro* effects following exposure of the PENS conjugate on cellular viability and oxidative stress response in the

mammalian neuronal cell line-PC12 was imperative before utilizing such a novel conjugate for any real world applications. Our results suggest that cellular viability was less adversely affected by PENS than by the deltamethrin. Also, ROS production following PENS exposure indicated that the newly developed conjugate was responding in a similar manner as that of cells treated with deltamethrin only.

5. A PHYSIOLOGICALLY RELEVANT APPROACH TO CHARACTERIZE THE MICROBIAL RESPONSE TO COLLOIDAL PARTICLES IN FOOD MATRICES WITHIN A SIMULATED GASTROINTESTINAL TRACT*

5.1. Introduction

Recent advances in colloid science have availed new technologies in diverse areas of our lives. Many research groups have postulated the use of small particles in a variety of consumer products including cosmetics and topical creams, drugs, and food packaging. [148-154]. The use of these particle-enabled products in their intended (and potentially unintended) manner would result in either individual colloids or particles incorporated into larger composites entering into the human body [55, 56]. This is especially relevant for colloidal silver particles. For these materials, the physical properties (e.g. size) influence the chemical properties (e.g. the production of bioavailable metals and redox surface chemistry). Colloidal silver is unique due to its high surface area to volume ratio, which is the main reason for the reportedly enhanced antimicrobial activity [7, 155-158].

These particles, because of their supposed antimicrobial properties, have been postulated as ideal candidates for antimicrobial surface coatings, antimicrobial paints and even food and drink additives. The demand for natural orange juice with high

---

*Reprinted with permission from Sooresh, A., et al., *A Physiologically Relevant Approach to Characterize the Microbial Response to Colloidal Particles in Food Matrices within a Simulated Gastrointestinal Tract.* Food and Chemical Toxicology, 2012. **50**(9): p. 2971-2977. Copyright 2012 Elsevier.

nutritional value and sensory characteristics with minimum heat treatment is on the rise [159, 160]. Non-thermal processing techniques (such as IR and UV) as a substitute for thermal processing have been extensively studied in order to extend the shelf life and maintain the freshness of the juice [161]. However, these techniques are not only energy-intensive but also require costly equipment for processing. Moreover, orange juice even if properly refrigerated has a short shelf life due to microbial spoilage [160, 162]. Hence, colloid science (such as nanotechnology) can potentially provide answers to some of the challenges facing food processing [150].

The physical and chemical properties and observed antimicrobial effects of colloidal silver can also influence their reaction with commensal microbial populations within the gastrointestinal tract. Some of these responses could be detrimental to surrounding tissues by causing inflammation and alterations in the immune response depending on the physicochemical nature of the colloid, the target microbial populations and the physiological conditions existing within specific locations of the gastrointestinal tract. The microbial populations within the gastrointestinal tract have coevolved with us and it directly influences gastrointestinal tract form, function, and stability. The microbial consortia within the intestines are vital to many aspects of normal host physiology, immune development, and in controlling infections. When colloid-containing foods are ingested, these particles are exposed to the spectrum of pH levels that exist from the stomach to the large intestines. These conditions could facilitate the release of colloids from the food matrix and/or metal ions from the particle core. Food-incorporated, aggregated, or free particles could get disseminated within the

gastrointestinal tract. Changes in the pH of the surrounding environment will modify the particles' size, increase the amount of leached metal ions, and influence the production of reactive oxygen species from the surface of the colloid [6, 58-61]. Perturbations in the microbial communities could be expected when there are changes associated with the colloid's surface or, as has previously been reported, when a digestion procedure is incorporated into the experimental design [62-65].

In this section, silver particles suspended in orange juice were investigated over dose-response and time course experimental designs. The focus was on relating the physicochemical properties of colloidal silver particles (e.g. size, size distribution, the production of bioavailable metals, particle surface charge and solution pH) to its influence on microbial cells within the small intestines of the gastrointestinal tract. First, the differences between planktonic bacterial cultures versus bacterial biofilms were analyzed using "digested" and "undigested" colloidal silver particles and silver nitrate salt solution. By systematically analyzing bacterial responses and changes in size, pH, surface charge and bioavailable ionic silver from the particles before, during, and after the study, physicochemical properties to ecological effects can be related.

5.2. Materials and methods

5.2.1. Experimental design

Silver particles (<100nm, 99.5% metal basis) and silver nitrate (99.9999% metal basis) were purchased commercially (from Sigma-Aldrich, St. Louis, MO). Pulp-free orange juice was purchased from a retail store (Tropicana Manufacturing Company, Inc, Bradenton, FL, USA). The orange juice was filtered using a 0.2 μm target syringe filter

to remove residual pulp prior to use (Thermo Fischer Scientific, Beverly, MA, USA). Three sample concentrations of 10, 50, and 100 mg/L of the colloidal silver particles suspended in orange juice were prepared. Experimental control samples of 10, 50, and 100 mg/L of the silver nitrate salt suspended in orange juice were also prepared.

To study the interaction between colloidal suspensions and the microbial populations within the gastrointestinal tract, it was essential that the test materials (colloidal silver and silver nitrate) be incorporated in a food matrix (orange juice) and subsequently exposed to the pH changes postulated to occur within the gastrointestinal tract. Figure 1 outlines the experimental design of exposing the colloidal silver in juice and silver nitrate in juice samples to fluctuating pH conditions to simulate the gastrointestinal tract. The protocol of Glahn et al was used with slight modification and described in 4 steps [163]. Step 1: the pH of the starting material (colloidal silver in juice and silver nitrate in juice) was determined to be pH 4.0. Step 2: the pH of the colloidal silver in juice and silver nitrate in juice was adjusted to pH 2.0 using 5M HCl and 5% of pepsin solution (pepsin obtained from porcine gastric mucosa, Sigma-Aldrich, St. Louis, MO). This mixture was then placed in a water bath with shaking at 37°C for 1 hr. Step 3: the pH of each of these samples was raised to 6.0 with 1 M $NaHCO_3$. 25% of pancreatic-bile solution was added. Step 4: The pH was adjusted to 7 with 1 M NaOH. The volume was raised to 7.5 mL with 120 mM NaCl and 5 mM KCl.

5.2.2. Survival and growth patterns of E. coli ATCC 25922 strain

E. coli ATCC strain 25922 *(*American Type Culture Collection, Manassas, VA), a prototypical *E. coli* strain that is present in the gastrointestinal tract was used in this

study. *Luria-Bertani (LB) broth and* Tryptic Soy Agar (TSA) (Difco, Lawrence, KS) were used for culturing and plating purposes. The starting concentrations of colloidal silver in juice and silver nitrate in juice were 10, 50, and 100 mg/L. After the digestion and incubation with *E. coli* 25922, the samples were eventually diluted 10X in LB broth to yield final dosing concentrations of 7, 33, and 67 mg/L. As experimental controls, colloidal silver and silver nitrate were also suspended in phosphate buffer saline (PBS) solution. In this control study, the final concentration after 10X dilution in LB broth was also 7, 33, and 67 mg/L.

An overnight culture of *E. coli* was centrifuged to pellet the cells. The cell pellet was washed with PBS and its concentration was adjusted to approximately 10^7 CFU/mL (OD_{600}=0.1). An aliquot (7.5 μL) containing approximately 10^5 CFU was added to 50 mL tubes containing 7.5 mL of colloidal silver in juice or silver nitrate in juice. The experimental treatments were filtered orange juice (control), colloidal silver in juice, and silver nitrate in juice. The samples were incubated at 37°C in a water bath with shaking. Samples were removed at 0, 2 and 4 hours and the size of the surviving *E. coli* population was determined using TSA plates. The plates were incubated at 37°C for up to 48 hours prior to enumeration.

5.2.3. Biofilm inhibition assay

Biofilm assays were performed in 96-well round-bottomed polystyrene plates. The biofilm assay was described by Jesudhasan et al [164]. Briefly, an overnight culture of *E. coli* was adjusted to OD_{600}=1.30, washed in PBS, and diluted (20X) in LB broth, LB containing colloidal silver, and LB containing silver nitrate. After exposure for 1

hour, 100 μL aliquots from each experimental treatment were added to 8 replicate wells. The plates were incubated at 37°C for 4 d without shaking. After incubation, the samples were removed using a pipette, and the plates were washed with distilled water. The wells were stained with 0.1% crystal violet (Fisher, Hanover Park, IL) for 15 min. The excess dye was removed by washing with distilled water. The dye associated with the attached biofilms was dissolved in 200 μL of 95% ethanol for 10 min. An aliquot (125 μL) was transferred to an optically clear flat-bottom 96-well plate (Corning, Lowell, MA) and OD_{590} was measured.

5.2.4. Cell membrane integrity

The integrity of the bacterial cell membranes after exposure to the experimental treatments was confirmed using the LIVE/DEAD BacLight™ Bacterial Viability kit (L7012, Molecular Probes Inc., Eugene, OR). The LIVE/DEAD BacLight™ assay was used per the manufacturer's instructions. Live cells are supposed to have intact membranes and are impermeable to propidium iodide (PI), which only influxes into cells with disrupted membranes. Syto-9 is a membrane-permeable dye that can enter all cells. The combination of these two dyes provides a rapid and reliable method for discriminating live (fluorescence green) and dead bacteria (fluorescence red). Staining protocol was followed as proposed by the manufacturer. The fluorescence was measured in a micro plate reader. Each experiment was repeated 9 times. Analyses of viable *E. coli* cells after exposures to either colloidal silver in juice or silver nitrate in juice - i.e., percentages of viable and culturable cells and percentages of viable but nonculturable cell state (VBNC) was determined using conventional plate count procedures [165].

5.2.5. Particle characterization

The colloidal silver in juice sample was characterized for size (i.e., hydrodynamic diameter), zeta potential (i.e., surface charge) and dissociated silver ion content (i.e. Ag^{+}) at specific time points in the experimental design. The hydrodynamic diameter and zeta potential of samples was measured using a Zeta Sizer Nano Series ZEN 3600 Spectrometer (Malvern Instruments Ltd, Malvern, Worcestershire, UK). The dissociated silver ions (Ag^{+}) in the particle suspensions were measured using a silver/sulfide ion selective half-cell electrode (ISE) and a silver/silver chloride (Ag/AgCl) reference electrode (Thermo Fisher Scientific, Beverly, MA, USA).

5.2.6. Statistical analysis

Each experiment described was replicated at least three times and repeated at least three times on different days. The data from each of the independently replicated experiments was statistically analyzed using the Student's t test for pair comparison. Probabilities less than 0.05 were considered significant at $p < 0.05$.

5.3. Results

This study investigated the interaction between particles (i.e. colloidal silver) incorporated in a food matrix (i.e. orange juice) and candidate microbial population found within the gastrointestinal tract (namely *E. coli* ATCC strain 25922) using an *in vitro* simulation of the pH changes occurring during digestion.

5.3.1. Experimental design

Figure 5.1 outlines the methodology used in this study that more accurately represents the state that the colloidal silver would be if ingested with a food matrix such as orange juice (i.e., the gastrointestinal tract would not be exposed to "undigested" colloidal silver, but rather exposed to "digested" silver).

The systematic scheme showcases a simulated "digestion" protocol integrated with bacterial bioassays and particle characterization. The bacterial bioassays include growth curves, biofilm formation, and viable but not culturable (VBNC) cell status. The particle characterization includes analyses of particle size, zeta potential, and free silver metal ion at different time points at each step of the digestion protocol. These time points correspond to locations of the gastrointestinal tract where a significant pH change is observed (i.e., *Step 1* = pH 4.0, *Step 2* = pH 2.0, *Step 3* = pH 6.0, and *Step 4* = pH 7.0).

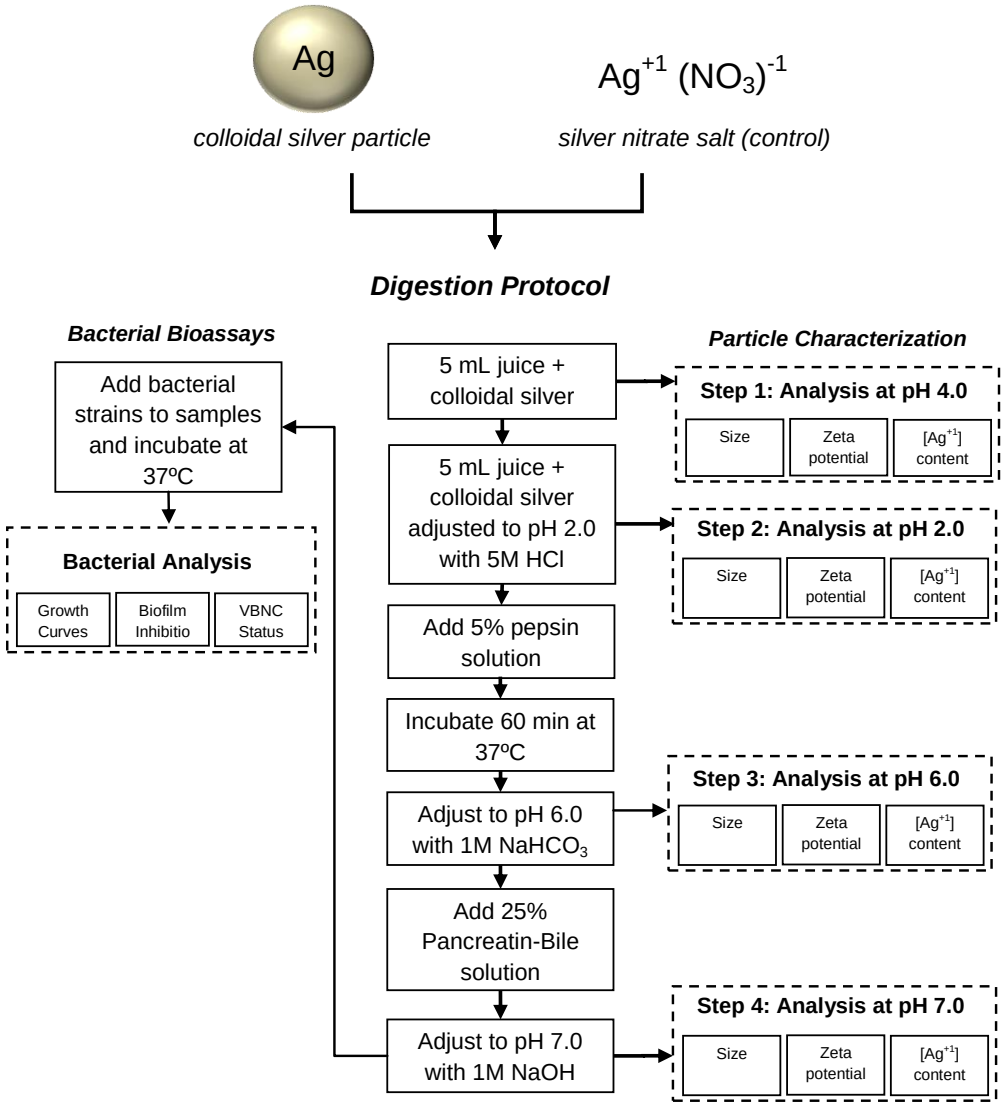

Figure 5.1. Experimental design. The response of colloidal silver in juice and silver nitrate in juice to microbial populations via bacterial bioassays was investigated in a simulated digestion protocol that mimics the conditions within the gastrointestinal tract.

5.3.2. Survival and growth patterns of E. coli ATCC 25922 strain

Figure 5.2 shows the survival of *E. coli* ATCC strain 25922 on exposure to digested orange juice (control), colloidal silver in orange juice, and silver nitrate in

orange juice. For all experiments, the exposure time points are on par for the time of digestion after ingestion, i.e. 4 hours is the average residence time of foods in the gastrointestinal tract [166]. The experiments were performed over dose (7, 33, and 67 mg/L) and time (0, 2, and 4 hr). The results show that the growth of *E. coli* was completely inhibited by the silver nitrate in orange juice over concentration and over time. However, neither the orange juice nor the colloidal silver in orange juice showed any effect on the growth rate of *E. coli* even after 4 hours of incubation time. This reduced toxicity effect may be attributed to the fact that the colloidal particles in the juice suspension stay intact as particles and do not leach silver ions from the particle surface during the digestion process. The silver nitrate, on the other hand, contains more bioavailable silver ions as compared to silver particles and therefore decreased *E. coli* cell growth rates.

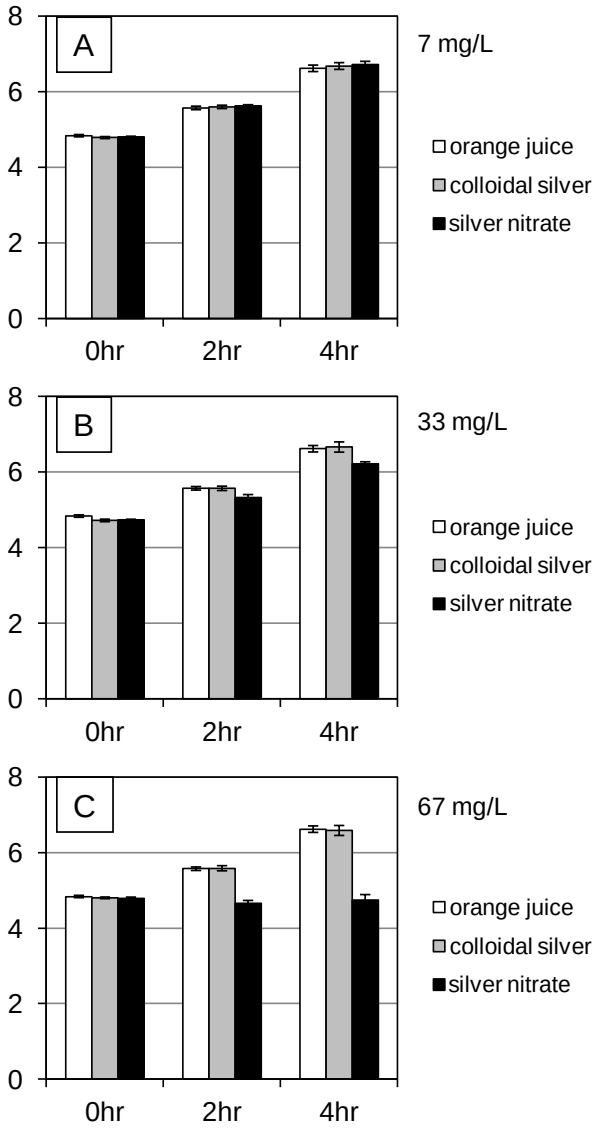

Figure 5.2. Survival and growth patterns of E. coli ATCC 25922 strain in orange juice with digestion. The survival of E. coli ATCC strain 25922 on exposure to) digested orange juice (control), colloidal silver in orange juice, and silver nitrate in orange juice over doses of (A) 7 mg/L, (B) 33 mg/L and (C) 67 mg/L.

As experimental controls, colloidal silver and silver nitrate were also suspended in phosphate buffer saline (PBS) solution. Figure 5.3 shows the survival and growth patterns of *E. coli* ATCC 25922 strain in PBS with digestion.

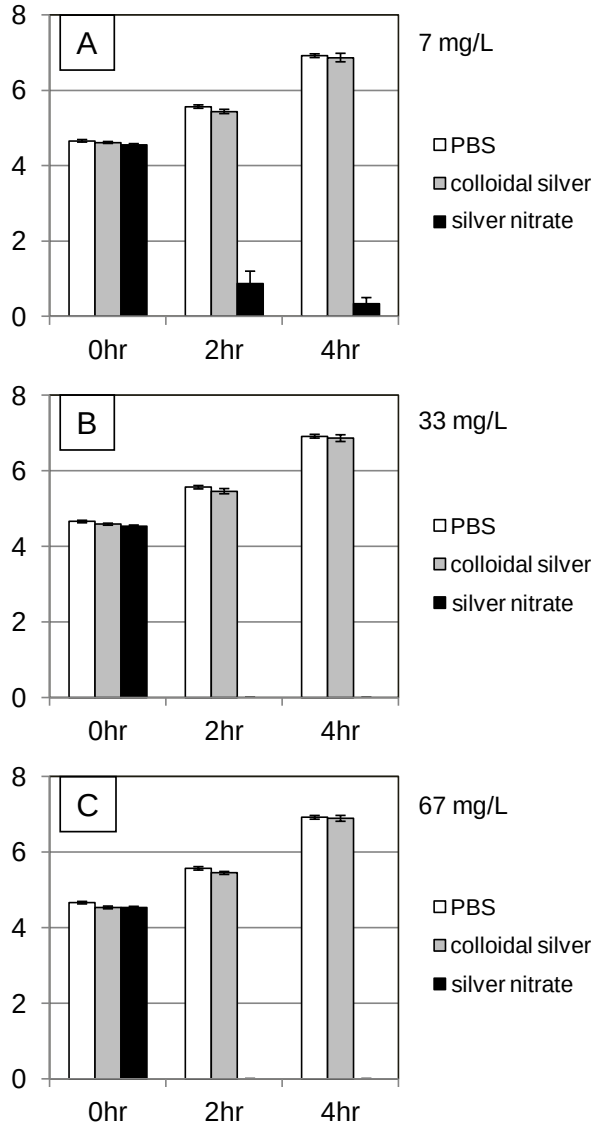

Figure 5.3. Survival and growth patterns of *E. coli* ATCC 25922 strain in PBS with digestion. The survival of *E. coli* ATCC strain 25922 on exposure to PBS (control), colloidal silver in PBS, and silver nitrate in PBS over doses of (A) 7 mg/L, (B) 33 mg/L and (C) 67 mg/L.

5.3.3. Biofilm inhibition assay

Though studying the effects of particles on unattached (planktonic) bacterial cells in suspension is both critical and traditional to evaluate toxicity, the effects on bacterial cells in biofilms may, however, be more realistic. Results of colloidal silver in juice and silver nitrate in juice are shown in Figure 5.4. Using data from Figure 5.2, we proceeded to re-evaluate the effects of "digested" versus "undigested" colloidal silver and silver nitrate in orange juice on biofilm formation. For this study, we only investigated effects at the high dose, i.e., 67 mg/L. These results showed that unlike the previous data set (Figure 5.2), the colloidal silver inhibited biofilm formation significantly when compared to (1) "undigested" colloidal silver particles, (2) "digested" silver nitrate, and (3) "undigested" silver nitrate.

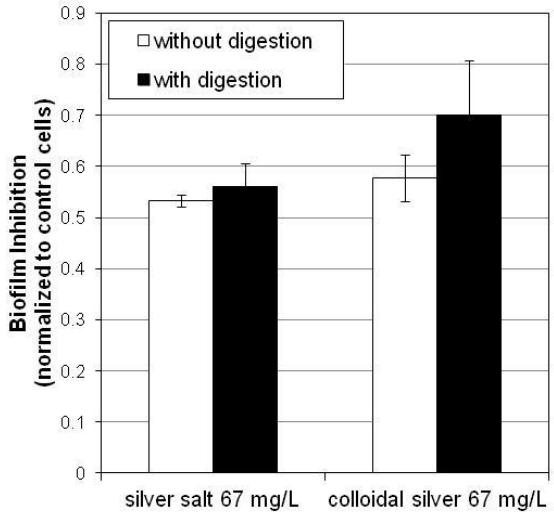

Figure 5.4. Biofilm inhibition assay. Biofilm inhibition after exposure to colloidal silver in orange juice and silver nitrate in orange juice were evaluated at 67 mg/L. Data is represented as biofilm inhibition vs. sample concentration. The black bars represent the effect of "digested" colloidal silver in juice and silver nitrate in juice sample while the white bars represent the effects of the "undigested" samples.

5.3.4. Cell membrane integrity

The inhibition on *E. coli* growth was observed by using the plate count assays in which *E. coli* was incubated in the presence of colloidal silver particles and silver nitrate. A LIVE/DEAD BacLight™ Bacterial Viability kit was used to evaluate the membrane integrity of the bacterial cells as depicted in Figure 5.5. As shown in the micrographs, colloidal silver and silver nitrate caused fairly high percentages of compromised cells at the dose of 33 and 7 mg/L, respectively. Dose-response relationships were plotted for silver colloids/salt versus the growth of *E. coli*. When the dosages of colloidal silver were raised from 7 to 67 mg/L, the percentages of "dead" cells (lacking membrane integrity) increased from 0% to 95%. Although the digested silver nitrate had a greater viable but not culturable (VBNC) state on the cells at a lower concentrations in comparison to digested colloidal silver particles, both the silver colloids and silver nitrate created a completely VBNC state. Specifically, the percent VBNC after exposure to silver colloids at the 7 mg/L dose was 15%; at 33 mg/L dose was 39%; and 67 mg/L was 3%. For the silver nitrate exposure, only the lowest dose (7 mg/L) resulted in any type of viable cell population. The percent VBNC for this exposure group was 34%. Information reported in the Figure 5.5 is the average of all cells counted in approximately 10 images per concentration per replicate.

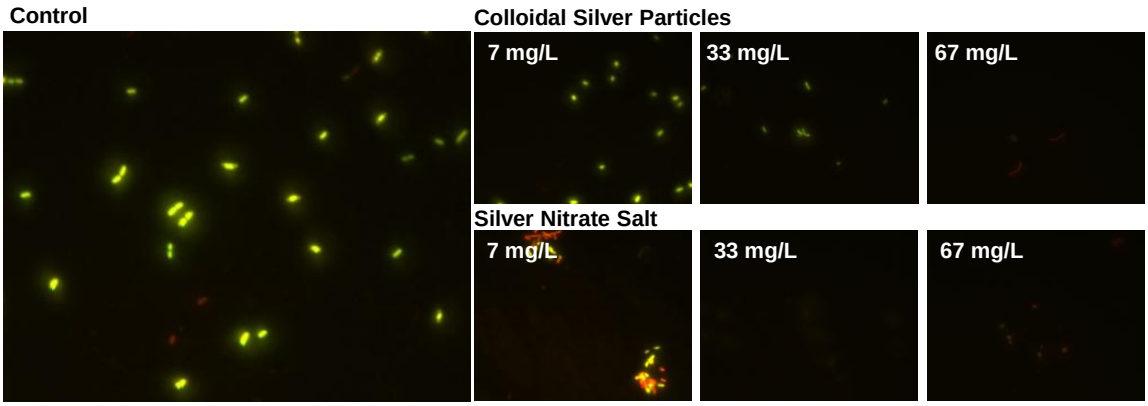

Figure 5.5. Cell membrane integrity. Fluorescent microscopic images of E. coli ATCC 25922 after exposure to colloidal silver in juice and silver nitrate in juice after incubation for 4 hours.

5.3.5. Particle characterization

Silver ion concentration is frequently reported as "total silver" measured in ppm measurements. In our study, for the colloidal silver in juice samples, total silver consists of silver in two distinct forms – silver particles and silver ions. While the dynamic light scattering technique measures the hydrodynamic diameter and surface charge of silver particles, the ISE (ion selective electrode) probe detects the silver ion content in the suspensions. Hence the colloidal silver in juice samples were characterized for size distribution, zeta potential, and dissociated silver ion concentration over the four steps in the digestion protocol to study the effects of silver particle characteristics in the digestion process. Figure 5.6 shows the size distribution profile of the silver particles in orange juice at the 3 specific dosing concentrations used in this study: 7, 33, and 67 mg/L.

Changes in size distribution over time and concentration. The changes in the size and size distribution of the colloidal silver suspensions at each step of the digestion protocol are shown in Figure 5.6. At the lowest pH of the digestion protocol, i.e., pH 2.0, the size profile of the particles exhibited a bimodal distribution for each concentration used in the study. On the other hand, at the highest pH of the digestion protocol, i.e., pH 7.0 the size profile of the particles exhibited a unimodal distribution for each concentration used in the study. Also, at pH 7.0, the width of the size peak is the narrowest and the height of the peak is at its maximum for each concentration. Hence, the average hydrodynamic diameter of the silver particles at the final step in the digestion protocol (pH 7.0) was less than 200 nm at every concentration providing evidence that the particles in suspension were indeed in the nanometer scale.

Changes in zeta potential over time and concentration. For the zeta potential measurements, the colloidal silver in juice suspension consistently measured slightly negative as shown in table 5.1. There was little fluctuation in the measured zeta potential value over the digestions steps and among the concentrations used in the study, implying that the surface charge of the particles were unaffected before and after digestion.

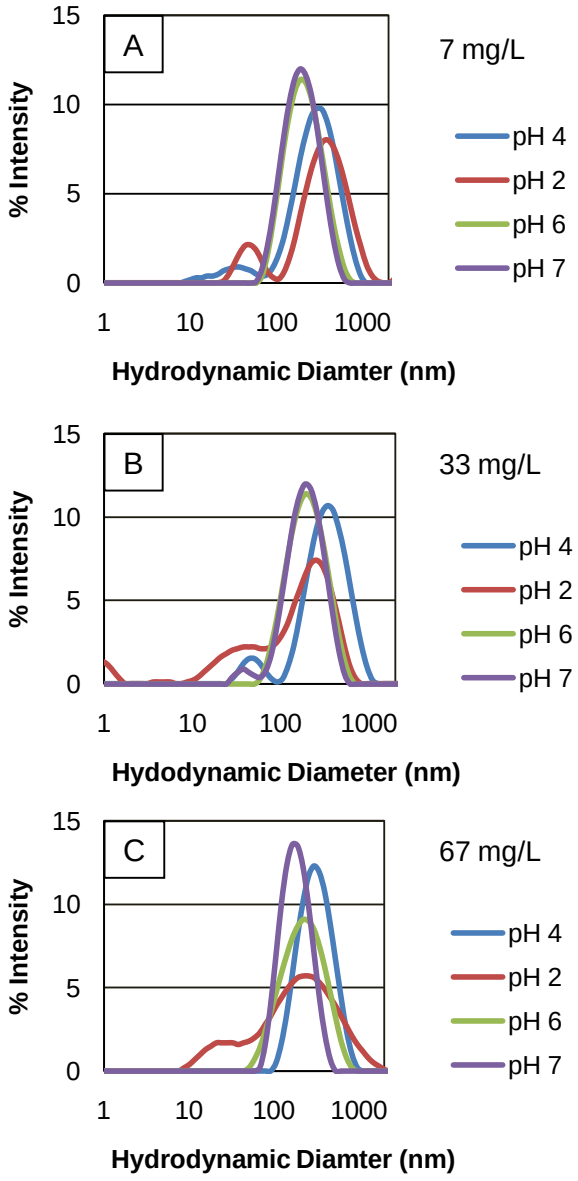

Figure 5.6. Changes in size distribution over time and concentration. The dynamic light scattering profile of colloidal silver particles in orange juice at each step of the digestion protocol was plotted. Data is represented as % intensity vs. hydrodynamic diameter of colloidal silver in juice at (A) 7 mg/L, (B) 33 mg/L, and (C) 67 mg/L.

Table 5.1. Colloidal silver particle surface charge over time and concentration. The table includes the zeta potential values of the colloidal silver particles. Step 1 = analysis at pH 4.0, Step 2 = analysis at pH 2.0, Step 3 = analysis at pH 6.0, and Step 4 = analysis at pH 7.0.

Steps in Digestion Process	Zeta Potential (mV)		
	7 mg/L	33 mg/L	67 mg/L
Step 1 = pH 4	-6.07	-6.69	-2.32
Step 2 = pH 2	-0.838	-0.526	-0.731
Step 3 = pH 6	-6.77	-6.05	-0.749
Step 4 = pH 7	-6.77	-7.01	-5.91

Changes in dissociated silver ion concentration over time and concentration. For the dissociated silver (Ag^+) ion measurements, the iso-electric probes were calibrated using standard $AgNO_3$ salt solutions. The probe measures the electric potential as a "mV" reading over concentration. The literature suggests a 58 mV per decade increase in concentration is needed to ensure calibration [167]. In order to effectively translate the probe's readings to a concentration of Ag^+ ions for the colloidal silver juice samples, another calibration graph was plotted. This time, however, silver nitrate in orange juice suspensions was used. Again, the 58 mV per decade increase in concentration was observed. The results are represented in Table 5.2. The table shows the dissociated Ag^+ ion concentration decreasing over the steps in the digestion protocol for all concentration ranges. We conclude that the simulated digestion procedure contributed towards quenching the toxicity of colloidal silver because there are significantly less bioavailable Ag^+ ions after digestion when compared to the sample before digestion.

Table 5.2. Colloidal silver particle and bioavailable silver metal ion detection over time and concentration. The table shows the dissociated Ag+ concentration over the steps in the digestion process for the 7 mg/L, 33 mg/L and 67 mg/L concentrations. Step 1 = analysis at pH 4.0, Step 2 = analysis at pH 2.0, Step 3 = analysis at pH 6.0, and Step 4 = analysis at pH 7.0.

Steps in the Digestion Process	**7 mg/L**	
	Actual ISE reading (mV)	Dissociated Ag+ ion (mg/L)
Step 1 = pH 4	31.8	6.84×10^{-4}
Step 2 = pH 2	14.2	3.63×10^{-4}
Step 3 = pH 6	-90.2	8.48×10^{-6}
Step 4 = pH 7	-125.3	2.40×10^{-6}
Steps in the Digestion Process	**33 mg/L**	
	Actual ISE reading (mV)	Dissociated Ag+ ion (mg/L)
Step 1 = pH 4	21.5	4.72×10^{-4}
Step 2 = pH 2	6.6	2.76×10^{-4}
Step 3 = pH 6	-112.6	3.79×10^{-6}
Step 4 = pH 7	-150.3	9.75×10^{-7}
Steps in the Digestion Process	**67 mg/L**	
	Actual ISE reading (mV)	Dissociated Ag+ ion (mg/L)
Step 1 = pH 4	10.5	3.18×10^{-4}
Step 2 = pH 2	-8.4	1.61×10^{-4}
Step 3 = pH 6	-152.1	9.14×10^{-7}
Step 4 = pH 7	-167.4	5.27×10^{-7}

There were little changes in colloidal silver in juice size distributions, zeta potential measurements, and leaching of bioavailable silver ions over the steps in the digestion protocol. Therefore, we conclude that the effects observed in bacterial growth and the ability to form a biofilm were due to the exposure to intact silver particles and

not to leaching silver ions from the particle surface. Hence, this study has provided us with a physiological-relevant approach to characterize microbial responses to colloidal particles that would be applicable for a variety of safety assessments.

5.4. Discussion

Colloidal silver has been regarded as an inert suspension of particles and used regularly throughout the 19^{th} and 20^{th} centuries as a therapy to illness. In addition, colloidal silver is believed to be antimicrobial to a variety of microbes. These more "traditional" colloidal suspensions of silver particles include a polydisperse size population with a polymer or acidic surface capping agent as well as residual ions from the starting material such as Ag+, SO_4^-, or NO_3^-. When the entire population of silver particles is on the size scale of 20-30 nanometers, the effects of the particles are different than free ionic silver [168]. The toxicity of silver particles to bacteria has been previously examined [169-171], and the possible mechanism of silver particle toxicity is that the particles adsorb onto the surface of the cell, damage bacterial membrane, and cause death [169, 170]. Another possible mechanism of silver particle toxicity is the leaching of silver metal ion from the particle surface that crosses the cell wall and membrane and participate in mimicry, thus interfering with normal protein function. The toxicity of colloidal silver particles to bacteria in culture medium is well studied [6, 59, 172-174]; however, the physicochemical properties of silver particles when present in foods or drinks and subsequent behavior in the gastrointestinal tract have not been reported.

This research is significant because it addresses a contemporary issue namely, colloidal particles and their potential human health impacts that arise due to the emerging applications of particles in foods. Colloidal-induced toxicological pathways are not well understood. Questions such as: Are there direct interferences? Are there indirect consequences? are still unanswered. There are also not many methods available to gauge colloidal particle toxicity in complex matrices like food in order to assess the risk of use.

5.5. Summary

The results from the bacterial viability assays and physicochemical characterization studies confirm that the colloidal silver in the juice suspension stay intact as particles and do not leach silver ions from the particle surface during the "digestion" process. "Digested" particles have little effect on planktonic bacteria colonies, but do inhibit biofilm formation. Hence, we conclude that the state in which bacterial cells are and gastrointestinal digestion both play a significant role in quenching the potential toxicity of silver particles towards commensal bacteria in the gastrointestinal tract. This study provides a framework for a physiological relevant approach to characterize microbial responses to colloidal particles that would be applicable to safety and toxicity assessments. The experimental design of the colloidal silver in juice and silver nitrate in juice samples subjected to a simulated digestion protocol that mimics the conditions within the gastrointestinal tract allows for a more representative study of the species response to Ag in the gastrointestinal tract.

6. SUMMARY AND FUTURE RESEARCH DIRECTIONS

6.1. Summary

The unique properties of nanomaterials are being exploited by various academic laboratories, commercial sectors, as well as government agencies, in order to add value to existing products and enable new product development. These technical advances in the rapidly growing field of nanotechnology must be balanced with detailed toxicity assessments to assess the benefits and risks of such emerging technology. If the risks are considered earlier in the stage of a new technology, then the costs of identifying the important environmental and/or health impacts once that technology has been widely diffused can be minimized.

The research objectives described in this dissertation are novel and relevant, given this explosive nature of the nanotechnology sector. There is an urgent need to responsibly design products and develop new technologies with adequate attention devoted to understanding the risks. This was achieved via material characterization techniques, predictive toxicity assays and hazard identification capabilities. The findings of this work will help the scientific community make more informed decisions about the design features and steps that should be taken for the safe use of nanotechnology.

The overall aim of this study was to investigate two scenarios of a nano-enabled product:

1. A nano-enabled product that is beyond scientific journal phase and currently in the market place (i.e., a current nanotechnology), and

2. A nano-enabled product that is still in the basic science phase (i.e., a novel nanotechnology).

The extensive utilization of nanomaterials for new products for the building envelope is expected to expand rapidly; however, the uncertainly regarding safety of these novel materials to humans and the environment requires study in parallel to their incorporation into consumer products. One way to gather information critical to the development of safe nanomaterials is a product life cycle approach. Three brands of commercially-available TiO_2 NPs were incorporated into lab-formulated paint and lacquer products. This specific research investigated a nano-enabled white paint product and a lacquer formulation as a case study, with TiO_2 NP as a "model" NP. Real world end-of-life stages were mimicked by subjecting the nano-enabled products to wear-and-tear scenarios. The pristine and end-of-life powders were analyzed via material characterization techniques and toxicity assessments. Electron microscopy and elemental analysis confirmed the presence of TiO_2 NPs in the worn-and-torn paint and wood matrices for all three NP types. FTIR, on the other hand, proved to be a useful characterization tool for the nano-enabled paint samples, but the nano-enabled wood samples warrant further investigation. These results validate the usefulness of TEM, SEM and EDX as a predictive tool for analyzing worn-and-torn nano-enabled products. FTIR as a characterization technique, however, is only valid when relatively high concentrations of the NPs are incorporated into the products.

While there is a vast body of nanotoxicology literature on pristine, as produced NPs, studies that test a nano-enabled product or the end-of-life stages of a nano-enabled

product is scare. To address this gap in the literature, toxicity of the nano-enabled products in their pristine and end-of-life stage was assessed *in vitro* using immortalized human lung epithelial cells, A549. Results from cell viability and reactive oxygen species generation assays showed differential toxicological responses between pristine and worn-and-torn powders, and among the three NP types. Thus, a life cycle approach will help provide methodologies for understanding nanomaterial properties in the context of developed consumer products. A proactive approach such as the application of a life cycle coupled with *in vitro* toxicity testing for a current nano-based application will provide critical information that will help evaluate potential health and environmental risks and benefits of a nano-scale technology. Furthermore, mimicking real world scenarios and developing products "in-house" provides a more realistic platform for data interpretation and the identification of risk triggers.

The novel synthetic scheme presented for the creation of a nanosilver core-deltamethrin shell conjugate to be used as an active agent against insect vectors is a refreshing concept. This nanoconjugate and miniature biological system has the potential to effectively address many of the shortcomings of traditionally utilized pesticides such as inconsistent reapplication. Every day, people and animals contract debilitating and life threatening diseases due to bites from infected flies, ticks, and mosquitoes. The current methods utilized to fight against these diseases are only partially effective or safe for humans and animals. When it comes to insect vector control, a conceptual paradigm shift is urgently needed. As a proof of concept, we conjugated nanosilver to the pyrethroid pesticide deltamethrin. Firstly, electron microscopy and FTIR verified the

presence of a 15 nm nanosilver core surrounded by deltamethrin. Secondly, when the conjugate was exposed to mosquitoes for a 24-hour bioassay, mortality was observed at $9x10^{-4}$ ppm. Silver was detected in the hemolymph of mosquitoes exposed to the conjugate. We concluded that the newly developed nanoconjugate did not inactivate the primary function of the pesticide and was effective in killing mosquitoes at low concentrations. By simply altering the nano-biochemistry of the synthesis scheme, we open up the possibilities of creating several other NP-pesticide core-shell nanoconjugate models that can be tested in other biological systems. This is a paradigm-shifting technology and will have a significant impact on both basic understanding of nano-chemistry as well as application of such novel technology towards vector control.

In an effort to evaluate the safety of our newly developed conjugate, PENS was tested in neuronal cultured cells to compare the cytotoxic responses to the unconjugated pesticide deltamethrin – a known neurotoxic agent and pristine silver NPs. The pheochromocytoma of the rat adrenal medulla, PC12 cell line was chosen as a model neuronal culture system. After 24 hours of incubation, cell viability and intracellular reactive oxygen species (ROS) were measured. Bright field images of high dose exposures to dosing solutions were also acquired to evaluate cell morphology. Exposure to PENS resulted in a 17% decline in viability at the highest concentration of 45 μM while exposure to deltamethrin caused a 47% decrease. These results suggest that cellular viability was less adversely affected by PENS than by the deltamethrin. Also, ROS production following PENS exposure indicated that the newly developed conjugate was responding in a similar manner as that of cells treated with deltamethrin only. Thus,

the promise of nanotechnology to improve the everyday activities of our life seems unlimited.

The synthesis, characterization, efficacy studies, and *in vitro* toxicity of the novel nanoconjugate not only opens up research avenues for new technological breakthroughs towards vector control but also enhances the collaborations over cross-disciplinary fields. The findings of this work will provide a useful initial framework in prioritizing future nanotechnological research needs and have a significant impact on material scientists, toxicologists and engineers alike.

Lastly, designing an *in vitro* digestion model to explore the effect of orally ingested AgNPs is significant because it addresses a contemporary issue namely, NPs and their potential human health impacts that arise due to the emerging applications of particles in foods. There are also not many methods available to gauge NP toxicity within the gastrointestinal tract in order to assess the risk of intended and unintended use. Furthermore, simulating human digestion scenarios is physiologically relevant and provides a more realistic platform for interpretation, validation and correlation of results.

6.2. Future research directions

Due to practical limitations such as resources, several research opportunities could not be pursued in great detail in this current work. The following section outlines some interesting directions for future research.

6.2.1. Aerosol detection and characterization during TiO_2 sanding process

As mentioned in Section 2, the Taber test is one of the most commonly used test for simulating the abrasive damage during the service life of a product. As a result of sanding the surface of the nano-enabled product, NPs are released into the air. The uncertainties concerning possible hazard to health, safety and the environment due to NP release from a surface are unknown. Measuring and quantifying this airborne particle concentration could be a noteworthy future research direction. The development of an exposure chamber system coupled with an aerosol generator methodology would prove to be a robust aerosolized particle characterization system. The released particles can be analyzed using an aerodynamic particle sizer to measure the particle size distribution in the micrometer size range (0.5 – 20 μm) and a scanning mobility particle sizer for the determination of the number size distribution can be employed to measure relatively smaller particles, in the range of 10 - 800 nm. A battery of other useful characterization techniques such as a hand-held aerosol monitor, membrane filter elements for determining the dust concentration or a condensation particle counter for measuring the particle concentration can be built into the chamber.

6.2.2. Characterization of AgNPs in digestive fluids

Engineered NPs are being explored to improve current technologies, and AgNPs, in particular, are being incorporated for innovative food packaging applications to provide longer shelf-life for foods, better barrier properties, improved heat resistance and temperature control, among other advantages [153, 175]. The anti-microbial and anti-fungal protections offered by AgNPs make these NPs ideal candidates not only in food

packaging and processing applications (such as antimicrobial kitchenware coatings), but also in food itself [6, 7, 150, 161]. However, in order to increase the safety of nano-enabled food product while decreasing the uncertainty surrounding its exposures, research in developing a physiologically relevant model to assess the safety of engineered nanomaterials is needed. If these NPs are used in food/food packaging applications without fully understanding the consequences, then we threaten the security of our food supply chain and increase our susceptibility of pathogenic microbes, such as *Clostridium spp.*, and the onset of autoimmune diseases, like Celiac disease [175, 176].

Section 5 investigated the physicochemical changes and possible perturbations to microbial communities within the gastrointestinal tract. However, electron microscopy studies were not included to visually analyze changes in the particle sizes and morphology. Additionally NP in the mouth (i.e., in artificial saliva) wasn't included in the digestion model. In order to address this gap, the introduction and characterization of NPs within this digestive model is a novel and powerful approach to assess physicochemical changes that AgNPs undergo during digestion. This information is critical in identifying hazards within a risk assessment framework. An *in vitro* digestion model is a three step procedure that simulates the digestion process in the gastrointestinal tract of humans i.e., the conditions in the mouth, the stomach and the small intestine. The model mimics the human system by applying physiologically relevant conditions, such as chemical composition of digestive fluids, pH and residence time of food within each compartment [177]. The large intestine is not taken into

consideration in this model because *in vivo* food absorption and digestion are known to occur in the small intestine.

Preliminary results. The digestive fluids, i.e., artificial saliva, gastric juice, duodenal juice and bile juice were prepared in the laboratory using milli-Q ultrapure water (18.2 mΩ) as previously published [177]. Before incubations, the digestive fluids are heated to 37˚C. The digestion experiment is started with the introduction of 6 mL of artificial saliva into 1 ml of 10 μg/mL AgNP solution. The mixture is rotated head-over-heels for 5 min. Subsequently, 12 mL of gastric juice is added and this mixture is rotated head-over-heeds for 2 hours. Finally, 12 mL of duodenal juice, 6 mL of bile juice and 2 mL of $NaHCO_3$ solution are added. The mixture is rotated head-over-heels for 2 hours. The pH of the samples after every step is continuously monitored.

Samples at the end of every digestion step – i.e., AgNP + salvia, AgNP + saliva + gastric juice, AgNP + saliva + gastric juice + duodenal and bile juice were characterized for size, shape, aggregation states and topography using transmission and scanning electron microscopy. Chemical compositions were confirmed using energy dispersive X-ray spectroscopy.

Figure 6.1 shows the SEM, TEM and EDX of undigested and digested AgNPs. Figure 6.1A and Figure 6.1B are the SEM and TEM of undigested AgNPs i.e., AgNPs suspended in milli-Q water, respectively. The micrographs reveal fairly aggregated, 200nm sized AgNPs. EDX confirms these electron dense particles to be silver. Figure 6.1D through Figure 6.1L are the SEM, TEM and EDX spectra of the AgNPs in the digestive fluids. Since the digestive fluids are made up of both inorganic as well as

organic compounds, imaging the AgNPs in the digestive fluids becomes challenging. However, EDX spectra confirmed the presence of silver at each stage of the digestion implying that human gut epithelium is likely to be exposed to AgNPs if ingested (Figure 6.1F, Figure 6.1I and Figure 6.1L).

Figure 6.1D and Figure 6.1E are SEM and TEM of the AgNP in stage 1 of the digestion model, i.e., in the artificial saliva (pH 6.8), respectively. SEM reveals the presence of AgNPs embedded within a matrix (Figure 6.1D). In addition to inorganic salts, the artificial saliva consisted of organics such as urea, amylase, uric acid and mucin. This matrix was therefore formed as a result of these organic compounds in the simulated saliva preparation. The electron dense portions of the TEM (Figure 6.1E) and Ag peaks in the EDX spectra (Figure 6.1F) confirm the presence of AgNPs in stage 1 of the digestion model.

Figure 6.1G and Figure 6.1H are SEM and TEM of the AgNP in stage 2 of the digestion model, i.e., in the stomach (pH 2-3), respectively. The significant decrease in pH from a neutral regime to a highly acidic environment resulted in micron-sized Ag aggregates. Similar to stage 1, both SEM and TEM reveal silver-embedded in a complex organic matrix. EDX confirms the presence of silver (Figure 6.1I). Additionally, EDX revealed a chlorine peak. This chlorine peak is due to the addition of hydrochloric acid during the gastric juice preparation. The role of the hydrochloric acid was to lower the pH from 6.8 to 2 in order to mimic conditions in the stomach. Figure 6.1J and Figure 6.1K are SEM and TEM of the AgNP in stage 3 of the digestion model, i.e., in the small intestine (pH 8.1-8.2), respectively. The small intestine is made up of duodenal and bile

juice. Yet again, microscopy reveals AgNPs to be embedded within an organic matrix and EDX confirms the presence of silver within this dense organic matrix.

6.2.3. Use of co-culture models

Although *in vitro* cultures provide an easier, cheaper, and more ethical alternative to *in vivo* studies, many limitations exist. The relevance of isolated cells in petri dishes to communicative tissues in the body is often questioned. Though it is widely agreed *in vitro* studies have their limitations, the benefits, such as reduced cost and reproducibility, win out. There is currently a large global effort to improve *in vitro* systems by making them more representatives of *in vivo* conditions. One such improvement is seen in the use of co-culture systems (cultures containing more than one cell type) over monocultures (cultures consisting of one cell line). *In* vivo organs and tissues consist of multiple cell types. Communication between cells is known to have large impacts on cellular function. Therefore, in comparing *in vitro* cultures to biological systems, it stands to reason that including as many components of the respective tissue will increase biological relevance. For example, human colorectal epithelial cells (Caco-2) are often used in "gut" cultures for investigation of digestion, disease, or drug development. This single system, though relevant as a human derived cell line largely referenced in the literature, can be improved upon by addition of mucous producing cells of the intestine and/or bacteria of the micro biome. In co-cultures, a cellular response of one cell type may trigger in a response in a second cell type that would not be seen in monocultures. Thus, *in vitro* co-culture models are more sophisticated and better representative of conditions than monocultures.

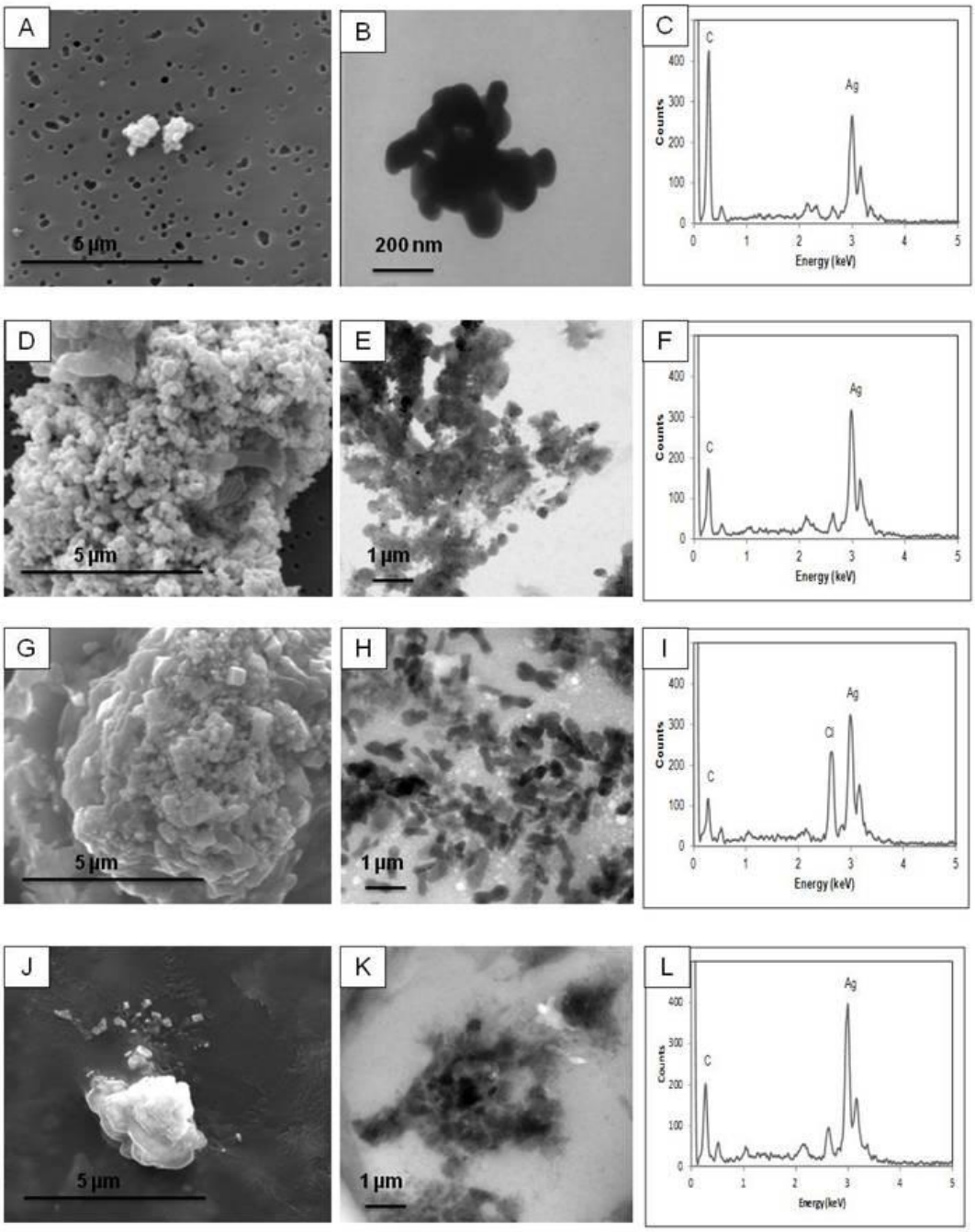

Figure 6.1. Material characterization via SEM, TEM and EDX of undigested and digested AgNPs.

REFERENCES

[1] McNeil, S.E., *Nanotechnology for the Biologist.* Journal of Leukocyte Biology, 2005. **78**(3): p. 585-594.

[2] Chen, X. and S.S. Mao, *Titanium Dioxide Nanomaterials: Synthesis, Properties, Modifications and Applications.* Chemical Reviews, 2007. **107**(7): p. 2891-2959.

[3] Salvador, A., et al., *Analytical Methodologies for Atomic Spectrometric Determination of Metallic Oxides in Uv Sunscreen Creams.* Journal of Pharmaceutical and Biomedical Analysis, 2000. **22**(2): p. 301-306.

[4] Pfaff, G. and P. Reynders, *Angle-Dependent Optical Effects Deriving from Submicron Structures of Films and Pigments.* Chemical Reviews, 1999. **99**(7): p. 1963-1981.

[5] Wijnhoven, S.W.P., et al., *Nano-Silver - a Review of Available Data and Knowledge Gaps in Human and Environmental Risk Assessment.* Nanotoxicology, 2009. **3**(2): p. 109-138.

[6] Sondi, I. and B. Salopek-Sondi, *Silver Nanoparticles as Antimicrobial Agent: A Case Study on E-Coli as a Model for Gram-Negative Bacteria.* Journal of Colloid and Interface Science, 2004. **275**(1): p. 177-182.

[7] Marambio-Jones, C. and E.M.V. Hoek, *A Review of the Antibacterial Effects of Silver Nanomaterials and Potential Implications for Human Health and the Environment.* Journal of Nanoparticle Research, 2010. **12**(5): p. 1531-1551.

[8] Aitken, R.J., et al., *A Multidisciplinary Approach to the Identification of Reference Materials for Engineered Nanoparticle Toxicology.* Nanotoxicology, 2008. **2**(2): p. 71-78.

[9] *Woodrow Wilson International Center for Scholars, 2011.* The Project on Emerging Nanotechnologies: Nanotechnology Consumer Products Inventory. Available from: http://www.nanotechproject.org/cpi/.

[10] Roco, M.C., C.A. Mirkin, and M.C. Hersam, *Nanotechnology Research Directions for Societal Needs in 2020: Summary of International Study.* Journal of Nanoparticle Research, 2011. **13**(3): p. 897-919.

[11] *National Institute of Standards and Technology (NIST),* 2009. US Deparment of Commerce: Environmental Leaching of Nanoparticles from Consumer Products. Available from: http://www.nist.gov/mml/csd/inorganic/leachnano.cfm.

[12] Lewinski, N., V. Colvin, and R. Drezek, *Cytotoxicity of Nanopartides.* Small, 2008. **4**(1): p. 26-49.

[13] Oberdörster, G., E. Oberdörster, and J. Oberdörster, *Nanotoxicology: An Emerging Discipline Evolving from Studies of Ultrafine Particles.* Environmental Health Perspectives, 2005. **113**(7): p. 823-839.

[14] Shukla, R.K., et al., *ROS-Mediated Genotoxicity Induced by Titanium Dioxide Nanoparticles in Human Epidermal Cells.* Toxicology in Vitro, 2011. **25**(1): p. 231-241.

[15] Oberdörster, G., et al., *Principles for Characterizing the Potential Human Health Effects from Exposure to Nanomaterials: Elements of a Screening Strategy.* Particle and Fibre Toxicology, 2005. **2**(8): p. 1-35.

[16] Auffan, M., et al., *Towards a Definition of Inorganic Nanoparticles from an Environmental, Health and Safety Perspective.* Nature Nanotechnology, 2009. **4**(10): p. 634-641.

[17] Sepeur, *European Coatings Tech Files. Nanotoxicology : Technical Basics and Applications* Hannover: Vincentz Network, 2008.

[18] Baan, R.A., *Carcinogenic Hazards from Inhaled Carbon Black, Titanium Dioxide, and Talc Not Containing Asbestos or Asbestiform Fibers: Recent Evaluations by an IARC Monographs Working Group.* Inhalation Toxicology, 2007. **19**(SUPPL. 1): p. 213-228.

[19] *IARC (International Agency for Research on Cancer): IARC Monographs on the Evaluation of Carcinogenic Risks to Humans*, 2010. p. 9-38.

[20] Saber, A.T., et al., *Nanotitanium Dioxide Toxicity in Mouse Lung Is Reduced in Sanding Dust from Paint.* Particle and Fibre Toxicology, 2012. **9**(4): p. 1-15.

[21] Nazarenko, Y., et al., *Potential for Exposure to Engineered Nanoparticles from Nanotechnology-Based Consumer Spray Products.* Journal of Exposure Science and Environmental Epidemiology, 2011. **21**(5): p. 515-528.

[22] Warheit, D.B., et al., *Pulmonary Toxicity Study in Rats with Three Forms of Ultrafine-Tio2 Particles: Differential Responses Related to Surface Properties.* Toxicology, 2007. **230**(1): p. 90-104.

[23] Sweet, L. and B. Strohm, *Nanotechnology - Life-Cycle Risk Management.* Human and Ecological Risk Assessment, 2006. **12**(3): p. 528-551.

[24] Som, C., et al., *The Importance of Life Cycle Concepts for the Development of Safe Nanoproducts.* Toxicology, 2010. **269**(2-3): p. 160-169.

[25] Mueller, N.C. and B. Nowack, *Exposure Modeling of Engineered Nanoparticles in the Environment.* Environmental Science and Technology, 2008. **42**(12): p. 4447-4453.

[26] Gottschalk, F. and B. Nowack, *The Release of Engineered Nanomaterials to the Environment.* Journal of Environmental Monitoring, 2011. **13**(5): p. 1145-1155.

[27] Abbott, L.C. and A.D. Maynard, *Exposure Assessment Approaches for Engineered Nanomaterials.* Risk Analysis, 2010. **30**(11): p. 1634-1644.

[28] Grieger, K.D., et al., *Analysis of Current Research Addressing Complementary Use of Life-Cycle Assessment and Risk Assessment for Engineered Nanomaterials: Have Lessons Been Learned from Previous Experience with Chemicals?* Journal of Nanoparticle Research, 2012. **14**(7): p. 958-981.

[29] Ju-Nam, Y. and J.R. Lead, *Manufactured Nanoparticles: An Overview of Their Chemistry, Interactions and Potential Environmental Implications.* Science of The Total Environment, 2008. **400**(1-3): p. 396-414.

[30] Tolaymat, T.M., et al., *An Evidence-Based Environmental Perspective of Manufactured Silver Nanoparticle in Syntheses and Applications: A Systematic Review and Critical Appraisal of Peer-Reviewed Scientific Papers.* Science of The Total Environment, 2010. **408**(5): p. 999-1006.

[31] Patel, K., et al., *Synthesis of Nanosized Silver Colloids by Microwave Dielectric Heating.* Journal of Chemical Sciences, 2005. **117**(1): p. 53-60.

[32] Vorobyova, S.A., A.I. Lesnikovich, and N.S. Sobal, *Preparation of Silver Nanoparticles by Interphase Reduction.* Colloids and Surfaces A: Physicochemical and Engineering Aspects, 1999. **152**(3): p. 375-379.

[33] Sharma, V.K., R.A. Yngard, and Y. Lin, *Silver Nanoparticles: Green Synthesis and Their Antimicrobial Activities.* Advances in Colloid and Interface Science, 2009. **145**(1-2): p. 83-96.

[34] Pillai, Z.S. and P.V. Kamat, *What Factors Control the Size and Shape of Silver Nanoparticles in the Citrate Ion Reduction Method?* Journal of Physical Chemistry B, 2004. **108**(3): p. 945-951.

[35] Lee, P.C. and D. Meisel, *Adsorption and Surface-Enhanced Raman of Dyes on Silver and Gold Sols.* Journal of Physical Chemistry, 1982. **86**(17): p. 3391-3395.

[36] Teow, Y., et al., *Health Impact and Safety of Engineered Nanomaterials.* Chemical Communications, 2011. **47**(25): p. 7025-7038.

[37] Ju-Nam, Y. and J.R. Lead, *Manufactured Nanoparticles: An Overview of Their Chemistry, Interactions and Potential Environmental Implications.* Science of the Total Environment, 2008. **400**(1–3): p. 396-414.

[38] Dadosh, T., *Synthesis of Uniform Silver Nanoparticles with a Controllable Size.* Materials Letters, 2009. **63**(26): p. 2236-2238.

[39] Soukupová, J., et al., *Comprehensive Study on Surfactant Role on Silver Nanoparticles (Nps) Prepared Via Modified Tollens Process.* Materials Chemistry and Physics, 2008. **111**(1): p. 77-81.

[40] Gan, X., et al., *Effect of Silver Nanoparticles on the Electron Transfer Reactivity and the Catalytic Activity of Myoglobin.* Chembiochem, 2004. **5**(12): p. 1686-1691.

[41] Hamal, D.B. and K.J. Klabunde, *Synthesis, Characterization, and Visible Light Activity of New Nanoparticle Photocatalysts Based on Silver, Carbon, and Sulfur-Doped Tio2.* Journal of Colloid and Interface Science, 2007. **311**(2): p. 514-522.

[42] Sylvestre, J.P., et al., *Surface Chemistry of Gold Nanoparticles Produced by Laser Ablation in Aqueous Media.* Journal of Physical Chemistry B, 2004. **108**(43): p. 16864-16869.

[43] Yang, M.X., et al., *Lithographic Fabrication of Model Systems in Heterogeneous Catalysis and Surface Science Studies.* Langmuir, 1998. **14**(6): p. 1458-1464.

[44] Rezaei-Zarchi, S., et al., *Use of Silver Nanoparticles as an Electron Transfer Facilitator in Electrochemical Ligand-Binding of Haemoglobin.* Journal of Applied Electrochemistry, 2007. **37**(9): p. 1021-1026.

[45] Schmid, G. and B. Corain, *Nanoparticulated Gold: Syntheses, Structures, Electronics, and Reactivities.* Eur J Inorg Chem, 2003. **17**: p. 3081–98.

[46] Brust, M. and C.J. Kiely, *Some Recent Advances in Nanostructure Preparation from Gold and Silver Particles: A Short Topical Review.* Colloids Surf A: Physicochem Eng Asp, 2002. **202**: p. 175–86.

[47] Haick, H., *Chemical Sensors Based on Molecularly Modified Metallic Nanoparticles.* J Phys D-Appl Phys 2007. **40**: p. 7173–86.

[48] Chaloupka, K., Y. Malam, and A.M. Seifalian, *Nanosilver as a New Generation of Nanoproduct in Biomedical Applications.* Trends in Biotechnology, 2010. **28**(11): p. 580-588.

[49] Burda, C., et al., *Chemistry and Properties of Nanocrystals of Different Shapes.* Chemical Reviews, 2005. **105**(4): p. 1025-1102.

[50] Charles P. P. Jr., *Introduction to Nanotechnology (1st Edition)*, 2003, Hoboken, NJ: Wiley-Interscience.

[51] Poole, C.P. and F.J. Owens, *Introduction to Nanotechnology*, 2003, Hoboken, NJ: Wiley-Interscience.

[52] Rotello, V.M., *Nanoparticles: Building Blocks for Nanotechnology*. 1st Ed ed. 2003, New York: Springer.

[53] Ahamed, M., M.S. AlSalhi, and M.K.J. Siddiqui, *Silver Nanoparticle Applications and Human Health.* Clinica Chimica Acta, 2010. **411**(23-24): p. 1841-1848.

[54] Rai, M., A. Yadav, and A. Gade, *Silver Nanoparticles as a New Generation of Antimicrobials.* Biotechnology Advances, 2009. **27**(1): p. 76-83.

[55] Kreyling, W.G., et al., *Translocation of Ultrafine Insoluble Iridium Particles from Lung Epithelium to Extrapulmonary Organs Is Size Dependent but Very Low.* Journal of Toxicology and Environmental Health-Part A, 2002. **65**(20): p. 1513-1530.

[56] Takenaka, S., et al., *Pulmonary and Systemic Distribution of Inhaled Ultrafine Silver Particles in Rats.* Environmental Health Perspectives, 2001. **109**: p. 547-551.

[57] Sooresh, A., et al., *A Physiologically Relevant Approach to Characterize the Microbial Response to Colloidal Particles in Food Matrices within a Simulated Gastrointestinal Tract.* Food and Chemical Toxicology, 2012. **50**(9): p. 2971-2977.

[58] Sawai, J., et al., *Hydrogen Peroxide as an Antibacterial Factor in Zinc Oxide Powder Slurry.* Journal of Fermentation and Bioengineering, 1998. **86**(5): p. 521-522.

[59] Feng, Q.L., et al., *A Mechanistic Study of the Antibacterial Effect of Silver Ions on Escherichia Coli and Staphylococcus Aureus.* Journal of Biomedical Materials Research, 2000. **52**(4): p. 662-668.

[60] Sawai, J. and T. Yoshikawa, *Quantitative Evaluation of Antifungal Activity of Metallic Oxide Powders (Mgo, Cao and Zno) by an Indirect Conductimetric Assay.* Journal of Applied Microbiology, 2004. **96**(4): p. 803-809.

[61] Sawai, J., *Quantitative Evaluation of Antibacterial Activities of Metallic Oxide Powders (ZnO, MgO and CaO) by Conductimetric Assay.* Journal of Microbiological Methods, 2003. **54**(2): p. 177-182.

[62] Hur, S.J., et al., *In Vitro Human Digestion Models for Food Applications.* Food Chemistry, 2011. **125**(1): p. 1-12.

[63] Moreda-Pineiro, J., et al., *In-Vivo and in-Vitro Testing to Assess the Bioaccessibility and the Bioavailability of Arsenic, Selenium and Mercury Species in Food Samples.* Trac-Trends in Analytical Chemistry, 2011. **30**(2): p. 324-345.

[64] Astwood, J.D., J.N. Leach, and R.L. Fuchs, *Stability of Food Allergens to Digestion in Vitro.* Nature Biotechnology, 1996. **14**(10): p. 1269-1273.

[65] Fu, T.T., U.R. Abbott, and C. Hatzos, *Digestibility of Food Allergens and Nonallergenic Proteins in Simulated Gastric Fluid and Simulated Intestinal Fluid - a Comparative Study.* Journal of Agricultural and Food Chemistry, 2002. **50**(24): p. 7154-7160.

[66] Hansen, S.F., et al., *Categorization Framework to Aid Hazard Identification of Nanomaterials.* Nanotoxicology, 2007. **1**(3): p. 243-250.

[67] Scientific Community on Emerging and Newly Identified Health Risks, (SCENIHR), *The Appropriateness of Existing Methodologies to Assess the Potential Risks Associated with Engineered and Adventitious Products of Nanotechnologies*, 10th March 2006. Available from:

http://ec.europa.eu/health/ph_risk/committees/04_scenihr/docs/scenihr_o_003b.pdf

[68] *The Global Market for Metal Oxide Nanoparticles to 2020*. Future Markets, Inc, March 2013. p. 322.

[69] Saber, A.T., et al., *Inflammatory and Genotoxic Effects of Nanoparticles Designed for Inclusion in Paints and Lacquers.* Nanotoxicology, 2012. **6**(5): p. 453–471.

[70] Baan, R.A., *IARC (International Agency for Research on Cancer): IARC Monographs on the Evaluation of Carcinogenic Risks to Humans*, 2010. **93**: p. 9-38.

[71] *The Global Market for Nanomaterials 2002-2016: Production Volumes, Revenues and End User Market Demand*, April 2012. p. 371. Available from: http://www.marketresearchreports.biz/analysis-details/the-global-market-for-nanomaterials-2002-2016-production-volumes-revenues-and-end-user-market-demand

[72] Allen, N.S., et al., *Photocatalytic Surfaces: Environmental Benefits of Nanotitania.* The Open Materials Science Journal, 2009. **3**: p. 6-27. Available from: http://www.benthamscience.com/open/tomsj/articles/V003/6TOMSJ.pdf

[73] Ozgenc, O., S. Hiziroglu, and U.C. Yildiz, *Weathering Properties of Wood Species Treated with Different Coating Applications.* BioResources, 2012. **7**(4): p. 4875-4888.

[74] Vlad-Cristea, M., et al., *Nanocharacterization Techniques for Investigating the Durability of Wood Coatings.* European Polymer Journal, 2012. **48**(3): p. 441-453.

[75] Vorbau, M., L. Hillemann, and M. Stintz, *Method for the Characterization of the Abrasion Induced Nanoparticle Release into Air from Surface Coatings.* Journal of Aerosol Science, 2009. **40**(3): p. 209-217.

[76] Göhler, D., et al., *Characterization of Nanoparticle Release from Surface Coatings by the Simulation of a Sanding Process.* Annals of Occupational Hygiene, 2010. **54**(6): p. 615-624.

[77] Carp, O., *Photoinduced Reactivity of Titanium Dioxide.* Progress in Solid State Chemistry, 2004. **32**(1-2): p. 33-177.

[78] Mills, A., R.H. Davies, and D. Worsley, *Water-Purification by Semiconductor Photocatalysis.* Chemical Society Reviews, 1993. **22**(6): p. 417-425.

[79] Allen, N.S., et al., *Degradation and Stabilisation of Polymers and Coatings: Nano Versus Pigmentary Titania Particles.* Polymer Degradation and Stability, 2004. **85**(3 SPEC. ISS.): p. 927-946.

[80] Allen, N.S. and J.F. McKellar, *Photochemistry of Dyed and Pigmented Polymers*. London: Applied Science Publishers, July 1980.

[81] Allen, N.S., et al., *Behaviour of Nanoparticle (Ultrafine) Titanium Dioxide Pigments and Stabilisers on the Photooxidative Stability of Water Based Acrylic and Isocyanate Based Acrylic Coatings.* Polymer Degradation and Stability, 2002. **78**(3): p. 467-478.

[82] Beattie, I.R. and T.R. Gilson, *Oxide Phonon Spectra.* Journal of the Chemical Society A: Inorganic, Physical, Theoretical, 1969. **0**(0): p. 2322-2327.

[83] López, T., et al., *Characterization of Iron-Doped Titania Sol-Gel Materials.* Journal of Materials Chemistry, 2002. **12**(3): p. 714-718.

[84] Luo, H.L., J. Sheng, and Y.Z. Wan, *Preparation and Characterization of TiO_2/Polystyrene Core–Shell Nanospheres Via Microwave-Assisted Emulsion Polymerization.* Materials Letters, 2008. **62**(1): p. 37-40.

[85] Mohamed, M.M., et al., *Synthesis and Structural Characterization of Tio2 and V2o5/Tio2 Nanoparticles Assembled by the Anionic Surfactant Sodium Dodecyl Sulfate.* Microporous and Mesoporous Materials, 2006. **97**(1–3): p. 66-77.

[86] Wang, J., et al., *Heat Treatment of Nanometer Anatase Powder and Its Photocatalytic Activity for Degradation of Acid Red B Dye under Visible Light Irradiation.* Inorganic Materials, 2008. **44**(6): p. 608-614.

[87] Erdem, B., et al., *XPS and FTIR Surface Characterization of Tio2 Particles Used in Polymer Encapsulation.* Langmuir, 2001. **17**(9): p. 2664-2669.

[88] Borm, P.J.A., et al., *The Potential Risks of Nanomaterials: A Review Carried out for Ecetoc.* Particle and Fibre Toxicology, 2006. **3**(11): p. 1-35.

[89] Shi, H., et al., *Titanium Dioxide Nanoparticles: A Review of Current Toxicological Data.* Particle and Fibre Toxicology, 2013. **10**(15): p. 1-33.

[90] Bravo, A., et al., *Bacillus Thuringiensis: A Story of a Successful Bioinsecticide.* Insect Biochemistry and Molecular Biology, 2011. **41**(7): p. 423-431.

[91] Elango, G., et al., *Efficacy of Medicinal Plant Extracts against Malarial Vector, Anopheles Subpictus Grassi.* Parasitology Research, 2011. **108**(6): p. 1437-1445.

[92] Zaim, M. and P. Guillet, *Alternative Insecticides: An Urgent Need.* Trends Parasitol 2002. **18**: p. 161–163.

[93] Castillo, J.C., A.E. Robertson, and M.R. Strand, *Characterization of Hemocytes from the Mosquitoes Anopheles Gambiae and Aedes Aegypti.* Insect Biochemistry and Molecular Biology, 2006. **36**(12): p. 891-903.

[94] Wang, L., W. Zhao, and W. Tan, *Bioconjugated Silica Nanoparticles: Development and Applications.* Nano Research, 2008. **1**(2): p. 99-99-115.

[95] Saxena, P.N., L.K.S. Chauhan, and S.K. Gupta, *Cytogenetic Effects of Commercial Formulation of Cypermethrin in Root Meristem Cells of Allium Sativum: Spectroscopic Basis of Chromosome Damage.* Toxicology, 2005. **216**(2-3): p. 244-252.

[96] Owen, J.D., *Absolute-Configuration of Most Potent Isomer of Pyrethroid Insecticide by Crystal-Structure Analysis* Journal of the Chemical Society-Perkin Transactions 1, 1975(19): p. 1865-1868.

[97] Owen, J.D., *Structure of Rel-(Alphar), (1r, Trans)-Alpha-Cyano-3-Phenoxybenzyl 3-(2,2-Dichlorovinyl)-2,2-Dimethylcyclopropanecarboxylate, Non-Insecticidal Components of Cypermethrin* Acta Crystallographica Section B-Structural Science, 1981. **37**(JUN): p. 1311-1314.

[98] Segal-Rosenheimer, M. and Y. Dubowski, *Heterogeneous Ozonolysis of Cypermethrin Using Real-Time Monitoring Ftir Techniques.* Journal of Physical Chemistry C, 2007. **111**(31): p. 11682-11691.

[99] Armenta, S., et al., *Mid-Infrared and Raman Spectrometry for Quality Control of Pesticide Formulations.* Trac-Trends in Analytical Chemistry, 2005. **24**(8): p. 772-781.

[100] Lin-Vien, D., et al., *The Handbook of Infrared and Raman Characteristic Frequencies of Organic Molecules*. Academic Press. 1991.

[101] Mo, L.X., et al., *Preparation and Characterization of Silver Citrate Nano-Emulsion and Nano-Silver Film*, in *Surface Engineering*, M.K. Lei, X.P. Zhu, and K.W. Xu, Editors. 2008. p. 698-701.

[102] Li, X.A., J.J. Lenhart, and H.W. Walker, *Dissolution-Accompanied Aggregation Kinetics of Silver Nanoparticles.* Langmuir 2010. **26**(22): p. 16690-16698.

[103] Zaim, M. and P. Guillet, *Alternative Insecticides: An Urgent Need.* Trends in Parasitology, 2002. **18**(4): p. 161-163.

[104] Sudakin, D., *Prethroid Insecticides: Advances and Challenges in Biomonitoring.* Clinical Toxicology 2006. **44**: p. 31-37.

[105] Erstfeld, K.M., *Environmental Fate of Synthetic Pyrethroids During Spray Drift and Field Runoff Treatments in Aquatic Microcosms.* Chemosphere 1999. **39**: p. 1737-1769.

[106] Sooresh, A., et al., *Surface Functionalization of Silver Nanoparticles: Novel Applications for Insect Vector Control.* ACS Applied Materials and Interfaces, 2011. **3**(10): p. 3779-3787.

[107] Jeon, H.J., S.C. Yi, and S.G. Oh, *Preparation and Antibacterial Effects of Ag-Sio2 Thin Films by Sol-Gel Method.* Biomaterials, 2003. **24**(27): p. 4921-4928.

[108] J.I. Kim, C.W. and J.L.E. KJ Wilkinson, *Environmental Colloids and Particles: Behaviour, Structure and Characterisation*. 2006: John Wiley and Sons, Chichester.

[109] Roco, M.C. and W.S. Bainbridge, *Societal Implications of Nanoscience and Nanotechnology: Maximizing Human Benefit.* Journal of Nanoparticle Research, 2005. **7**(1): p. 1-13.

[110] Niemeyer, C.M., *Nanoparticles, Proteins, and Nucleic Acids: Biotechnology Meets Materials Science.* Angewandte Chemie-International Edition, 2001. **40**(22): p. 4128-4158.

[111] Schmid, G., *Nanoparticles: From Theory to Application*. 1st Ed ed. 2004: Wiley-VCH, Weinheim

[112] Oberdorster, G., E. Oberdorster, and J. Oberdorster, *Nanotoxicology: An Emerging Discipline Evolving from Studies of Ultrafine Particles.* Environmental Health Perspectives, 2005. **113**(7): p. 823-839.

[113] US EPA, *Nanoscale Silver in Disinfectant Spray (External Review Draft)*, 2010: Washington, D. C.

[114] Sun, R.W.Y., et al., *Silver Nanoparticles Fabricated in Hepes Buffer Exhibit Cytoprotective Activities toward Hiv-1 Infected Cells.* Chemical Communications, 2005(40): p. 5059-5061.

[115] Wright, J.B., et al., *Efficacy of Topical Silver against Fungal Burn Wound Pathogens.* American Journal of Infection Control, 1999. **27**(4): p. 344-350.

[116] Lee, H.J., S.Y. Yeo, and S.H. Jeong, *Antibacterial Effect of Nanosized Silver Colloidal Solution on Textile Fabrics.* Journal of Materials Science, 2003. **38**(10): p. 2199-2204.

[117] Kah, M., et al., *Nanopesticides: State of Knowledge, Environmental Fate, and Exposure Modeling.* Critical Reviews in Environmental Science and Technology, 2012. **43**(16): p. 1823-1867.

[118] WHO, *Malaria Vector Control and Personal Protection*, 2006. p. vi, 62 p.

[119] Foldbjerg, R., et al., *Pvp-Coated Silver Nanoparticles and Silver Ions Induce Reactive Oxygen Species, Apoptosis and Necrosis in Thp-1 Monocytes.* Toxicology Letters, 2009. **190**(2): p. 156-162.

[120] Kim, T.H., *Size-Dependent Cellular Toxicity of Silver Nanoparticles.* Journal of Biomedical Materials Research. Part A, 2012. **100A**(4): p. 1033-1043.

[121] Ott, M., et al., *Mitochondria, Oxidative Stress and Cell Death.* Apoptosis, 2007. **12**(5): p. 913-922.

[122] Li, H.Y., et al., *Oxidative Stress of Deltamethrin on Rat Nervous System.* Journal of Industrial Hygiene and Occupational Diseases, 2005. **23**(2): p. 97-101.

[123] Li, T., et al., *Effects of Deltamethrin on Intracellular Free Ca^{2+} Concentration and Apoptosis in Rat Neural Cells.* Journal of Industrial Hygiene and Occupational Diseases, 2002. **20**(6): p. 427-429.

[124] Kale, M., et al., *Lipid Peroxidative Damage on Pyrethroid Exposure and Alterations in Antioxidant Status in Rat Erythrocytes: A Possible Involvement of Reactive Oxygen Species.* Toxicology Letters, 1999. **105**(3): p. 197-205.

[125] Giray, B., A. Gürbay, and F. Hincal, *Cypermethrin-Induced Oxidative Stress in Rat Brain and Liver Is Prevented by Vitamin E or Allopurinol.* Toxicology Letters, 2001. **118**(3): p. 139-146.

[126] Maiti, P.K., et al., *Loss of Membrane Integrity and Inhibition of Type-I Iodothyronine 5'-Monodeiodinase Activity by Fenvalerate in Female Mouse.* Biochemical and Biophysical Research Communications, 1995. **214**(3): p. 905-909.

[127] Shafer, T.J. and W.D. Atchison, *Transmitter, Ion Channel and Receptor Properties of Pheochromocytoma (PC12) Cells - a Model for Neurotoxicological Studies.* Neurotoxicology, 1991. **12**(3): p. 473-492.

[128] Teng KK, G.L., *Cultured PC12 Cells: A Model for Neuronal Function and Differentiation. In: Cell Biology: A Laboratory Handbook* Ed. E. (Celis JE. 1994, San Diego: Academic Press.

[129] Cheng, B., S. Christakos, and M.P. Mattson, *Tumor Necrosis Factors Protect Neurons against Metabolic-Excitotoxic Insults and Promote Maintenance of Calcium Homeostasis.* Neuron, 1994. **12**(1): p. 139-153.

[130] Coyle, J.T. and P. Puttfarcken, *Oxidative Stress, Glutamate, and Neurodegenerative Disorders.* Science, 1993. **262**(5134): p. 689-695.

[131] De Erausquin, G.A., E. Costa, and I. Hanbauer, *Calcium Homeostasis, Free Radical Formation, and Trophic Factor Dependence Mechanisms in Parkinson's Disease.* Pharmacological Reviews, 1994. **46**(4): p. 467-482.

[132] Keller, J.N., et al., *Increased Sensitivity to Mitochondrial Toxin-Induced Apoptosis in Neural Cells Expressing Mutant Presenilin-1 Is Linked to Perturbed Calcium Homeostasis and Enhanced Oxyradical Production.* Journal of Neuroscience, 1998. **18**(12): p. 4439-4450.

[133] Huang, Y.L., et al., *Nf-E2 Related Factor 2 Activation and Heme Oxygenase-1 Induction by Tert-Butylhydroquinone Protect against Deltamethrin-Mediated Oxidative Stress in Pc12 Cells.* Chemical Research in Toxicology, 2007. **20**(9): p. 1242-1251.

[134] Li, H., et al., *Effect of Glutathione Depletion on Nrf2/Are Activation by Deltamethrin in Pc12 Cells.* Arh Hig Rada Toksikol, 2013. **64**(1): p. 87-97.

[135] Li, H.Y., et al., *The Pesticide Deltamethrin Increases Free Radical Production and Promotes Nuclear Translocation of the Stress Response Transcription Factor Nrf2 in Rat Brain.* Toxicol Ind Health, 2011. **27**(7): p. 579-90.

[136] Li, H.Y., Y.F. Zhong, and N. Shi, *Effect of Deltamethrin on Production of Reactive Oxygen Species in PC12 Cells.* Journal of Industrial Hygiene and Occupational Diseases, 2008. **26**(11): p. 654-658.

[137] Li, H.Y., S.Y. Wu, and N. Shi, *Transcription Factor Nrf2 Activation by Deltamethrin in Pc12 Cells: Involvement of Ros.* Toxicology Letters, 2007. **171**(1-2): p. 87-98.

[138] Powers, C.M., et al., *Silver Nanoparticles Compromise Neurodevelopment in PC12 Cells: Critical Contributions of Silver Ion, Particle Size, Coating, and Composition.* Environmental Health Perspectives, 2011. **119**(1): p. 37-44.

[139] Carlson, C., et al., *Unique Cellular Interaction of Silver Nanoparticles: Size-Dependent Generation of Reactive Oxygen Species.* Journal of Physical Chemistry B, 2008. **112**(43): p. 13608-13619.

[140] Haase, A., et al., *Effects of Silver Nanoparticles on Primary Mixed Neural Cell Cultures: Uptake, Oxidative Stress and Acute Calcium Responses.* Toxicological Sciences, 2012. **126**(2): p. 457-468.

[141] Hussain, S.M., et al., *The Interaction of Manganese Nanoparticles with Pc-12 Cells Induces Dopamine Depletion.* Toxicological Sciences, 2006. **92**(2): p. 456-463.

[142] Rahman, M.F., et al., *Expression of Genes Related to Oxidative Stress in the Mouse Brain after Exposure to Silver-25 Nanoparticles.* Toxicology Letters, 2009. **187**(1): p. 15-21.

[143] Yang, Z., et al., *A Review of Nanoparticle Functionality and Toxicity on the Central Nervous System.* Journal of the Royal Society Interface, 2010. **7**: p. S411-S422.

[144] Lee, P.C. and D. Meisel, Journal of Physical Chemistry, 1982. **86**(17): p. 3391-3395.

[145] Sivaraman, S.K., et al., *A Green Protocol for Room Temperature Synthesis of Silver Nanoparticles in Seconds.* Current Science, 2009. **97**(7): p. 1055-1059.

[146] Yazawa, K., et al., *Distinct Mechanisms Underlie Distinct Polyphenol-Induced Neuroprotection.* FEBS Letters, 2006. **580**(28-29): p. 6623-6628.

[147] Conte, A., S. Pellegrini, and D. Tagliazucchi, *Effect of Resveratrol and Catechin on Pc12 Tyrosine Kinase Activities and Their Synergistic Protection from B-Amyloid Toxicity.* Drugs under Experimental and Clinical Research, 2003. **29**(5-6): p. 243-255.

[148] Ponder, S.M., et al., *Surface Chemistry and Electrochemistry of Supported Zerovalent Iron Nanoparticles in the Remediation of Aqueous Metal Contaminants.* Chemistry of Materials, 2001. **13**(2): p. 479-486.

[149] Obare, S.O. and G.J. Meyer, *Nanostructured Materials for Environmental Remediation of Organic Contaminants in Water.* Journal of Environmental Science and Health Part a-Toxic/Hazardous Substances & Environmental Engineering, 2004. **39**(10): p. 2549-2582.

[150] Chaudhry, Q., et al., *Applications and Implications of Nanotechnologies for the Food Sector.* Food Additives and Contaminants, 2008. **25**(3): p. 241-258.

[151] Biancaniello, P.L., A.J. Kim, and J.C. Crocker, *Colloidal Interactions and Self-Assembly Using DNA Hybridization.* Physical Review Letters, 2005. **94**(5): p. 058302.

[152] Nelson, E.C. and P.V. Braun, *Enhancing Colloids through the Surface.* Science, 2007. **318**(5852): p. 924-925.

[153] Bouwmeester, H., et al., *Review of Health Safety Aspects of Nanotechnologies in Food Production.* Regulatory Toxicology and Pharmacology, 2009. **53**(1): p. 52-62.

[154] Akerman, M.E., et al., *Nanocrystal Targeting in Vivo.* Proceedings of the National Academy of Sciences of the United States of America, 2002. **99**(20): p. 12617-12621.

[155] Damm, C., H. Munstedt, and A. Rosch, *The Antimicrobial Efficacy of Polyamide 6/Silver-Nano- and Microcomposites.* Materials Chemistry and Physics, 2008. **108**(1): p. 61-66.

[156] Morones, et al., *The Bactericidal Effect of Silver Nanoparticles.* Nanotechnology, 2005. **16**(10): p. 2346-2353.

[157] Thomas, V., et al., *A Versatile Strategy to Fabricate Hydrogel-Silver Nanocomposites and Investigation of Their Antimicrobial Activity.* Journal of Colloid and Interface Science, 2007. **315**(1): p. 389-395.

[158] Panacek, A., et al., *Silver Colloid Nanoparticles: Synthesis, Characterization, and Their Antibacterial Activity.* Journal of Physical Chemistry B, 2006. **110**(33): p. 16248-16253.

[159] Potty, V.H., *Physio-Chemical Aspects, Physiological Functions, Nutritional Importance and Technological Significance of Dietary Fibres - a Critical*

Appraisal. Journal of Food Science and Technology-Mysore, 1996. **33**(1): p. 1-18.

[160] de Souza, M.C.C., et al., *Stability of Unpasteurized and Refrigerated Orange Juice.* Brazilian Archives of Biology and Technology, 2004. **47**(3): p. 391-397.

[161] Morris, C., A.L. Brody, and L. Wicker, *Non-Thermal Food Processing/Preservation Technotogies: A Review with Packaging Implications.* Packaging Technology and Science, 2007. **20**(4): p. 275-286.

[162] Emamifar, A., et al., *Evaluation of Nanocomposite Packaging Containing Ag and Zno on Shelf Life of Fresh Orange Juice.* Innovative Food Science & Emerging Technologies, 2010. **11**(4): p. 742-748.

[163] Glahn, R.P., et al., *Caco-2 Cell Ferritin Formation Predicts Nonradiolabeled Food Iron Availability in an in Vitro Digestion/Caco-2 Cell Culture Model.* J Nutr, 1998. **128**(9): p. 1555-61.

[164] Jesudhasan, P.R., et al., *Transcriptome Analysis of Genes Controlled by Luxs/Autoinducer-2 in Salmonella Enterica Serovar Typhimurium.* Foodborne Pathog Dis, 2010. **7**(4): p. 399-410.

[165] Oliver, J.D., *The Viable but Nonculturable State in Bacteria.* Journal of microbiology, 2005. **43**(1): p. 93.

[166] Abrahamsson, B., et al., *Gastro-Intestinal Transit of a Multiple-Unit Formulation (Metoprolol Cr/Zok) and a Non-Disintegrating Tablet with the Emphasis on Colon.* International Journal of Pharmaceutics, 1996. **140**(2): p. 229-235.

[167] Ngeontae, W., et al., *New Silver Selective Electrode Fabricated from Benzothiazole Calix 4 Arene: Speciation Analysis of Silver Nanoparticles.* Sensors and Actuators B-Chemical, 2008. **134**(2): p. 377-385.

[168] Wijnhoven, S.W.P., et al., *Nano-Silver - a Review of Available Data and Knowledge Gaps in Human and Environmental Risk Assessment.* Nanotoxicology, 2009. **3**(2): p. 109-U78.

[169] Lok, C.N., et al., *Proteomic Analysis of the Mode of Antibacterial Action of Silver Nanoparticles.* J Proteome Res, 2006. **5**(4): p. 916-24.

[170] Sondi, I. and B. Salopek-Sondi, *Silver Nanoparticles as Antimicrobial Agent: A Case Study on E. Coli as a Model for Gram-Negative Bacteria.* J Colloid Interface Sci, 2004. **275**(1): p. 177-82.

[171] Sotiriou, G.A. and S.E. Pratsinis, *Antibacterial Activity of Nanosilver Ions and Particles.* Environ Sci Technol, 2010.

[172] Nel, A., et al., *Toxic Potential of Materials at the Nanolevel.* Science, 2006. **311**(5761): p. 622-627.

[173] Ratte, H.T., *Bioaccumulation and Toxicity of Silver Compounds: A Review.* Environmental Toxicology and Chemistry, 1999. **18**(1): p. 89-108.

[174] Johnston, H.J., et al., *A Review of the in Vivo and in Vitro Toxicity of Silver and Gold Particulates: Particle Attributes and Biological Mechanisms Responsible for the Observed Toxicity.* Critical Reviews in Toxicology, 2010. **40**(4): p. 328-346.

[175] Duncan, T.V., *Applications of Nanotechnology in Food Packaging and Food Safety: Barrier Materials, Antimicrobials and Sensors.* J Colloid Interface Sci, 2011. **363**(1): p. 1-24.

[176] Staiano, M., et al., *Nanostructured Silver-Based Surfaces: New Emergent Methodologies for an Easy Detection of Analytes.* ACS Applied Materials and Interfaces, 2009. **1**(12): p. 2909-2916.

[177] Versantvoort, C.H.M., et al., *Applicability of an in Vitro Digestion Model in Assessing the Bioaccessibility of Mycotoxins from Food.* Food and Chemical Toxicology, 2005. **43**(1): p. 31-40.